Multidecadal variability in the North Atlantic

Dissertation

in fulfilment of the requirements for the degree of Dr. rer. nat

of the Faculty of Mathematics and Natural Sciences

at Kiel University

submitted by

Jing Sun

May 2021

Department of Marine Meteorology,

Research Division of Ocean Circulation and Climate Dynamics,

GEOMAR Helmholtz Centre for Ocean Research Kiel

First Referee: Prof. Dr. Mojib Latif

Second Referee: Prof. Dr. Arne Biastoch

Date of the oral examination: 02 August 2021

Approved for Publication: 02 August 2021

Abstract

The North Atlantic (NA) region plays a key role in the global climate system and exhibits pronounced multidecadal climate variability. There is a controversy about the nature of the multidecadal climate variability in the NA region. This thesis provides an enhanced understanding about the multidecadal variability in the NA sector by applying and analyzing climate models and investigating observations, especially about the mechanisms for sea surface temperature (SST) and Atlantic meridional overturning circulation (AMOC) variability. Firstly, different driving factors operating on the extratropical and tropical NA SST on different timescales are investigated by using observations and model simulations. Secondly, a coupled air-sea multidecadal mode is discovered in the NA region by analyzing the fully coupled Kiel Climate Model (KCM). Thirdly, possible AMOC slowing is discussed by analyzing observational datasets and historical simulations with climate models.

In the first part of this thesis, the different influences on the NA SST variability are examined based on observations and climate models. This analysis is conducted by using the basin-averaged NA SST index (NASST) and the low-pass filtered version, termed Atlantic multidecadal oscillation (AMO) index. In particular, the relationships of the two indices with some of its mechanistic drivers including Atlantic meridional overturning circulation (AMOC), North Atlantic Oscillation (NAO), subpolar gyre (SPG) and El Niño–Southern Oscillation (ENSO) are investigated. The results show that the NASST index lumps together SST variability driven by different mechanisms and operating on different timescales. Meanwhile, the AMO index emphasizes the SST variability over the extratropical NA, which is connected to the AMOC in climate models. In addition, models with a large cold bias over the NA exhibit a relatively weak linkage between the AMOC and AMO.

The second part discusses the roles of ocean circulation and atmosphere-ocean coupling in the multidecadal climate variability in the NA region. A multidecadal mode is found in KCM, where both ocean circulation and atmosphere-ocean coupling are essential. A fast positive feedback and a delayed negative feedback are crucial for the multidecadal mode. The positive ocean-atmosphere feedback is between the SST and low-level atmospheric circulation over the Southern Greenland area. SPG and AMOC mutually influence each other and together provide the delayed negative feedback necessary for maintaining the oscillation. The stochastic heat-flux variability associated with the NAO keeps exciting the mode.

A number of climate models predict that the AMOC will slow if the anthropogenic greenhouse gas emissions continue to rise unabatedly. However, there are debates about as to whether the AMOC is already slowing. The NA warming hole, which is a region where the SST cooled despite the global surface ocean warmed, has been suggested to be an indicator of anthropogenic AMOC slowing. The cooling may reflect diminishing AMOC-related northward upper-ocean heat transport. In the last part of the thesis, by using observational datasets since the beginning of the 20th century, the Atlantic SST variability linked to the net radiative forcing is identified and this pattern hardly accounts for any variance in the NA warming hole. In the NA warming hole, the so-called interhemispheric SST dipole pattern dominates that well records long-term internal AMOC variability in climate models. Furthermore, historical simulations with climate models in the ensemble mean only predict minor AMOC slowing. This part demonstrates the importance of natural internal AMOC variability in recent AMOC slowing and the need for systematic and sustained direct observations of the AMOC.

Zusammenfassung

Die Nordatlantikregion (NA) spielt eine Schlüsselrolle im globalen Klimasystem und weist eine ausgeprägte multidekadische Variabilität auf. Es gibt eine Kontroverse über die Art der multidekadischen Klimavariabilität in der NA-Region. Diese Arbeit bietet einen verbesserten Einblick in die multidekadische Variabilität im nordatlantischen Raum in Klimamodellen und Beobachtungen, insbesondere in Bezug auf die atlantischen Meeresoberflächentemperaturen (SSTs) und die Atlantischen meridionale Umwälzzirkulation (AMOC). Zunächst werden verschiedene Antriebsmechanismen, die auf verschiedenen Zeitskalen auf die extratropischen und tropischen NA SSTs wirken, mithilfe von Beobachtungen und Modellsimulationen untersucht. Zweitens wird ein gekoppelter multidekadischer Atmosphäre-Ozean Mode in dem voll gekoppelten Kieler Klimamodell (KCM) beschrieben. Drittens wird eine mögliche anthropogene Abschwächung der AMOC durch die Analyse von Beobachtungsdatensätzen diskutiert.

Im ersten Teil der Arbeit werden die verschiedenen Einflüsse auf die NA SST-Variabilität anhand von Beobachtungen und Modellen untersucht. Diese Analyse wird unter Verwendung des beckengemittelten NA SST-Index (NASST) und der tiefpassgefilterten Version des Indexes, des sogenannten Atlantic Multidecadal Oscillation (AMO) Index, durchgeführt. Insbesondere werden die Beziehungen der beiden Indizes zusammen mit ihren eigenen mechanistischen Treiber wie die atlantische meridionale Umwälzzirkulation (AMOC), die Nordatlantische Oszillation (NAO), der subpolare Wirbel (SPG) und El Niño-Southern Oscillation (ENSO), untersucht. Die Ergebnisse zeigen, dass der NASST-Index die SST-Variabilität beschreibt, die durch unterschiedliche Mechanismen auf unterschiedlichen Zeitskalen gesteuert wird. Währenddessen betont der AMO-Index die SST-Variabilität im extratropischen NA, die mit der AMOC verbunden ist. Darüber hinaus weisen Modelle mit einem viel zu kalten NA („cold SST bias“) eine relativ schwache Verknüpfung zwischen der AMOC und der AMO auf.

Der zweite Teil der Arbeit diskutiert die Rolle der Ozeanzirkulation und der Atmosphäre-Ozean-Kopplung für die multidekadische Klimavariabilität in der NA-Region. Ein multidekadischer Mode findet sich in KCM, bei der sowohl die Ozeanzirkulation als auch die Atmosphäre-Ozean-Kopplung wesentlich sind. Eine schnelle positive Rückkopplung und eine verzögerte negative Rückkopplung sind für den multidekadischen Mode

entscheidend. Das positive Feedback findet zwischen der SST und der atmosphärischen Zirkulation mit einem Druckzentrum über Südgrönland statt. SPG und AMOC beeinflussen sich gegenseitig und liefern zusammen die verzögerte negative Rückkopplung, die zur Aufrechterhaltung der Oszillation erforderlich ist. Der mit der NAO verbundene stochastische Wärmefluss regt den Mode kontinuierlich an.

Eine Reihe von Klimamodellen sagen voraus, dass sich die AMOC verlangsamen wird, wenn die anthropogenen Treibhausgasemissionen unvermindert weiter ansteigen. Es gibt jedoch eine Debatte darüber, ob sich die AMOC bereits verlangsamt hat. Das nordatlantische Erwärmungsloch, eine Region, in der sich die SST abkühlte trotz der Erwärmung der Meeresoberfläche im globalen Mittel, wurde als Indikator für die anthropogen bedingte Verlangsamung der AMOC vorgeschlagen. Die Abkühlung könnte einen abnehmenden AMOC-bedingten Wärmetransport nach Norden im oberen Ozean widerspiegeln.

Im letzten Teil der Arbeit wird anhand von Beobachtungsdatensätzen die mit dem globalen Strahlungsantrieb verbundene atlantische SST Variabilität seit Beginn des 20. Jahrhunderts identifiziert. Dieses Muster erklärt jedoch kaum eine Varianz im Bereich des Erwärmungslochs. Dort dominiert der interhemisphärische SST-Dipol, der die langfristige interne AMOC Variabilität in Klimamodellen beschreibt. Außerdem zeigen die historischen Simulationen mithilfe der Klima-Modellen im Ensemblemittelwert nur eine geringe Verlangsamung der AMOC. Dieser Teil der Dissertation zeigt die Bedeutung der natürlichen internen Variabilität der AMOC und die Notwendigkeit systematischer und nachhaltiger direkter AMOC Beobachtungen.

Contents

Chapter 1 Introduction

The North Atlantic (NA) Ocean is one of the few basins where the atmosphere can communicate with the deep ocean via the deep water formation, which is important for the Atlantic Meridional Overturning Circulation (AMOC; Stommel 1958, 1961; Buckley and Marshall 2016). The AMOC in coupled climate models often exhibits pronounced variability on decadal to multidecadal timescales (Zhang et al. 2019). In general, the AMOC consists of a northward upper branch of warm and saline water and a southward lower branch of cold and fresh water, the North Atlantic Deep Water (NADW; Dickson and Brown 1994). The subsequent large northward heat transport makes the Atlantic Ocean being a unique ocean basin with substantial cross-equator ocean heat transport (Bryan 1962; Ganachaud and Wunsch 2000; Trenberth and Solomon 1994). This is important to the climate system, for instance, in setting the mean position of the Inter-Tropical Convergence Zone (Marshall et al. 2014).

On decadal to multidecadal timescales, Atlantic sea surface temperatures (SSTs) exhibit significant basin-scale fluctuations. The NA SST, and its low-pass filtered version which is often referred to as Atlantic multidecadal oscillation/variability (AMO/V, AMO hereafter; Kerr 2000; Enfield et al. 2001; Sutton and Hodson 2005), have been linked to climate variations over many regions, such as NA tropical cyclone activity (Goldenberg et al. 2001; Klotzbach and Gray 2008), Sahel summer rainfall (Folland et al. 1986; Zhang and Delworth 2006), sea ice sheet melt (Holland et al. 2008) and sea-level anomalies (McCarthy et al. 2015). There is ongoing discussion about the driving mechanisms, both internally and externally (Zhang et al. 2019). Atlantic meridional heat transport associated with AMOC is thought to lead ocean heat content anomalies and potentially impacts on SST (Knight et al. 2005; Zhang 2007; Deser et al. 2010; Latif and Keenlyside 2011; Wills et al. 2019). In addition, several hypotheses have been proposed that external radiative forcing is a primary driver (Booth et al. 2012; Bellomo et al. 2018; Mann et al. 2021).

Anthropogenic global warming is the long-term increase of global average temperature which can be attributed to human activity (Pachauri et al. 2014). Anthropogenic global warming has been detected during last decades in observations and climate models (Pierce et al. 2006; Chemke et al. 2020). A number of climate models predict that the AMOC will slow under the global warming. However, due to the limited direct observations of AMOC

and the pronounced internal variability over the NA, it remains unclear as to whether a sustained anthropogenic AMOC slowing already has been underway.

The following sections provide the introduction to the NA SST, ocean circulation, ocean-atmosphere coupling and anthropogenic global warming. The definitions of NA SST indices and different driving factors are discussed in Section 1.1. A brief introduction of ocean circulation and the roles of ocean and atmosphere in the NA region are addressed in Section 1.2. General descriptions about the climate model biases are mentioned in Section 1.3. The possible AMOC slowdown and NA warming hole under global warming are introduced in Section 1.4. The outline and scientific questions of this thesis are given in Section 1.5.

1.1 North Atlantic sea surface temperature index

Both instrumental data and proxy data have shown that NA SSTs exhibit strong multidecadal variability, which is referred to as AMO. A North Atlantic basin-averaged SST index (NASST) is often used to discuss mechanisms of SST variability over the NA region (80°W to 0°E, 0–65°N). In order to emphasize the "multidecadal" character, the conventional AMO index is often defined as a 10-year running mean (or low-pass filtered) NASST with external forcing signal removed. Linear detrending method (Enfield et al. 2001) and other nonlinear detrending methods are used to remove global-scale externally forced signal, for example, removing global mean SST as a proxy (Trenberth and Shea 2006) or signal-to-noise ratio maximizing empirical orthogonal function (EOF) analysis (Ting et al. 2009).

Figure 1a shows the observed AMO index, defined as the basin average SST anomalies over the NA from the Hadley Centre Sea Ice and Sea Surface Temperature data set (Rayner et al. 2003). A nonlinear detrending method is used to remove the externally forced trend. The index shows pronounced multidecadal variability and the SST spatial pattern (Fig. 1b) is characterized by dipole pattern across Atlantic Ocean. The NA shows a "horseshoe" pattern, especially stronger in the subpolar region, whereas the South Atlantic exhibits weaker negative SST anomalies.

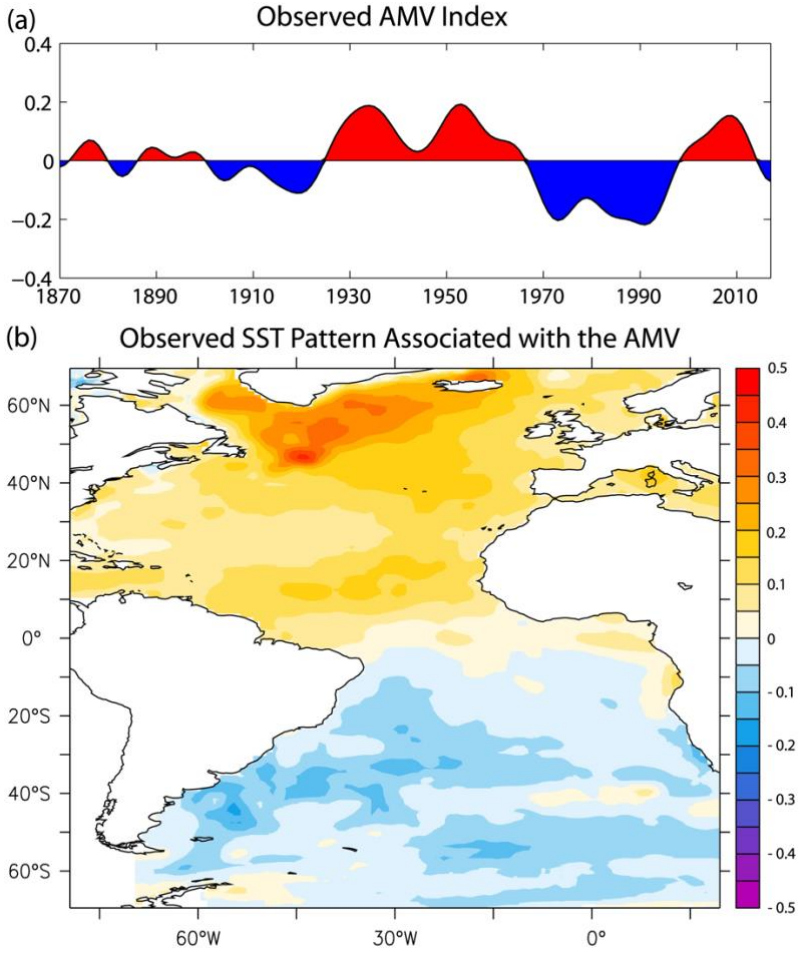

Fig. 1.1 Observed AMO index and SST spatial pattern associated with AMO derived from Hadley Centre Sea Ice and Sea Surface Temperature data set data set (Rayner et al., 2003). (a) Observed AMO index (K), defined as the 10-year low-pass-filtered area-weighted average of residual SST anomalies over the North Atlantic (80°W to 0°E, 0–65°N). The residual SST anomaly at each grid point is computed by removing the local component regressed on the global mean SST anomaly. This nonlinear detrending method for AMO has also been used in Gulev et al. (2013) and Frankignoul et al. (2017) to remove the nonuniform global scale signal, but it neglects the contribution of AMO to the global scale signal. (b) Observed SST pattern (K) associated with AMO, that is, regression of residual SST anomalies on the observed AMO index shown in (a). The regression corresponds to 1 standard deviation of the observed AMO index. Source: Zhang et al. 2019, Fig. 2.

Bjerknes (1964) pointed out that the driving mechanisms of NA SST differ on two different timescales: on long-term (multidecadal) timescales, ocean dynamics plays an active role; while on short-term (interannual) timescales, NA SST is driven by the atmosphere. Many following studies using observational data and climate models support Bjerknes' hypothesis (e.g., Hasselmann 1976; Cayan 1992; Delworth et al. 1993; Kushnir 1994; Delworth and Mann 2000; Latif et al., 2004; Gulev et al. 2013). On multidecadal timescales, the AMOC is

thought to play a primary role in SST variability via meridional oceanic heat transport, especially in the extratropical NA (Delworth et al. 2017). On the other hand, the tropical Atlantic SST exhibits pronounced short-term variability and different mechanisms have been proposed to explain the tropical Atlantic SST variability such as cloud feedback (Brown et al. 2016), atmospheric circulation, ITCZ shifts (Zhang and Delworth 2005; Robson et al. 2014), and thermodynamic coupled processes such as the wind–evaporation–SST feedback (Xie and Carton 2004).

The SST variability in the tropical and extratropical NA sectors is shown to be related to different driving factors. The NASST index may lump together SST variability originating from different mechanisms. In this thesis, by using observations and climate models, the relationships between the NA basin-averaged SST indices and some potential drivers are investigated. A statistic method, cross-spectral analysis is used which can provide information about the relationship of two time series in the frequency domain.

1.2 Ocean circulation and air-sea interactions in the North Atlantic

1.2.1 Ocean circulation in the NA

Ocean circulation plays an important role in redistributing the heat in the NA, which is important for the global climate system. In Atlantic Ocean, both meridional overturning circulation and horizontal circulation are important to the oceanic meridional heat transport (Dong and Sutton 2002). The horizonal circulation in the NA consists a cyclonic circulation over subpolar basin (subpolar gyre, SPG) and an anticyclonic circulation in the subtropic basin (subtropical gyre) (Rhein et al. 2011). On interannual timescales, the strength and variability of SPG is suggested to be related to surface wind stress (Curry et al. 1998; Böning et al. 2006). On decadal or longer timescales, the SPG is found to be linked to buoyancy fluxes related to the atmosphere (Eden and Jung 2001; Msadek and Frankignoul 2009).

The AMOC, which is defined as the zonally integrated volume flux, is characterized by a northward flow of warm water in the upper layer and a southward flow of cold water in the lower layer. On interannual timescales, both observational and modeling studies have shown that the AMOC is influenced by wind driven Ekman transport, the wind-stress curl variability and western boundary currents (McCarthy et al. 2012; Zhao and Johns 2014). On longer

timescales, the AMOC is linked to deep water formation in subpolar region associated with the local buoyancy forcing (Delworth et al. 1993).

Climate model studies suggest that the SPG has considerable impacts on the AMOC through deep water formation (Delworth et al. 1993; Lohmann et al. 2009; Born and Mignot 2012). Warm and salty tropical and subtropical water is transported to subpolar region through advection, which affects the production of the Labrador Sea Water (LSW), a major component of the North Atlantic Deep Water (NADW) and contributor to the lower limb of the AMOC.

In this thesis, the roles of the Atlantic Ocean circulation (meridional overturning circulation and horizontal circulation) and their interactions, in the multidecadal variability in the NA are studied by using a control integration of a fully coupled climate model, Kiel Climate Model (KCM; Park et al. 2009).

1.2.2 Potential drivers of AMOC variability

Many hypotheses have been put forward to explain the driving mechanisms of the AMOC variability. However, no consensus has been reached. They are briefly categorized into the following classes: 1) the thermal dynamic ocean response to stochastic atmospheric forcing, 2) a damped ocean mode with dynamical origins, 3) a fully coupled mode.

Hasselmann (1976) raised that ocean variability is the red-noise response to the integrated stochastic or white noise forcing of the atmosphere, As supported by later studies (e.g., Frankignoul et al. 1998; Delworth and Greatbach 2000; Dong and Sutton 2005; Mecking et al. 2014). For example, Delworth and Greatbach (2000) found that the low-frequency NA thermohaline circulation can be interpreted as a linear response to atmospheric surface flux. One leading atmospheric mode over NA is the North Atlantic Oscillation (NAO; Hurrell 1995). Several studies show that the ocean can response to wind stress immediately but response to the NAO-induced heat flux slowly (Bjerknes 1964; Eden and Willebrand 2001; Eden and Jung 2001). NAO can affect the convection in the Labrador Sea, thus influencing the AMOC (Dickson et al. 1996; Latif et al. 2006; Medhaug et al. 2012).

Some studies indicate the importance of oceanic dynamics and two-way air-sea interactions in the NA multidecadal variability. Eden and Greatbatch (2003) found that the decadal variability in the NA is driven by a combination of a delayed negative feedback due to

overturning circulation anomalies and a fast wind-driven positive feedback. This is done by using a realistic ocean model coupled with a simplified stochastic atmospheric model, in which oceanic processes played an active role. Additionally, air-sea interactions are also highlighted to play a critical role in the NA multidecadal variability (Timmermann et al. 1998; Sutton et al. 2018).

Furthermore, a number of studies show that the variability originates from internal ocean dynamics, without the role of atmosphere. For example, some studies suggest a mechanism involving anomalies from the east to the west of the NA basin via westward propagating baroclinic Rossby waves, which can lead interdecadal (20-30 years) AMOC variability (te Raa and Dijkstra 2002; Sévellec and Fedorov 2013).

The roles of the ocean circulation and air-sea interactions in the NA multidecadal variability are under debate. A three-way interaction between the SPG, the AMOC and the atmosphere, which operates in the KCM, has been found in this thesis, which according to my knowledge, has not been previously described. The interactions among the SPG, the AMOC and the atmosphere provide a better understanding about the nature of the multidecadal climate variability in the NA region.

1.3 Climate model bias

Instrumental datasets are not long enough to concretely investigate the causes and characteristics of the multidecadal climate variability in the NA. For example, instrumental SSTs with relatively good spatial coverage are only available for about 150 years, and other variables such as subsurface ocean temperatures and ocean-circulation parameters are even shorter. For example, observations of the AMOC only started in 2004 (Cunningham et al. 2007, Kanzow et al. 2007).

The limited observations are the reasons that control climate model integrations of multi-centennial to millennial timescales are heavily used to explore the nature of internal multidecadal variability in the Atlantic. However, most models exhibit pronounced SST cold biases in the NA (Drews and Greatbatch 2016; Flato et al. 2014; Wang et al. 2014). The cold SST bias may contaminate the origin of multidecadal NA SST variability, making it difficult to understand and predict climate dynamics in the NA. Therefore, it is important to eliminate the cold biases in climate model simulations. In this thesis, the results show that models

suffering from a large cold bias exhibit a relatively weak linkage between the AMOC and AMO and vice versa. Therefore, in this thesis, a freshwater-flux-corrected control integration of a fully coupled climate model, KCM, is used. Park et al. (2016) corrected sea surface salinity biases of the NA and the results of AMOC, gyre circulation and SST have been improved compared with a control run without employing the correction.

1.4 AMOC slowdown and North Atlantic warming hole

The change of the AMOC in observations is found to influence not only the climate in the NA, but also global climate processes, such as shifting rainfall pattern (Liu et al. 2020), salinity and temperature changes in the Southern Ocean (Stouffer et al. 2006; Zhu and Liu 2020). There is no consensus if the recently observed AMOC weakening (Smeed et al., 2014) is part of a long-term decline in response to anthropogenic global warming or within internal variability (Roberts et al. 2014; Jackson et al. 2016) due to the limited temporal coverage of observations. Direct ocean-circulation observations, e.g., the RAPID array (Rapid Climate Change-Meridional Overturning Circulation and Heatflux Array–Western Boundary Time Series) at 26.5°N (Cunningham et al. 2007), or moored observations of the Deep Western Boundary Current (DWBC) in the northwestern Atlantic (Toole et al. 2017), only cover the last one and a half decades. Some climate models have revealed that the AMOC will slow down if the anthropogenic greenhouse gases continue to rise unabatedly (Gregory et al. 2005; Stocker et al. 2013). On the other hand, some historical simulations with climate models suggest that sustained anthropogenic AMOC slowing is within the range of natural variability (Latif et al. 2019; Lobelle et al. 2020) and observation-based estimations suggest that the AMOC is stable on decadal timescales since the 1990s (Fu et al. 2020).

There is a conspicuous cooling in the subpolar NA SST in spite of large part of global surface ocean warming, which is referred to as the North Atlantic warming hole (Fig 1.2). Some recent studies indicate that the NA warming hole may be caused by the reduced northward oceanic heat transport as a consequence of AMOC slowing under global warning (Drijfhout et al. 2012; Gervais et al. 2018). The surface temperature in the subpolar NA is used in recent studies as a fingerprint of AMOC, which indicate a weakening of AMOC by about 3±1 Sv ($1Sv = 10^6 m^3/s$) since the mid-twentieth century (Rahmstorf et al. 2015; Caesar et al. 2018). However, there is a controversy about the cause of the warming hole. Some other studies indicate that the cooling can be explained by anthropogenic aerosol emissions (Booth et al.

2012; Keil et al. 2020). In addition, unforced AMOC variability could also drive the warming hole over subpolar NA region as control integrations of climate models without external forcing can produce long-term (multidecadal to multi-centennial) internal AMOC variability of similar strength (e.g., Delworth et al. 1993; Park and Latif 2008).

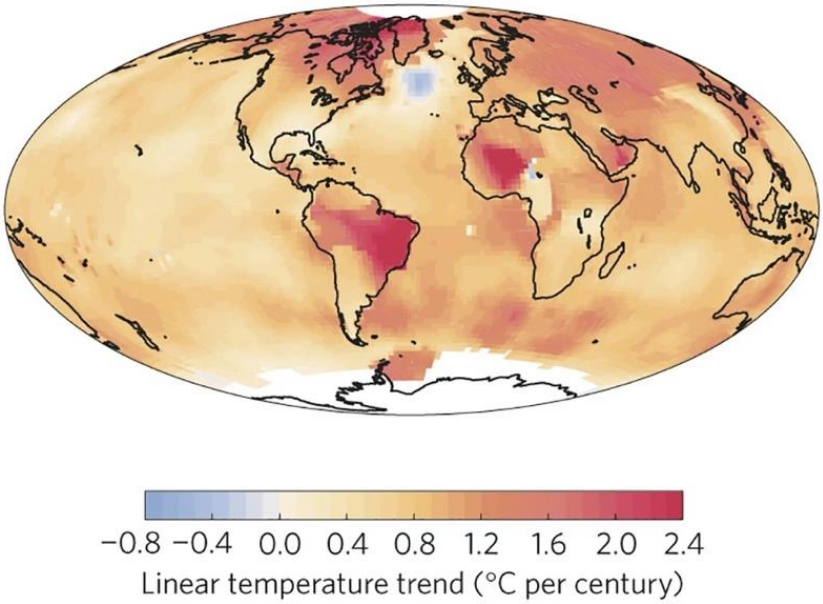

Fig 1.2 Linear trends of annual surface temperature since AD 1901. Based on the temperature data of NASA GISS (Hansen et al. 1999). Global equal area map (Hammer projection) for 1901–2013; white indicates insuffcient data. Source: Rahmstorf et al. 2015, Fig. 1a.

As to the debates about AMOC changes in response to global warming, in this thesis, a statistical method, Principal Oscillation Pattern, is conducted into the observational SST datasets. An ensemble mean of historical simulations of climate models is also analyzed. The results can help to understand the role of the natural internal AMOC variability in recent AMOC weakening and mechanisms of the SST cooling in NA warming hole in observations.

1.5 Thesis outline and scientific questions

Many quantities in the NA climate system have shown pronounced multidecadal variability in both climate models and observations, especially the SST and AMOC variability. The SST shows a basin-wide pattern and has wide-range influences on global climate. The

AMOC carries large amounts of heat and salt to high latitudes, strongly influencing the NA. The nature of the internal multidecadal variability over the NA and how SST and AMOC respond to global warming, however, are not well understood. This thesis attempts to understand: 1) different driving factors in tropical and extratropical regions of the NA SSTs, 2) the interactions between different climate variables over the NA, including surface pressure, winds, ocean circulation and SST on multidecadal timescales, 3) the mechanisms of the recent possible AMOC slowdown and cooling in the NA warming hole in observations. The following questions are discussed in the Chapters 3-5, which are reprints of two published papers, and one manuscript submitted. Each chapter includes an introduction, data and methodology, results, and discussion sections.

1. *What are the driving mechanisms of NA SST over different regions on different timescales in observations and climate models and how does climate model bias influence these results?*

2. *How do ocean circulation and atmosphere-ocean coupling influence the NA multidecadal variability and what is the role of stochastic atmospheric forcing?*

3. *Does AMOC slow in response to global warming? As an indirect indicator of AMOC in observation, what is the cause of the cooling of SST in NA warming hole?*

Chapter 2 will show the data and methods used in this thesis. Chapter 3 will investigate the different driving factors of NA SST by using climate models and observations. Chapter 4 addresses a coupled ocean-atmosphere multidecadal mode by analyzing a fully coupled climate model. It shows coexistence of a fast positive feedback and a slow negative feedback between SPG, AMOC and atmosphere over the subpolar NA. Multiple observed datasets since the beginning of the 20th century and results from a large ensemble of historical model simulations are used in Chapter 5. It investigates the recent debate about slowing of the AMOC and cooling in NA warming hole under global warming. Summary and discussions are given in Chapter 6.

Chapter 2 Data and methods

2.1 Data

Observational datasets

In this thesis, different observational datasets are used. Observed SSTs from Extended Reconstructed Sea Surface Temperature Version 5 (ERSST.v5, Huang et al. 2017) with 2° × 2° resolution and Kaplan Extended SST V2 (Kaplan et al. 1998) with 5° × 5° resolution are analyzed. Observed sea level pressures (SLPs) with 5° × 5° resolution are from Hadley Centre Sea Level Pressure dataset (HadSLP2r, Allan and Ansell 2006). The radiative forcing of four Representative Concentration Pathways (RCPs) scenarios is used (Van Vuuren et al. 2011). Climatology datasets are used for model comparison. The SST climatology is sourced from World Ocean Atlas 2018 (WOA18) with 1° × 1° resolution (Locarnini et al. 2018, https://www.nodc.noaa.gov/OC5/woa18/). Mixed Layer depth climatology with 2° × 2° resolution is based on a density threshold of 0.03 $kg \cdot m^{-3}$ (de Boyer Montégut et al. 2004). Annual sea level data is obtained from Copernicus https://cds.climate.copernicus.eu.

Climate models

A 3,000-years long, preindustrial control integration of a version of the KCM using a CO2-concentration of 286 ppm is analyzed in this thesis. A list of references of published studies employing different versions of the KCM, originally described in Park et al. (2009), can be obtained from https://www.geomar.de/kcms. This KCM version that is used here employs ECHAM5 (Roeckner et al. 2003) as atmospheric component, with a horizontal resolution of T42 (2.8° × 2.8°) and 19 vertical levels. The ocean-sea ice component is NEMO (Madec 2008) on a 2° Mercator mesh (ORCA2) horizontally and 31 vertical levels. The atmosphere model is coupled to the ocean-sea ice model via OASIS (Valcke et al. 2006). A surface freshwater-flux correction (FWC) is applied to the model over the NA (10°N–80°N), which not only largely eliminates upper-ocean salinity biases over that region but also considerably reduces the cold SST and upper-ocean temperature biases over the NA (Park et al. 2016).

Additionally, several preindustrial control integrations and historical integrations obtained from phase 5/6 of the Coupled Model Intercomparison Project (CMIP5/6; Taylor et al. 2012; Weyer et al. 2020) are used. The data from the CMIP5/6 models are linearly interpolated

onto 1° × 1° grids. The detailed descriptions about the CMIP5/6 models can be found in Chapter 3 and Chapter 5.

Climate indices

A number of climate indices are used in this thesis. The NAO index is based on the difference of normalized winter (December-March) SLP between Lisbon, Portugal and Stykkisholmur/Reykjavik, Iceland (Hurrell et al. 2013). This NAO index from 1865 to 2010 is retrieved from https://climatedataguide.ucar.edu/climate-data/hurrell-north-atlantic-oscillation-nao-index-station-based. The NASST index is defined here as the annual SST anomalies over the NA averaged over the region 0°–60°N, 75°–7.5°W. The same area average with low-pass filtering (11-yr running mean) applied, serves as the AMO index (Enfield et al. 2001). The Niño-3 index is defined as the SST anomalies averaged over 5°S–5°N and 150°–90°W (Rasmusson and Carpenter 1982). An AMOC index is defined as the maximum of the overturning streamfunction at 40° N (Zhang 2008). Finally, an SPG index is defined as the inverted area average of the barotropic streamfunction anomalies over the subpolar NA (50° N–58° N and 42° W–26°W), similar to a previous study (Lohmann et al. 2009).

2.2 Methods

The spatial pattern in this thesis is shown by linear regression coefficients of different variables on selected indices, where the indices have been normalized by their respective standard deviation σ. An F test is used to test the significance of the regression coefficients. The Student's t test and Monte Carlo simulation based on nonparametric random phase (Ebisuzaki 1997) are applied to test the significance of the correlation coefficients. Cross-spectral analysis is used to investigate the relationship between two time series in the frequency domain and this is shown in detail in Chapter 3. The power spectrum estimation is obtained by applying the Daniell window with length m to smooth 230 raw periodogram (Bloomfield 2004). The upper 90 % and 95 % confidence levels of the power spectra are calculated according to the Chi-squared distribution of the variance of the background noise.

Signal-to-noise maximizing EOF analysis

The global-scale external forcing signal in observations is estimated by using the signal-to-noise maximizing EOF (S/N EOF; Venzke et al. 1999) in Chapter 3. The S/N EOF method

assumes that the covariance matrix of the ensemble mean can be separated into two parts: the forced response and the internal climate variability. This method is described in detail in Chapter 3.

Principal Oscillation Pattern (POP) analysis

The Principal Oscillation Pattern (POP) analysis (Hasselmann 1988; von Storch et al. 1995) is a multivariate statistical technique designed to infer simultaneously the characteristic patterns and timescales of a vector time series. For practical purposes, the original process is usually reduced into the subspace of leading Empirical Orthogonal Function (EOFs, Lorenz 1956). POPs associated with real eigenvalues represent non-propagating, non-oscillatory patterns that decay exponentially. POPs associated with complex eigenvalues occur in complex conjugate pairs and can represent standing wave structures, propagating waves or, in general, an arbitrary amphidromic oscillation. POP analysis is shown in detail in Chapter 4 and Chapter 5.

Chapter 3 On the Interpretation of the North Atlantic Averaged Sea Surface Temperature

This chapter is a reprint of paper *"On the Interpretation of the North Atlantic Averaged Sea Surface Temperature"* published in Journal of Climate.

Citation: Jing Sun, Mojib Latif, Wonsun Park, and Taewook Park (2020). " On the Interpretation of the North Atlantic Averaged Sea Surface Temperature", *Journal of Climate*, 33(14): 6025-6045, https://doi.org/10.1175/JCLI-D-19-0158.1.

Jing Sun's contributions to this publication:

She did the analysis, produced all the figures. She wrote the first draft of the manuscript and revised the manuscript together with her co-authors.

On the Interpretation of the North Atlantic Averaged Sea Surface Temperature

JING SUN

GEOMAR Helmholtz Centre for Ocean Research Kiel, Kiel, Germany, and Ocean University of China, Qingdao, China

MOJIB LATIF

GEOMAR Helmholtz Centre for Ocean Research Kiel, and University of Kiel, Kiel, Germany

WONSUN PARK

GEOMAR Helmholtz Centre for Ocean Research Kiel, Kiel, Germany

TAEWOOK PARK

Korea Polar Research Institute, Incheon, South Korea

(Manuscript received 26 February 2019, in final form 18 April 2020)

ABSTRACT

The North Atlantic (NA) basin-averaged sea surface temperature (NASST) is often used as an index to study climate variability in the NA sector. However, there is still some debate on what drives it. Based on observations and climate models, an analysis of the different influences on the NASST index and its low-pass filtered version, the Atlantic multidecadal oscillation (AMO) index, is provided. In particular, the relationships of the two indices with some of its mechanistic drivers including the Atlantic meridional overturning circulation (AMOC) are investigated. In observations, the NASST index accounts for significant SST variability over the tropical and subpolar NA. The NASST index is shown to lump together SST variability originating from different mechanisms operating on different time scales. The AMO index emphasizes the subpolar SST variability. In the climate models, the SST-anomaly pattern associated with the NASST index is similar. The AMO index, however, only represents pronounced SST variability over the extratropical NA, and this variability is significantly linked to the AMOC. There is a sensitivity of this linkage to the cold NA SST bias observed in many climate models. Models suffering from a large cold bias exhibit a relatively weak linkage between the AMOC and AMO and vice versa. Finally, the basin-averaged SST in its unfiltered form, which has been used to question a strong influence of ocean dynamics on NA SST variability, mixes together multiple types of variability occurring on different time scales and therefore underemphasizes the role of ocean dynamics in the multidecadal variability of NA SSTs.

1. Introduction

The North Atlantic (NA) basin-averaged sea surface temperature (NASST) is often used to discuss mechanisms of SST variability over the NA region. An example is the Atlantic multidecadal oscillation or variability (AMO or AMV, AMO hereafter) index (Kerr 2000; Knight et al. 2005), which is characterized by multidecadal variations in NASST (e.g., Deser and Blackmon 1993; Kushnir 1994; Kilbourne et al. 2008). Climate variations over many regions have been linked to the AMO index. Examples are Northeast Brazilian and Sahel rainfall (Folland et al. 1986; Rowell et al. 1995), coastal climate around the NA (Enfield et al. 2001; Sutton and Hodson 2005), Atlantic hurricanes (Goldenberg et al. 2001), and Arctic sea ice (Day et al. 2012; Swart et al. 2015).

The mechanism of the AMO is not clear (Zhang et al. 2019). It is still under debate what the relative role is of processes such as stochastic atmospheric forcing, ocean dynamics, air–sea interactions, or external forcing (e.g., Latif and Keenlyside 2011; Ting et al. 2014; Bellomo et al. 2018). Moreover, in many studies the AMO is regarded as a physical mode with well-defined spatial pattern and period and unique mechanism, which is not justified on the basis of the current literature. Climate

Corresponding author: Jing Sun, jsun@geomar.de

DOI: 10.1175/JCLI-D-19-0158.1

models suggest that the low-frequency SST variability over the NA is partly related to the Atlantic meridional overturning circulation (AMOC) (e.g., Delworth et al. 1993; Timmermann et al. 1998; Delworth and Mann 2000; Latif et al. 2004; Knight et al. 2005; Msadek et al. 2013; McCarthy et al. 2015; Kim et al. 2018a,b). In these models, a strong AMOC is associated with an enhanced northward heat transport, which leads to anomalously warm NA SST and vice versa. Further, some previous work has shown that the AMOC can drive a monopolar SST anomaly pattern on multidecadal time scales that bears resemblance to the well-known AMO "horseshoe" SST pattern (e.g., Knight et al. 2005; Danabasoglu et al. 2012).

There are several methods of defining an AMO index from SST observations. The traditional definition is based on the area-weighted, linear detrended, and low-pass filtered NA-averaged (0°–60°N) SST anomalies (Enfield et al. 2001). The method of linear detrending cannot cleanly separate the internal multidecadal variability from the nonlinear externally forced global-scale signal including anthropogenic variability (Trenberth and Shea 2006; Frankcombe and England 2015). Besides linear detrending, other methods have been used to remove the global-scale externally forced signal, for example by using global mean SST as a proxy (Trenberth and Shea 2006; Mann and Emanuel 2006) or a signal-to-noise ratio maximizing empirical orthogonal function (EOF) analysis (Ting et al. 2009; Ruprich-Robert et al. 2017).

Some studies suggest that an SST-based AMO definition is insufficient to understand the mechanism of the AMO because it reflects multivariate low-frequency variability involving, for example, changes in salinity, ocean heat content, surface heat flux, subsurface temperature, and so on (e.g., Zhang 2007; Wang et al. 2010; Robson et al. 2012). A multivariate AMO index based on multivariate empirical orthogonal function (MEOF) analysis has been defined by Yan et al. (2019). Here we stick to the SST and study in detail SST-based indices defined over different regions and time scales with respect to their relationships to different phenomena such as the North Atlantic Oscillation (NAO) or El Niño–Southern Oscillation (ENSO), and linkages to ocean circulation. As SST is available for one and a half centuries, it can be used to study North Atlantic variability on time scales up to multidecadal.

In climate models, extratropical SST variability over the NA is often related to the AMOC on multidecadal time scales (Latif et al. 2004). Previous studies suggested that the relationship between AMOC and NA SST varies with latitude and time scale. At higher latitudes, the AMOC tends to lead the SST with a longer lead time than at lower latitudes (Zhang 2010; Wang and Zhang 2013). Several climate models studies have illustrated that the AMOC-induced heat transport cannot directly account for SST variability across the entire NA but influences SST mostly over the subpolar region on longer time scales (Zhang and Zhang 2015). Further, it has been suggested by several studies that multiyear to multidecadal SST variability over the subpolar NA is largely due to the delayed response of the oceanic wind-driven and meridional overturning circulation to the low-frequency portion of the NAO variability, which in turn drive changes in meridional heat transport (Eden and Willebrand 2001; Delworth et al. 2017).

With regard to tropical NA SST, some other mechanisms are needed to explain the variability such as cloud feedback (Brown et al. 2016; Yuan et al. 2016), local and large-scale wind changes (Carton et al. 1996; Kushnir et al. 2002; Hodson et al. 2014), changes in atmospheric circulation and intertropical convergence zone (ITCZ) shifts (Zhang and Delworth 2005; Robson et al. 2014), or thermodynamic coupled processes such as the wind–evaporation–SST (WES) feedback (Xie and Carton 2004; Amaya et al. 2017). Remote forcing by ENSO also accounts for a significant fraction of tropical NA SST variability (Enfield and Mayer 1997).

Recently, based on the simulations with atmosphere models coupled to slab-ocean models, some studies suggested that the AMO largely originates from stochastic forcing by the atmosphere (Clement et al. 2015; Cane et al. 2017), specifically the NAO. On the contrary, other recent studies suggested that stochastic atmospheric forcing alone cannot explain and ocean dynamics is crucial in generating NA SST multidecadal variability (O'Reilly et al. 2016; Zhang et al. 2016; Delworth et al. 2017; Zhang 2017; Garuba et al. 2018; Wills et al. 2019). Again other studies argue that the AMO is mostly driven by external forcing due to solar or atmospheric aerosol loading variability (Otterå et al. 2010; Booth et al. 2012). The role of aerosols in driving NA SST during the instrumental record, however, has been challenged by Zhang et al. (2013) by pointing out differences between the climate model simulation results of Booth et al. (2012) and the observations.

In this study we provide an interpretation of the annual basin-averaged NA SST, here referred to as NASST index, as well as of its low-pass filtered version, which serves as AMO index, and investigate the usefulness of the two indices in discussing origins of NA SST variability. We mainly address two questions. First, which processes contribute to the basin-averaged NA SST and on which time scale? Second, can the AMO, when defined by basin-averaged SST, be considered as a physical mode with well-defined spatial pattern and

period and unique mechanism? We study the influences of the NAO, AMOC, subpolar gyre (SPG), ENSO, and local and remote forcing on the SSTs over different regions of the NA. Most of these aspects have been studied previously and the results have been published in a number of complementary papers, as described above. Here, we investigate systematically how the different drivers are reflected in the NASST index and in the AMO index, two indices that are widely used in studies addressing climate variability over the NA sector and beyond.

We make use of observations and simulations with a number of climate models. Our focus is on internal variability and we therefore removed from the observations an estimate of the externally forced signal. Model data are from control runs without external forcing. We find that when calculated from instrumental SSTs, both the NASST index and the AMO index are composed of SST variability originating from different mechanisms operating on different time scales and therefore do not record a single mode of the climate system over the NA. In the climate models, there is a clear time scale separation such that the AMO index only describes SST variability over the extratropical NA, and this is significantly linked to the AMOC.

The paper is organized as follows: the data, climate models, and statistical methods used in this study are briefly described in section 2. Section 3 provides the results of our analysis pertaining to the SST variability over the NA. A summary and discussion of the major results are presented in section 4.

2. Material and methods

a. Data, climate models, and statistical methods

Observed SSTs during 1856–2010 with 2° × 2° resolution are from the Extended Reconstructed Sea Surface Temperature version 5 dataset (ERSST.v5, Huang et al. 2017). The NASST index is defined here as the annual SST anomalies over the NA averaged over the region 0°–60°N, 7.5°–75°W. The same area average with low-pass filtering (11-yr running mean) applied serves as the AMO index. We use the station-based NAO index from 1865 to 2010 (Hurrell et al. 2003; https://climatedataguide.ucar.edu/climate-data/hurrell-north-atlantic-oscillation-nao-index-station-based).

We analyze a multimillennial (3000 years long) preindustrial control integration of a version of the Kiel Climate Model (KCM; Park et al. 2009). A list of references of published studies employing different versions of the KCM can be obtained from https://www.geomar.de/en/research/fb1/fb1-me/research-topics/climate-modelling/kcms/. The KCM version used here employs ECHAM5 (Roeckner et al. 2003) as the atmospheric component, with a horizontal resolution of T42 (2.8° × 2.8°) and 19 vertical levels. The ocean–sea ice component is NEMO (Madec 2008) on a 2° Mercator mesh (ORCA2) horizontally, with increased meridional resolution of 0.5° near the equator and 31 vertical levels. The atmosphere model is coupled to the ocean–sea ice model via OASIS (Valcke et al. 2006). A surface freshwater-flux correction is applied over the NA, which not only largely eliminates upper-ocean salinity biases over that region but also considerably reduces the cold NA SST bias that is common to many climate models (Park et al. 2016).

TABLE 1. The 14 CMIP5 preindustrial control simulations used in this study. Start and end times are given as YYYYMM.

CMIP5 ID	Start time	End time
ACCESS1.0	030001	079912
ACCESS1.3	025001	074912
CanESM2	201501	301012
CCSM4	080001	130012
CESM1-BGC	010101	060012
CNRM-CM5	185001	269912
FGOALS-s2	185001	235012
GISS-E2-R	398101	453012
INM-CM4	185001	234912
MPI-ESM-LR	185001	284912
MPI-ESM-MR	185001	284912
MPI-ESM-P	185001	300512
MRI-CGCM3	185101	235012
NorESM1-M	070001	120012

Additionally, we analyze 14 preindustrial control integrations (model length varies from 500 to 1156 years; Table 1) obtained from phase 5 of the Coupled Model Intercomparison Project (CMIP5; Taylor et al. 2012). These climate models are chosen because they provide SST, sea level pressure (SLP), barotropic streamfunction, and meridional overturning streamfunction, the four variables used in the analysis below. The data from the CMIP5 models are linearly interpolated onto a 1° × 1° grid.

In the climate models, the NAO index is defined as the time series (PC) of the leading EOF of SLP anomalies over the North Atlantic region. The observed station-based NAO index is selected because it is longer than the PC-based NAO index, but the two indices are highly correlated. The Niño-3 index is used to assess the influence of the eastern equatorial Pacific SST on NA SST. It is defined as the SST anomalies averaged over 5°S–5°N and 90°–150°W. The SST climatology is from the NODC (Levitus) *World Ocean Atlas 2018* (Locarnini et al. 2018; https://www.nodc.noaa.gov/OC5/woa18/). We use annual-mean data. All data are linearly detrended prior to the analyses except for the observed SST, which is used after subtracting an estimate of the

global-scale external forcing signal. The detailed description of this method is given in section 2b. An AMOC index is obtained from the climate models and defined as the maximum of the overturning streamfunction in the Atlantic at 40°N. Most of the overturning streamfunction indices from the CMIP5 models are taken at this latitude.

We calculate patterns of linear regression coefficients of SST on the indices described above, where the indices have been normalized by their respective standard deviation σ. Pattern correlation is the Pearson product-moment coefficient (Pearson 1895) of linear correlation between two variables. An F test is used to test the significance of the regression coefficients. The Student's t test and Monte Carlo simulation based on nonparametric random phase (Ebisuzaki 1997) are applied to test the significance of the correlation coefficients. Cross-spectral analysis is used to investigate the relationship between two time series. The method provides information about the relationship of two time series in the frequency domain. The cross spectrum is defined as the Fourier transform of the cross-covariance function. The cross spectrum can be decomposed into its real part (cospectrum) and its imaginary part (quadrature spectrum) from which the coherence and phase spectra are obtained. To avoid ambiguity, the squared coherence is used. The limiting value for the squared coherence for a given α (e.g., $\alpha = 0.05$ corresponds to a confidence level of 95%) is given by

$$\kappa^2_{(1-\alpha)} = 1 - \alpha^{[2/(\mathrm{DoF}-2)]}. \tag{1}$$

DoF is the number of degrees of freedom determined by the choice of the smoothing window (Thompson 1979). We use the Hamming window and set the window length to 150 samples with an overlap of 80 samples (preindustrial control runs) and to 40 samples with overlap of 20 samples (observations) (e.g., von Storch and Zwiers 2001). Welch's method of overlapped averaged periodogram was applied (Welch 1967).

b. *Signal-to-noise maximizing EOF analysis*

We follow the method of Ting et al. (2009) that is based on historical runs with climate models to remove the global-scale external forcing signal from the SST. We chose 33 CMIP5 historical simulations (only one realization of each model) from 1850 to 2010 and the corresponding preindustrial control integrations (Table 2). In this method, a signal-to-noise maximizing EOF (S/N EOF) analysis is applied to the global SSTs to estimate the externally forced SST variability. We note that the CMIP5 historical runs are only used in this study to remove the external forcing trend and are not used in the subsequent analysis.

The S/N EOF method assumes that the covariance matrix of K number multimodel ensemble mean ($\mathbf{X}_M$) can be separated into two parts: one is the forced response ($\mathbf{X}_F$) and the other the internal climate variability in the kth ensemble integration ($\mathbf{X}^k_N$) or atmospheric noise:

$$\mathbf{X}_M = \mathbf{X}_F + \frac{1}{K}\sum_{k=1}^{K} \mathbf{X}^k_N. \tag{2}$$

If we apply a standard EOF method to the ensemble mean, the covariance matrix of the ensemble mean $\mathbf{C}_M$ consists of the covariance of the forced response $\mathbf{C}_F$ and that of the noise $\mathbf{C}_N$:

$$\mathbf{C}_M = \mathbf{C}_F + \frac{\mathbf{C}_N}{K}. \tag{3}$$

The standard EOF methodology is not well suited to separate the forced response from the noise. Therefore, the prewhitening procedure is applied to reduce the noise contamination in the ensemble mean. This procedure involves a transformation of the covariance matrix. That is, the covariance matrix is diagonalized:

$$\mathbf{F}^{\mathrm{T}}\mathbf{C}_N\mathbf{F} = K\mathbf{I}, \tag{4}$$

where $\mathbf{F}$ is the prewhitening operator and $\mathbf{I}$ is the identity matrix. If prewhitening is applied, the eigenvectors of the prewhitened $\mathbf{C}_M$ will be identical to those of the prewhitened $\mathbf{C}_F$. The noise covariance matrix $\mathbf{C}_N$ is estimated from the preindustrial control runs which, by definition, only yield the internal variability of the system. We then perform the singular value decomposition (SVD) of $\mathbf{C}_N$:

$$\mathbf{C}_N = \mathbf{E}_N\mathbf{\Lambda}_N\mathbf{P}^{\mathrm{T}}_N, \tag{5}$$

where $\mathbf{E}_N$ represents the eigenvectors matrix of $\mathbf{C}_N$ and $\mathbf{\Lambda}_N$ is the diagonal matrix of the square root of the corresponding eigenvalues. The prewhitening of the ensemble mean can be expressed as

$$\mathbf{X}'_M = \mathbf{F}^{\mathrm{T}}\mathbf{X}_M = \sqrt{K}\mathbf{\Lambda}^{-1}_N\mathbf{E}^{\mathrm{T}}_N\mathbf{X}_M. \tag{6}$$

Then an EOF analysis is performed on the transformed data matrix $\mathbf{X}'_M$. It can be shown that the leading EOF has the maximum signal-to-noise ratio and the first PC represents the time evolution of the most dominant forced response (Venzke et al. 1999). The PC1 (Fig. 1a) is taken as the time series of the forced SST response and the internal (unforced) components of the SST indices obtained by subtracting the PC1.

TABLE 2. The 33 CMIP5 historical (HIS) and preindustrial control (PI) simulations (with original resolution) used in the signal-to-noise maximizing EOF analysis. Start and end times are given as YYYYMM.

CMIP5 ID	HIS start time	HIS end time	PI start time	PI end time	Atmosphere resolution	Ocean resolution
ACCESS1.0	185001	200512	030001	079912	1.25° × 1.875°	0.3°–1° × 1°
ACCESS1.3	185001	200512	025001	074912	1.25° × 1.875°	0.3°–1° × 1°
BCC-CSM1.1	185001	201012	000101	050012	2.8° × 2.8°	0.3°–1° × 1°
BCC-CSM1.1-m	185001	201012	000101	040012	2.8° × 2.8°	0.3°–1° × 1°
CanESM2	185001	200512	201501	301012	2.8° × 2.8°	0.9° × 1.4°
CCSM4	185001	200512	080001	130012	0.94° × 1.25°	0.27–0.5° × 1.1°
CESM1-BGC	185001	200512	010101	060012	0.94° × 1.25°	0.3°–1° × 1°
CESM1-CAM5	185001	200512	000101	031912	0.94° × 1.25°	0.3°–1° × 1°
CESM1-FASTCHEM	185001	200512	007001	029112	0.94° × 1.25°	0.3°–1° × 1°
CESM1-WACCM	185001	200512	009601	029512	1.9° × 2.5°	0.3°–1° × 1°
CMCC-CESM	185001	200512	432401	449312	3.4° × 3.75°	0.5°–2° × 2°
CMCC-CM	185001	200512	155001	187912	0.75° × 0.75°	0.5°–2° × 2°
CMCC-CMS	185001	200512	368401	418312	3.71° × 3.75°	0.5°–2° × 2°
CNRM-CM5	185001	200512	185001	269912	1.4° × 1.4°	0.3°–1° × 1°
CNRM-CM5.2	185001	200512	185001	225912	1.4° × 1.4°	1.3° × 1.9°
GFDL CM3	186001	200512	000101	080012	2° × 2.5°	0.3°–1° × 1°
GFDL-ESM2G	186101	200512	000101	050012	2° × 2.5°	0.375–0.5° × 1°
GISS-E2-H	185001	200512	241001	294912	2° × 2.5°	0.3°–1° × 1°
GISS-E2-H-CC	185001	201012	208101	233112	2° × 2.5°	0.3°–1° × 1°
GISS-E2-R	185001	200512	398101	453012	2° × 2.5°	1° × 1.25°
GISS-E2-R-CC	185001	201012	205001	230012	2° × 2.5°	1° × 1.25°
HadGEM2-CC	185901	200512	185912	209912	1.25° × 1.875°	0.3°–1° × 1°
HadGEM2-ES	185901	200512	185912	243605	1.25° × 1.875°	0.3°–1° × 1°
INM-CM4	185001	200512	185001	234912	1.5° × 2°	0.5° × 1°
IPSL-CM5A-LR	185001	200512	180001	279912	1.9° × 3.75°	2° × 2°
IPSL-CM5B-LR	185001	200512	183001	212912	1.9° × 3.75°	2° × 2°
MIROC5	185001	201012	200001	266912	1.4° × 1.4°	0.5–1.4° × 1.4°
MPI-ESM-LR	185001	200512	185001	284912	1.87° × 1.875°	1.5° × 1.5°
MPI-ESM-MR	185001	200512	185001	284912	1.87° × 1.875°	0.4° × 0.4°
MPI-ESM-P	185001	200512	185001	300512	1.87° × 1.875°	1.5° × 1.5°
MRI-CGCM3	185001	200512	185101	235012	1.12° × 1.125°	0.5° × 1°
NorESM1-M	185001	200512	070001	120012	1.9° × 2.5°	1° × 1.1°
NorESM1-ME	185001	200512	090101	115212	1.9° × 2.5°	0.5° × 1°

3. Results

a. SST indices

The external forcing component of the NASST index, as calculated by using the S/N EOF method, is shown in Fig. 1a. We note that the forced signal calculated by applying the S/N EOF method is rather different from a linear trend and exhibits a strong increase after 1980. Figures 1b–d depict some of the indices that are used in the subsequent regression analyses. The NAO index, NASST index, and AMO index calculated from observations are shown in Fig. 1b. The NAO indexes obtained from both observations and the climate models are inverted and the regression analyses are performed with these inverted indices. We depict from the KCM the NASST index, AMO index, NAO index (Fig. 1c), and AMOC index (Fig. 1d). The indices from the preindustrial control integration of the KCM are shown for the model years 2075–2235, which are chosen since this period has the highest covariance with the observed AMO index. The KCM's AMOC index exhibits pronounced multidecadal variability that is consistent with that in the KCM's AMO index.

b. Regression patterns

Figure 2 depicts the spatial SST-anomaly patterns derived from observations and the climate models, which are obtained by regressing the SSTs onto the standardized indices. The explained variances are given by the contours. The map of local SST regression coefficients on the NASST index (Fig. 1b) derived from observations (Fig. 2a) depicts the well-known basinwide positive SST anomalies over the NA, with maxima in the subpolar and tropical NA and a pronounced minimum between the two maxima in the western half of the basin. The SST-anomaly pattern derived from regression onto the AMO index, which by definition largely reflects the low-frequency SST variability, is similar but emphasizes more the subpolar anomalies (Fig. 2b). Explained

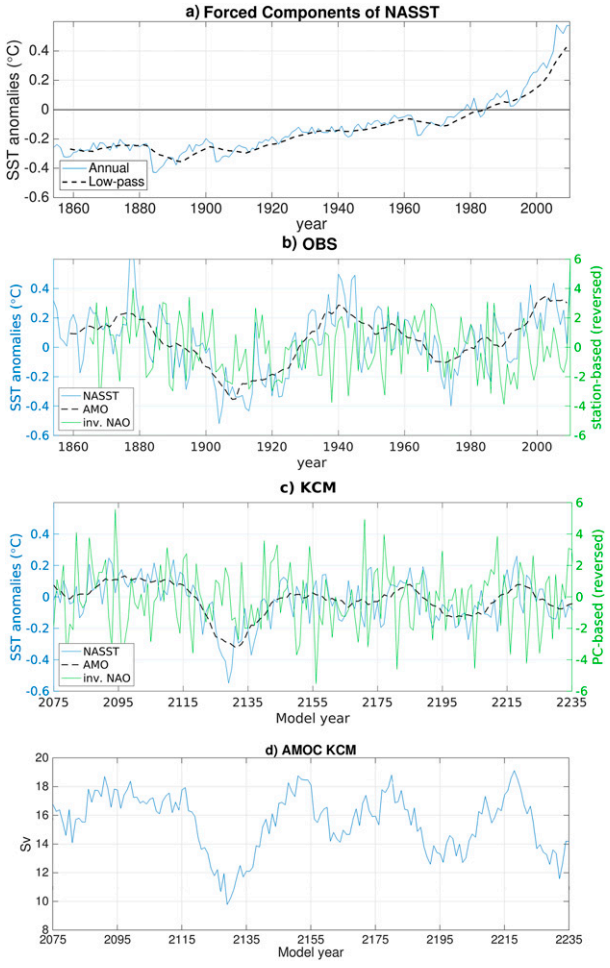

FIG. 1. (a) The externally forced component of the observed NA SST variability estimated by the S/N EOF. The blue curve indicates the forced component of observed NASST index (annual) and the black dashed curve indicates the forced component of observed AMO index (low-pass). (b) Observed indices. The blue curve indicates the NASST index 1854–2010, the black dashed curve indicates the AMO index 1859–2005, and the green curve indicates the station-based NAO index 1865–2010 (sign-reversed). (c) 160 years (model years 2075–2235, during which the covariance with the observed AMO index is maximum from the 3000-yr-long preindustrial control integration of the KCM). The blue curve indicates the NASST index, the black dashed curve indicates the AMO index, and the green curve indicates the PC-based NAO index (sign-reversed). (d) Same time span as in (c), but for the AMOC index in the KCM. The NASST index is defined as the annual SST anomalies over the NA averaged over the region 0°–60°N, 7.5°–75°W and the AMO index as the low-pass filtered (applying an 11-yr running mean) NASST index. The AMOC index is defined as the maximum of the overturning streamfunction in the Atlantic at 40°N. The NAO index in observations is defined as the difference of normalized SLP between Lisbon and Reykjavik. The NAO index in the KCM is defined as the first PC of SLP in the NA.

variances in the regression map associated with the NASST index (Fig. 2a) are larger over the tropical NA than over the subpolar NA. The explained variances over the tropical NA are considerably smaller in the regression map associated with the AMO index with a maximum of 0.2 as compared to 0.5 in the NASST-SST regression map. This is consistent with Zhang (2017) reporting that the low-frequency SST anomalies associated with the AMO are most pronounced in the subpolar NA region while the high-frequency NA SST varies primarily in the tropical NA, adding noise to the basin-averaged index definition (Wills et al. 2019). The AMO index explains slightly less variance in SST over the subpolar NA (Fig. 2b) than the NASST index (Fig. 2a), and the regressions are slightly smaller with the exception of the Labrador Sea, where they are larger.

The regression patterns associated with the observed NASST index and the observed AMO index share some similarities with the tripolar SST-regression pattern associated with the inverted NAO index (Fig. 2c): there are two maxima, one in the subpolar and the other in the subtropical NA, and a minimum between them. However, the minimum in the regression pattern associated with the NAO index is much more pronounced being negative. The pattern correlation between the NASST index–related (Fig. 2a) and the NAOindex related SST-regression pattern (Fig. 2c) amounts to 0.71, suggesting the NASST index–related pattern is significantly influenced by SST variability that is directly related to the NAO. The relationship between the NAO and NA SST on interannual time scales is known to be local in nature and largely originating from the action of the NAO-related surface heat fluxes (Frankignoul 1985; Cayan 1992). Anomalous Ekman transport also contributes to the generation of SST anomalies over the NA (Marshall et al. 2001). The pattern correlation between the regression patterns associated with the AMO index (Fig. 2b) and the NAO index (Fig. 2c) only amounts to 0.34, indicating that the AMO index–related pattern is less influenced by the NAO than the NASST index–related pattern and the ocean dynamics may be needed to explain the AMO index–related pattern.

The SST-regression pattern associated with the NASST index calculated from the preindustrial control integration of the KCM (Fig. 2d) captures the general spatial structure derived from the observations (Fig. 2a), but the KCM's SST anomalies are smaller over the tropical NA. In the observations, the explained variances in the NASST index–related pattern are larger over the tropical NA than over the subpolar NA, which also is the case in the KCM (Fig. 2d) and in the CMIP5 models' ensemble mean (see below; Fig. 2h). We note that the explained variance in most of the CMIP5 models exceeds 0.4 over limited regions of the tropical

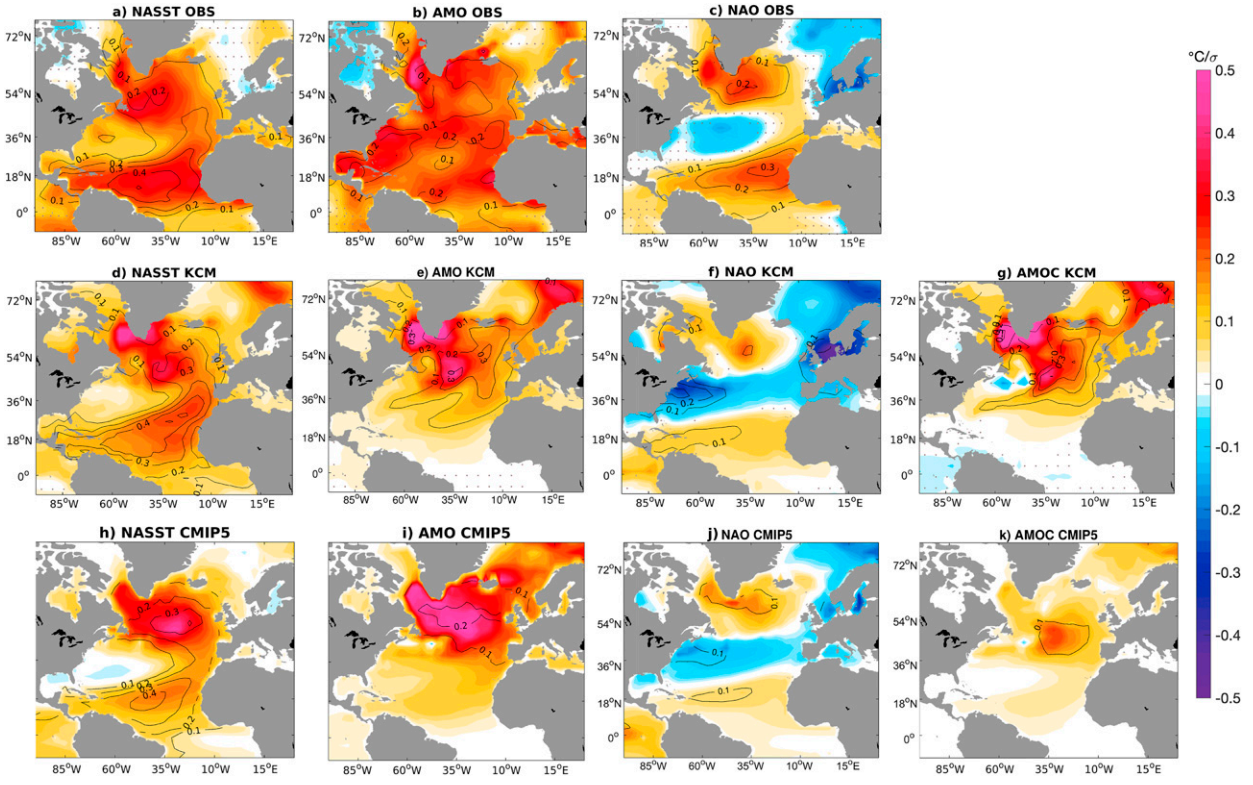

FIG. 2. (a) SST-anomaly pattern derived from regression onto the annual NASST index 1854–2010 in ERSST v5. (b) SST-anomaly pattern derived from regression onto the AMO index (low-pass filtered NASST index; see text for definition) during 1859–2005 in ERSST v5. (c) SST-anomaly pattern (sign-reversed) derived from regression onto the annual NAO index in 1865–2010. (d) As in (a), but for the regression coefficients calculated from the KCM. (e) As in (b), but for the regression coefficients calculated from the KCM. (f) As in (c), but for the regression coefficients calculated from KCM (sign-reversed). (g) SST-anomaly pattern derived from regression onto the annual AMOC index calculated from the KCM. (h) As in (a), but for the ensemble mean of regression coefficients calculated from 14 CMIP5 preindustrial control simulations. (i) As in (b), but for the ensemble mean of regression coefficients calculated from 14 CMIP5 preindustrial control simulations. (j) As in (c), but for the ensemble mean of regression coefficients calculated from 14 CMIP5 preindustrial control simulations (sign-reversed). (k) As in (g), but for the ensemble mean of regression coefficients calculated from 14 CMIP5 preindustrial control simulations. Note that the ensemble means from the CMIP5 models are calculated by averaging the regressions and explained variances from the individual models. Color shading indicates regressions; contours explaine variance. Dots means the regression is not significant at the 95% level, and the dots do not show in the CMIP5 ensemble mean. The regression coefficients correspond to a 1σ change of the corresponding indices.

NA and can be up to 0.6 (not shown). The explained variance exceeds 0.2 over the subpolar NA in most of the CMIP5 models with values up to 0.4 in limited regions (not shown), indicating a robustness of the pattern across the CMIP5 models. When calculating the SST regression on the KCM's AMO index (Fig. 2e), tropical NA SST anomalies are largely absent south of about 30°N. The ensemble-mean SST-regression pattern associated with the AMO index calculated from the 14 preindustrial control integrations of the CMIP5 models (Fig. 2i) is similar to that derived from the KCM in structure and magnitude. Most importantly, there are no signals over the tropical NA and significant SST anomalies with explained variances exceeding 10% are restricted to the mid- and high-latitude NA. Although the explained variances may become smaller when a multimodel ensemble average is calculated, they are only slightly smaller relative to those in the KCM, indicating a robustness of the AMO index-related pattern across the CMIP5 model ensemble. We note that there are large differences among the individual regression patterns associated with the AMO index across the CMIP5 model ensemble, but all patterns derived from the individual models exhibit relatively small SST anomalies over the tropical NA (not shown).

The regression pattern of the SST on the NAO index derived from the KCM (Fig. 2f) is consistent with that calculated from observations (Fig. 2c) featuring the tripolar SST-anomaly pattern. Compared with observations, the explained variances are smaller over the subpolar and tropical NA and larger over the midlatitude NA. The CMIP5 ensemble-mean NAO–SST

regression map (Fig. 2j) is characterized by similar regression coefficients and explained variances compared to those from the KCM. Overall, we conclude from both the observations and the climate models that the NASST index–related SST-anomaly pattern is strongly influenced by the NAO, whereas the AMO index–related pattern is less influenced by the NAO and only well developed over the extratropical NA. This suggests that the ocean dynamics play an important role in the AMO.

We next investigate the role of the AMOC in the NA SST variability. Figure 2g shows the SST regressions on the AMOC index calculated from the KCM. The AMOC-related SST regression pattern exhibits large positive SST anomalies over the mid- and high-latitude NA, especially over the subpolar region, but hardly any anomalies over the tropical NA. Such a structure is also observed in the ensemble-mean AMOC-related SST regression pattern derived from the CMIP5 models, but the regression coefficients and explained variances are relatively small (Fig. 2k) in comparison to the KCM. Previous studies show that the NA SST variability is not robust and varies considerably between climate models. For example, some of the CMIP5 models exhibit the largest explained variances with values of up to 0.4 over the eastern NA (not shown) whereas the ensemble-mean explained variances are on the order of 0.1 (Fig. 2k). One reason for the model differences could be the cold NA SST bias observed in the vast majority of the CMIP5 models that varies among the models (Ba et al. 2014; Keenlyside et al. 2016; Zhang and Wang 2013), which will be investigated below. Although the regression patterns in the individual CMIP5 models differ from each other considerably (not shown), the ensemble-mean AMOC-related SST-anomaly pattern supports the KCM's result that the AMOC only influences the extratropical NA SST.

In the KCM, the AMO index–related SST-regression pattern (Fig. 2e) is similar to the AMOC index–related SST-regression pattern (Fig. 2g), suggesting a major influence of the AMOC on the AMO. The temporal correlation between the AMO index and the annual AMOC index amounts to 0.70 at zero lag and to 0.75 when the AMOC index leads by two years. In comparison to the AMOC index–related pattern, the SST anomalies associated with the AMO index–related pattern extend farther south straddling the equatorial NA. In the CMIP5 models, the similarity between the AMO index–related and AMOC index–related SST-regression patterns is not as striking as in the KCM, but the CMIP5 models (Figs. 2i,k) agree with the KCM in that the largest regressions are seen over the extratropical NA and that the SST anomalies associated with the AMO index extend farther south. This suggests that the AMO index is composed of variability that additionally to the influence of the AMOC reflects tropical NA SST variability that is not related to the AMOC.

c. *Time scale separation of North Atlantic SST variability*

From the above regression analysis, we find that both the tropical and extratropical NA SST can be influenced by different factors. To identify these factors and their contributions over different parts of NA, another two SST indices are calculated: an extratropical NA SST index (E-NASST index hereafter) defined as the area-averaged SST over 40°–60°N, 7.5°–75°W and a tropical NA SST index (T-NASST index hereafter) defined as the area-averaged SST over 0°–20°N, 7.5°–75°W. Cross-spectral analysis is performed between the NASST index and T-NASST index and between the NASST index and E-NASST index (Fig. 3). In the observations, the NASST index is highly coherent with the T-NASST index on basically all time scales but with smaller squared coherence at periods longer than decadal (Fig. 3a). The squared coherence spectrum calculated between the NASST index and the E-NASST index fluctuates considerably with time scale (Fig. 3b), with peaks on interannual, decadal, and multidecadal time scale, and pronounced minima in between. We note the increase of the squared coherence toward longer periods in Fig. 3b.

In contrast to the observations, the climate models yield a clear time scale separation. In the KCM (Figs. 3c,d), the NASST index and the T-NASST index exhibit the highest squared coherence at the interannual to decadal time scale. The NASST index and the E-NASST index exhibit the largest squared coherence at the multidecadal time scale. We note that the NASST index and the T-NASST index are almost in phase at interannual time scales. At multidecadal time scales, the NASST index slightly lags the E-NASST index. We depict the power spectra of the three KCM indices in Fig. 4. The spectrum of the NASST index (Fig. 4a) exhibits increasing power toward longer time scales and features a peak at periods of about 30–50 years. In contrast, the spectrum of the T-NASST index exhibits largest power on short time scales and is basically flat on decadal and longer time scales (Fig. 4b). The spectrum of the E-NASST index (Fig. 4c) is steeper than that of the NASST index and also exhibits the multidecadal peak. Thus, among the three indices it is the E-NASST index that most robustly records multidecadal SST variability.

Recent studies suggest that SST anomalies in the midlatitudes can propagate into the tropics through cloud feedback (Brown et al. 2016; Yuan et al. 2016).

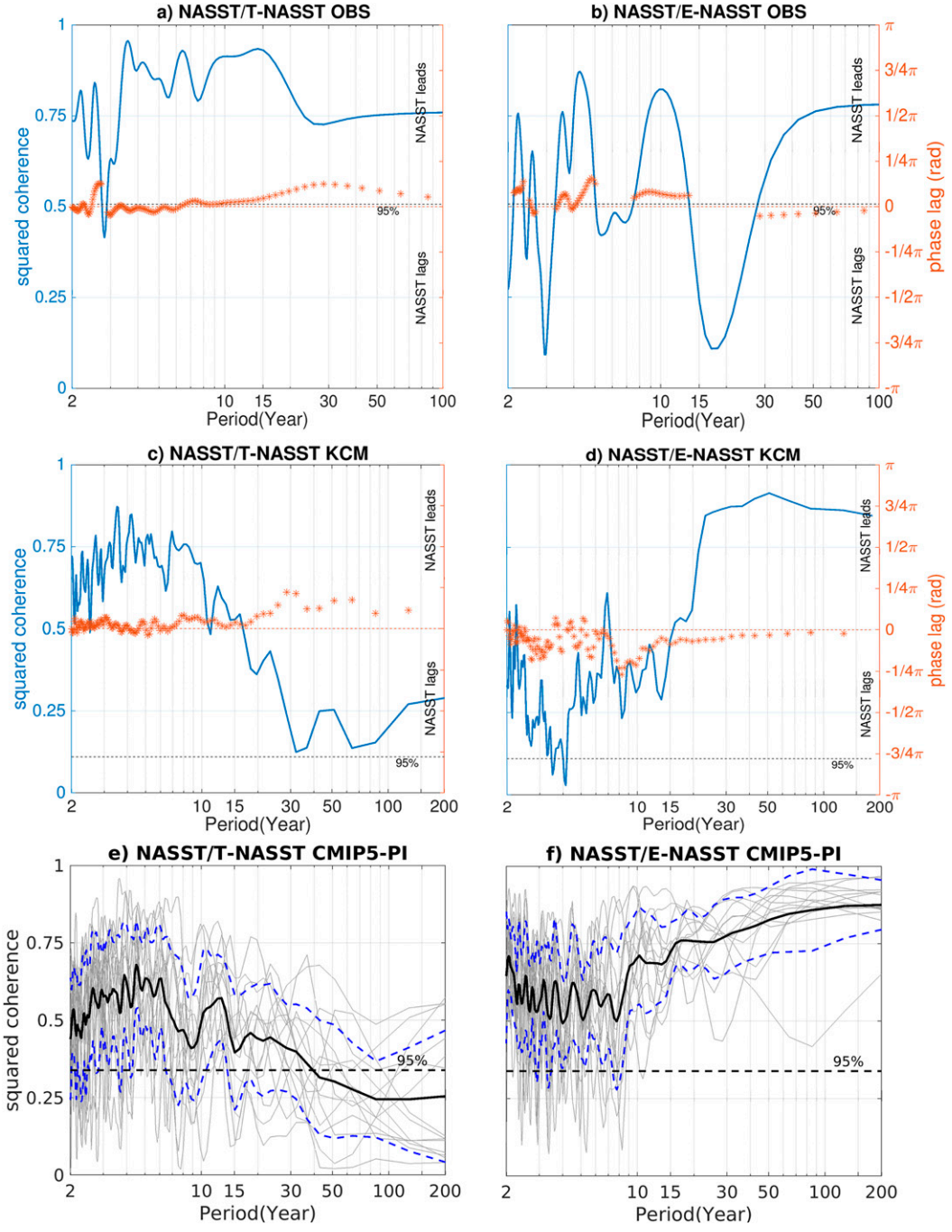

FIG. 3. Cross-spectral analysis between the NASST index and the SST indices, T-TASST (0°–20°N, 7.5°–75°W) and E-NASST (40°–60°N, 7.5°–75°W). Annual data are used. (a) Squared coherence (blue) and phase spectra (orange stars) between the NASST index and T-NASST index calculated from observations 1854–2010. (b) As in (a), but with the E-NASST index. (c),(d) As in (a) and (b), but for the KCM. The phase only is shown when the squared coherence exceeds the 95% confidence level (black dotted line). A phase lag of zero indicates that the two time series are in phase (orange dotted line) while a positive (negative) phase lag indicates that the NASST index leads (lags). (e) Squared coherence (gray lines) between NASST index and T-NASST index in the 14 CMIP5 preindustrial control runs; the thick black line indicates the ensemble mean of the squared coherence. (f) As in (e), but with the E-NASST index. Blue dashed curves indicate one standard deviation of the squared coherence across CMIP5 models. Black dashed curves indicate the ensemble mean 95% confidence level of the square coherence.

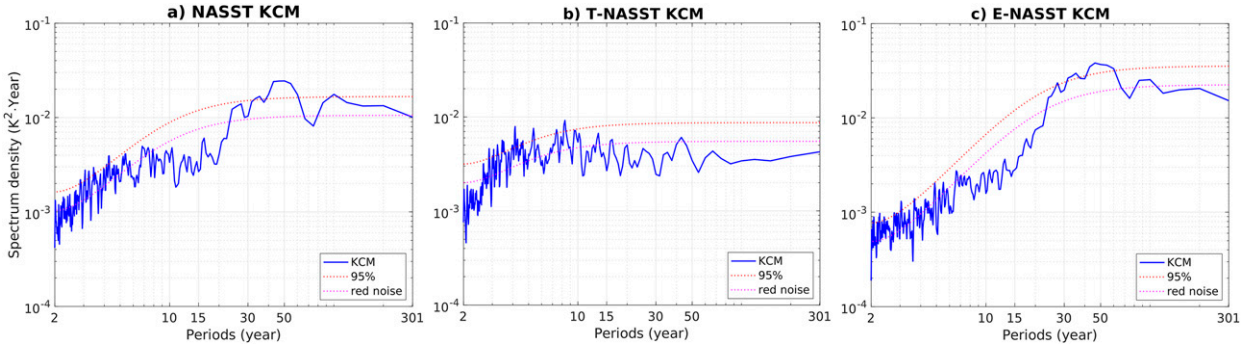

FIG. 4. (a) The power spectrum of NASST index (0°–60°N, 7.5°–75°W) in the KCM. The power spectrum is shown in the blue curve, the dashed pink curve represents the theoretical red noise spectrum, and the dashed red curve represents the 95% confidence level. Both the *x* axis and *y* axis use logarithmic scales, and the *x* axis shows the period in years. (b) As in (a), but for T-TASST (0°–20°N, 7.5°–75°W). (c) As in (a), but for E-NASST (40°–60°N, 7.5°–75°W).

We performed cross-spectral analysis between the T-NASST index and the E-NASST index (not shown). In both observations and in the KCM, the E-NASST index leads the T-NASST index by about $(1/2)\pi$ at interannual to decadal time scales but the squared coherence is far below the 95% confidence level. This suggests that the southward propagation of the SST anomalies is not a main factor contributing to the NA SST variability.

The ensemble-mean squared coherence between the NASST index, the T-NASST index, and the E-NASST index derived from the preindustrial control runs with the CMIP5 models (Figs. 3e,f) is similar to that obtained from the KCM. To visualize the ensemble spread, one standard deviation of the squared coherence and an averaged 95% confidence level (note that the length of the chosen model simulations varies) are also shown. Thus, there is a clear time scale separation in both the KCM and the CMIP5 models: the NASST index only is highly coherent with the T-NASST index on the interannual time scale. On the other hand, the NASST index only exhibits significant squared coherence with the E-NASST index on the multidecadal time scale. In conclusion, in the models the SST variability over the NA associated with the NASST index can be separated roughly into two components: a tropical component governed by interannual variability and an extratropical component governed by multidecadal variability. These results are consistent with Fig. 2 where the multidecadal NA SST variability, as expressed by the AMO index, mainly exists in the extratropical NA.

d. AMOC influence on NA SST variability

To further investigate the AMOC influence on NA SST, cross-spectral analysis is conducted between the AMOC index and the T-NASST index and between the AMOC index and the E-NASST index (Fig. 5). Since AMOC observations are limited, we only use model data in this analysis. The results obtained the KCM (Figs. 5a,b) yield a very clear picture: the T-NASST index is unrelated to the AMOC index at all time scales, while the E-NASST index is highly coherent with the AMOC index on multidecadal time scale with the AMOC index consistently leading. The KCM's results are supported by the ensemble-mean coherence spectrum derived from the preindustrial control runs with the CMIP5 models (Figs. 5c,d). Although model spread is large, the ensemble-mean squared coherence between the AMOC index and the E-NASST index is relatively high at the multidecadal time scale. Thus, the multidecadal extratropical NA SST variability in the models has a strong link to the AMOC.

e. Influence of model bias

As noted above, the relationship between AMOC and NA SST varies among the CMIP5 models. In many models, the displacement of the North Atlantic Current in the CMIP5 models results in a cold SST bias over the extratropical NA (Drews and Greatbatch 2016, 2017). To investigate the influence of the cold SST bias on the relationship between AMOC and NA SST in the CMIP5 models, we choose the three models (CanESM2, CESM1-BGC, and CNRM-CM5) exhibiting the largest SST bias over the extratropical NA (Fig. 6a), and the three models (FGOALS-s2, GISS-E2-R, and MPI-ESM-MR) exhibiting the smallest SST bias over that region (Fig. 6b). Clearly, the models with the smallest SST bias show high squared coherence at the multidecadal time scale (Fig. 6c). On the other hand, the models with the largest SST bias disagree more among each other, lack high squared coherence at the multidecadal time scale, and mostly show high squared coherence on the centennial time scale (Fig. 6d). As mentioned above, we use here a freshwater-flux

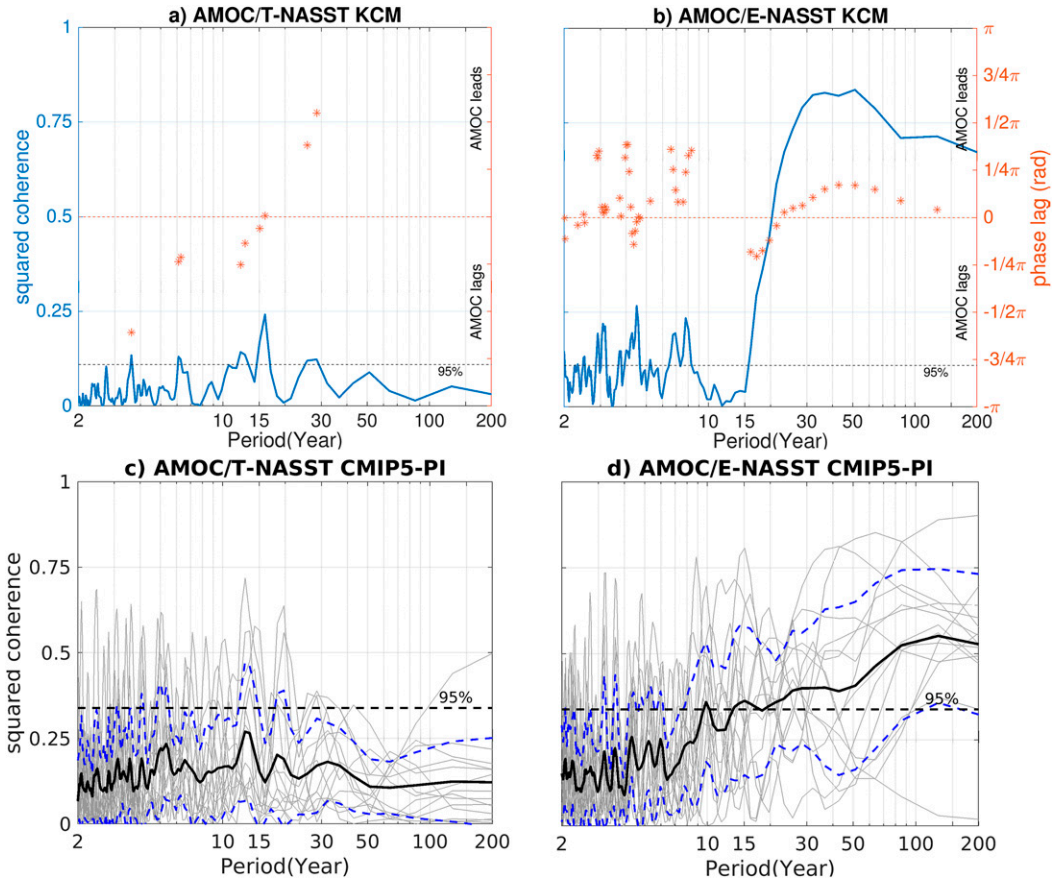

FIG. 5. Cross-spectral analysis between the AMOC index and the SST indices, T-TASST (0°–20°N, 7.5°–75°W) and E-NASST (40°–60°N, 7.5°–75°W). Annual data are used. (a) Squared coherence (blue) and phase spectra (orange stars) between the AMOC index and T-NASST index in the KCM. (b) As in (a), but with the E-NASST index. The phase only is shown when the squared coherence exceeds the 95% confidence level (black dotted line). A phase lag of zero indicates that the two time series are in phase (orange dotted line) while a positive (negative) phase lag indicates that the AMOC index leads (lags). (c),(d) As in (a) and (b), but for 14 CMIP5 preindustrial control runs. Blue dashed curves indicate one standard deviation of the squared coherence across CMIP5 models. Black dashed curves indicate the ensemble mean 95% level of the square coherence.

corrected KCM version with much reduced cold SST bias over the extratropical NA relative to the standard version. The corrected KCM version exhibits high squared coherence between the AMOC index and the E-NASST index at multidecadal time scale, as shown above (Fig. 5b), which is consistent with the three CMIP5 models exhibiting the smallest cold SST bias (Fig. 6c).

f. Lagged NA SST response to NAO variability

The NAO is another important factor that contributes to the NA SST variability. According to the discussion around Fig. 2, the NAO can induce a tripolar SST-anomaly pattern via anomalous surface heat fluxes. Cross-spectral analysis between the NAO index and the SST indices, T-NASST and E-NASST, is performed (Fig. 7). It should be mentioned that the NAO index used in the two cross-spectral analyses has not been inverted, because we wish to show the influence of the positive NAO phase on the NA SST variability. The results obtained from the observations and the climate models differ considerably. Considering the NAO index and the T-NASST index, we find in observations an enhanced squared coherence and an out-of-phase relationship at the biennial period (Fig. 7a). Additionally, there is a pronounced peak of the squared coherence between the NAO index and the T-NASST index with an out-of-phase relationship at a period of 15 years (Fig. 7a). Neither in the KCM (Fig. 7c) nor in the CMIP5 models (in the ensemble mean; Fig. 7e) is such a decadal peak found. We note that in the KCM's preindustrial control run the spectrum of the NAO index is consistent with white noise (not shown).

We next consider the relationship between the NAO index and the E-NASST index (Figs. 7b,d,f). Previous

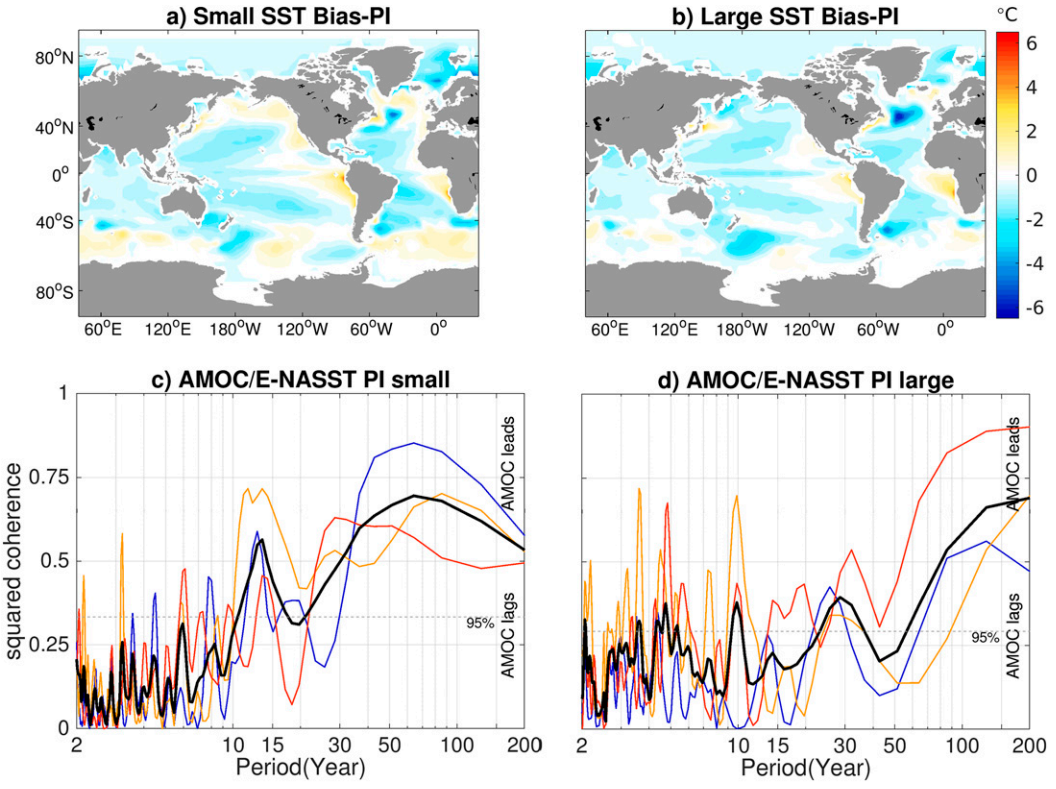

FIG. 6. Ensemble-mean long-term annual SST bias relative to Levitus climatology calculated from a selection of preindustrial control simulations with CMIP5 models: (a) mean SST bias from the three CMIP5 models (FGOALS-s2, GISS-E2-R, and MPI-ESM-MR) exhibiting the smallest SST bias over the North Atlantic and (b) mean SST bias from the three CMIP5 models (CanESM2, CESM1-BGC, and CNRM-CM5) exhibiting the largest SST bias over the North Atlantic. (c) Squared coherence between the AMOC index and the E-NASST index in the CMIP5 models with the smallest SST bias (colored lines) and the ensemble mean of these models (thick black line). A mean 95% confidence level is shown as the gray dashed line. (d) As in (c), but for the CMIP5 models with the largest SST bias. The phase is not shown in (c) and (d).

work by Eden and Willebrand (2001) suggested a two–time scale response of the NA ocean circulation to NAO variability that could influence SST over the extratropical NA: a fast barotropic response due to anomalous Ekman transport (intraseasonal time scale) and a delayed baroclinic response (time scale of 6–8 years) due to enhanced meridional overturning and a spinup of the subpolar gyre. The slow response is somewhat suggested by the observations, as the NAO index leads the E-NASST index at the multidecadal time scale (not shown), but the instrumental record is short and squared coherence at the multidecadal time scale, though enhanced, does not exceed the 95% confidence level (Fig. 7b). The fast response is not resolved by annual mean data.

The slow response is clearly simulated by the KCM, as suggested by the high squared coherence between the NAO index and the E-NASST index (Fig. 7d) as well as the high squared coherence between the AMOC index and the E-NASST index (Fig. 5b). In the KCM, the NAO index leads the E-NASST index by about $(1/4)\pi$, amounting to about 6–8 years. This time lag is consistent with that derived from the ocean model simulations in Eden and Willebrand (2001). Due to the large spread, the ensemble-mean squared coherences derived from the CMIP5 models (Fig. 7f) are insignificant at all time scales.

We conclude from the above analysis that the SST-anomaly pattern associated with the North Atlantic basin-averaged SST index (NASST index), which is based on annual data, lumps together tropical and extratropical SST variability although the two are related to different mechanisms. Climate models suggest that the extratropical part of the SST-anomaly pattern associated with the NASST index is linked to multidecadal AMOC variability. On the other hand, the models suggest that the tropical part is governed by interannual SST variability that is unrelated to the AMOC. The AMO index, defined as the low-pass filtered NASST index, only tracks extratropical NA SST variability in the climate models, although the

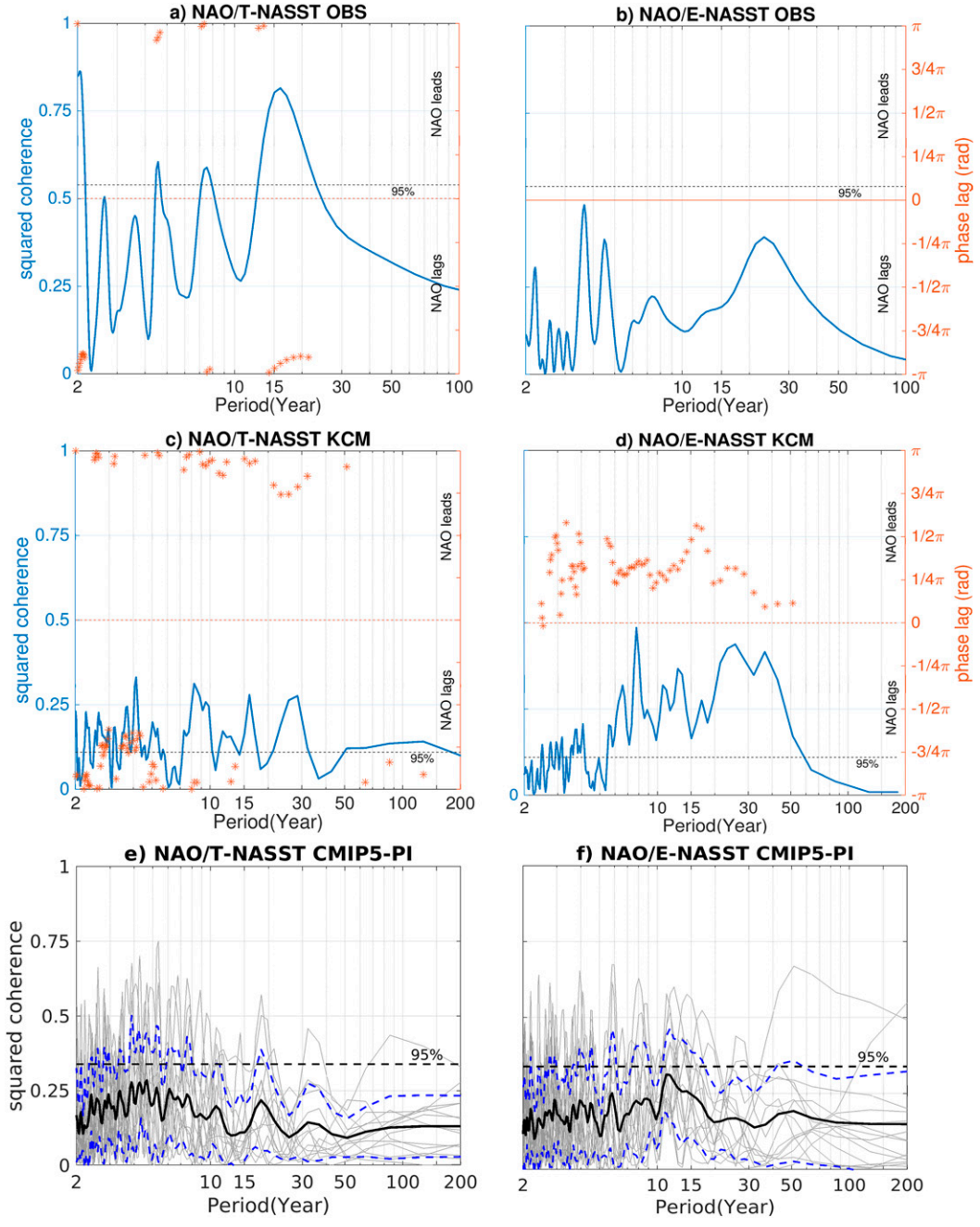

FIG. 7. Cross-spectral analysis between the NAO index and the SST indices, T-NASST (0°–20°N, 7.5°–75°W) and E-NASST (40°–60°N, 7.5°–75°W). Annual data are used. (a) Squared coherence (blue) and phase spectra (orange stars) between the NAO index and T-NASST index calculated from observations 1865–2010. (b) As in (a), but with the E-NASST index. (c),(d) As in (a) and (b), but for the KCM. The phase only is shown when the squared coherence exceeds the 95% confidence level (black dotted line). A phase lag of zero indicates that the two time series are in phase (orange dotted line) while a positive (negative) phase lag indicates that the NAO index leads (lags). (e),(f) Squared coherence (gray lines) between NAO index and T-NASST index in the 14 CMIP5 preindustrial control runs; the thick black line indicates the ensemble mean of the squared coherences. Blue dashed curves indicate one standard deviation of the squared coherence across CMIP5 models. Black dashed curves indicate the ensemble mean 95% confidence level of the square coherence.

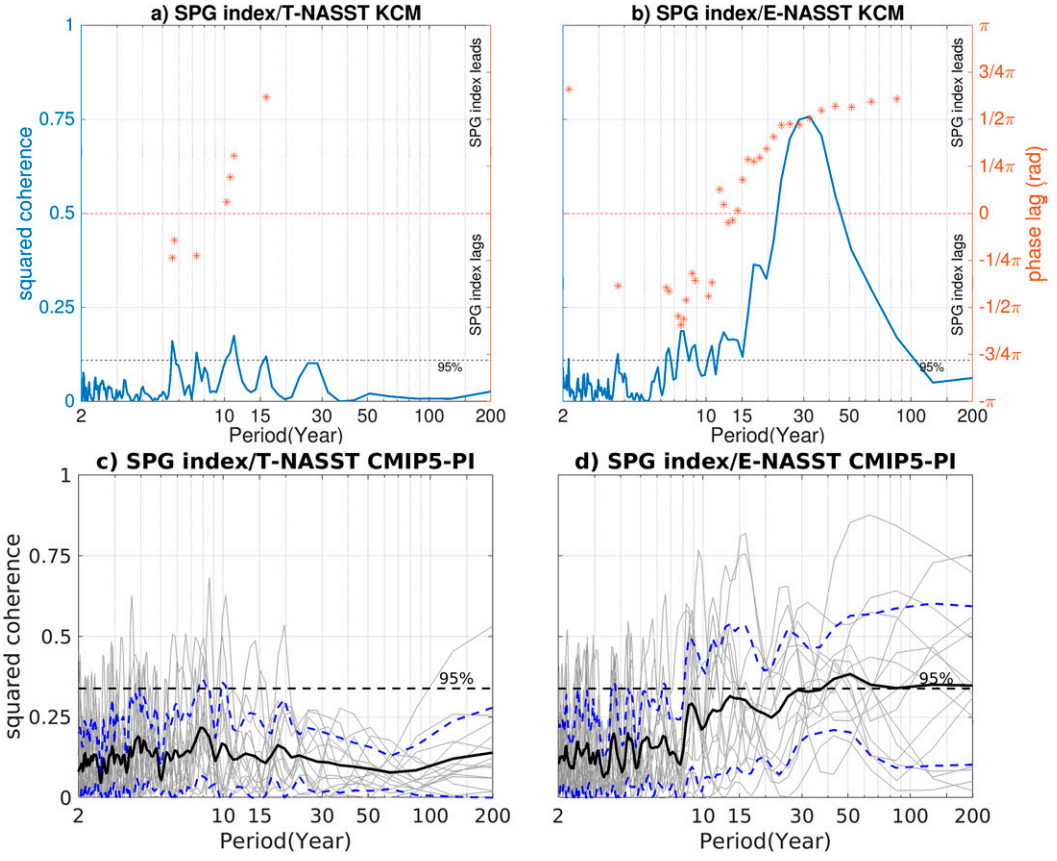

FIG. 8. Cross-spectral analysis between the SPG index and the SST indices, T-TASST (0°–20°N, 7.5°–75°W) and E-NASST (40°–60°N, 7.5°–75°W). Annual data are used. (a) Squared coherence (blue) and phase spectra (orange stars) between the SPG index and T-NASST index in the KCM. (b) As in (a), but with the E-NASST index. The phase only is shown when the squared coherence exceeds the 95% confidence level (black dotted line). A phase lag of zero indicates that the two time series are in phase (orange dotted line) while a positive (negative) phase lag indicates that the SPG index leads (lags). (c),(d) As in (a) and(b), but for 14 CMIP5 preindustrial control runs. Blue dashed curves indicate one standard deviation of the squared coherence across CMIP5 models. Black dashed curves indicate the ensemble mean 95% confidence level of the square coherence.

extratropical NA area is small in comparison to the full NA area over which the AMO index is defined. In the climate models, the SST variability associated with the AMO index is clearly linked to the AMOC. This link is very clear in the KCM. The CMIP5 models considerably differ among each other, which could be due to varying model biases over the NA (Fig. 6), but the ensemble-mean results also point toward the picture suggested by the KCM. The overturning observations at 26°N only starting in 2004 are too limited to draw robust conclusions about the connection between the AMO and the AMOC.

g. *SPG influence on NA SST*

Eden and Willebrand (2001) suggested that the delayed ocean circulation response to the NAO variability not only is related to the AMOC but also could be caused by an adjustment of the subpolar gyre. To investigate the importance of the subpolar gyre for the NA SST variability we compute from the climate models a subpolar gyre index (SPG index) defined as the inverted area average of the barotropic streamfunction over the region 50°–58°N, 26°–42°W. The SPG index calculated in this way is highly correlated with the PC1 of EOF1 calculated from the barotropic streamfunction over the same region, with a correlation coefficient of up to 0.92. The cross-spectral analysis results between the SPG index and the SST indices, T-NASST and E-NASST, are shown in Fig. 8. In the KCM, the T-NASST index is not strongly linked to the SPG index on any time scale (Fig. 8a), which is consistent with the CMIP5 preindustrial control runs (Fig. 8c). The E-NASST index, on the other hand, exhibits highly significant squared coherence with the SPG index in the KCM on the

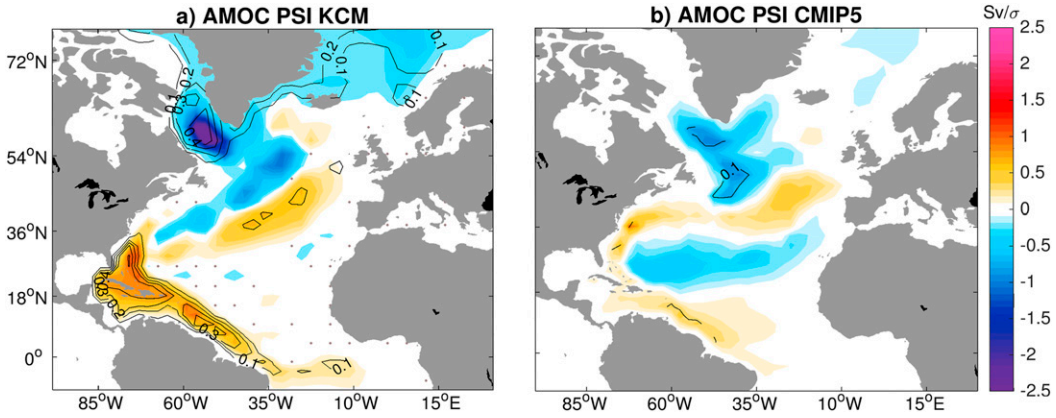

FIG. 9. (a) Barotropic streamfunction (PSI) anomalies pattern derived from regression onto the annual AMOC index calculated from the KCM. (b) As in (a), but calculated by the ensemble mean of 14 CMIP5 preindustrial control simulations. Note that the ensemble mean from the CMIP5 models is calculated by averaging the regressions and explained variances from the individual models. Color shading indicates regressions; contours explain variance. Dots mean the regression is not significant at 95% confidence level, and the dots do not show in the CMIP5 ensemble mean. The regression coefficients correspond to a 1σ change of the corresponding indices.

multidecadal time scale, with the SPG index leading by several years (Fig. 8b). The CMIP5 models somewhat support this result, as expressed by the enhanced ensemble-mean squared coherence between the E-NASST index and the SPG index at multidecadal time scale (Fig. 8d), but the ensemble-mean squared coherence is not as large as in the KCM. We note that in the KCM (Fig. 9a) and also on average in the CMIP5 models (Fig. 9b), a stronger AMOC is associated with an enhanced subpolar gyre. This is demonstrated by the regressions of the barotropic streamfunction (PSI) on the AMOC index. The strengthened subpolar gyre will enhance the northward heat transport into the extratropical NA, which leads to warmer SSTs over the subpolar NA and at least partly explains the relationship between the SPG index and the E-NASST index observed in the models (Figs. 8b,d).

h. Tropical Pacific influence on NA SST variability

Previous studies have shown that the tropical Atlantic SST variability is strongly related to local trade wind changes (e.g., Carton et al. 1996; Kushnir et al. 2002) and the wind–evaporation–SST (WES) feedback (Xie and Philander 1994). This picture is supported by the local correlation coefficients between SST and surface wind speed anomalies calculated from the KCM. The correlations between the two quantities over the tropical NA are relatively large and typically amount to about −0.6 in the region 15°–30°N (not shown). Besides the locally generated surface wind variability, ENSO has been shown to exert robust remote impacts on the SST over the tropical NA (Enfield and Mayer 1997). To study the ENSO influence on NA SST, we use the Niño-3 index and perform cross-spectral analysis with the T-NASST index and the E-NASST index. Figures 10a and 10b show the results derived from the observations. ENSO is highly coherent with T-NASST at interannual time scales, with ENSO leading (Fig. 10a). We note the large peak around a period of 15 years that also is seen in the coherence spectrum computed from the NAO index and the T-NASST index (Fig. 7a). The peak at interannual time scales (Fig. 10a) can also be found in the KCM (Fig. 10c) and in the ensemble-mean coherence spectrum calculated from the CMIP5 models (Fig. 10e).

The relationship between the Niño-3 index and the E-NASST index differs between the observations and the climate models. In the observations, there is statistically significant squared coherence at interannual time scales. This is the case neither in the coherence spectrum calculated from the KCM (Fig. 10d) nor in the ensemble-mean coherence spectrum calculated from the CMIP5 models (Fig. 10f). We conclude that the remote forcing by ENSO is an important component of tropical NA SST variability. It remains unclear to which extent ENSO also drives extratropical NA SST variability. The observations suggest some influence, which, however, is not supported by the climate models investigated in this study.

4. Summary and discussion

In this study, observations and climate model simulations are analyzed to aid interpretation of the North Atlantic averaged sea surface temperature (NASST). We investigate two indices: an annual index, termed the NASST index, and a low-pass filtered index that serves

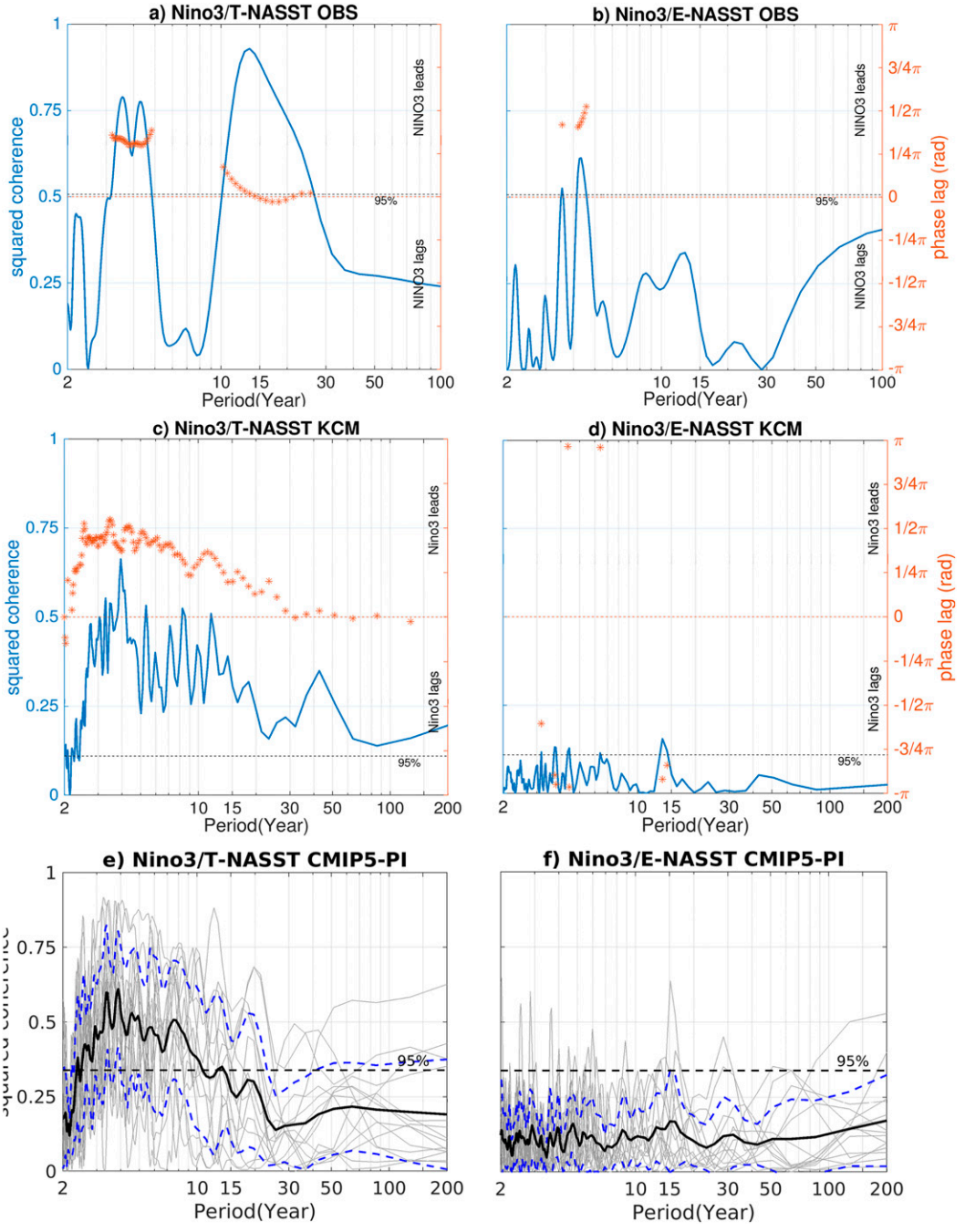

FIG. 10. Cross-spectral analysis between the Niño-3 index and the SST indices, T-TASST (0°–20°N, 7.5°–75°W) and E-NASST (40°–60°N, 7.5°–75°W). Annual data are used. (a) Squared coherence (blue) and phase spectra (orange stars) between the NASST index and T-NASST index calculated from observations 1854–2010. (b) As in (a), but with the E-NASST index. (c),(d) As in (a) and (b), but for the KCM. The phase only is shown when the squared coherence exceeds the 95% confidence level (black dotted line). A phase lag of zero indicates that the two time series are in phase (orange dotted line) while a positive (negative) phase lag indicates that the Niño-3 index leads (lags). (e) Squared coherence (gray lines) between the Niño-3 and T-NASST index in the 14 CMIP5 pre-industrial control runs; the thick black line indicates the ensemble mean of the squared coherence. (f) As in (e), but with the E-NASST index. Blue dashed curves indicate one standard deviation of the squared coherence across CMIP5 models. Black dashed curves indicate the mean 95% confidence level of the square coherence.

as the AMO index. The SST-anomaly pattern associated with the observed AMO index is similar to the pattern associated with the observed NASST index but highlights the extratropical SST variability. Moreover, in observations, the NASST index-related pattern is significantly influenced by SST variability that is directly related to the NAO, whereas the AMO index-related pattern is much less influenced by the NAO. In observations there is some weak evidence for the NAO leading the extratropical NA SST at the multidecadal time scale, suggesting a delayed ocean circulation influence on NA SST.

By using cross-spectral analysis, we argue that the two basin-averaged NA SST indices, the NASST index and the AMO index, are not appropriate to address the mechanisms of NA SST variability because relevant mechanisms operate on different time scales and over different regions of the NA. We thus conclude that neither NASST nor AMO constitutes a physical mode with a well-defined pattern and period and unique mechanism. Since observations are limited and to obtain further insight into the origin of NA SST variability, heavy use was made of data from preindustrial control integrations of the Kiel Climate Model (KCM) and of models participating in phase 5 of the Coupled Model Intercomparison Project (CMIP5). In the models, consistent with observations, the NASST index, is shown to be composed of SST variability originating from different factors: the NAO, AMOC, SPG, and ENSO. The SST variability associated with the AMOC is restricted to the mid- and high-latitude NA and the multidecadal time scale, consistent with previous studies using different climate models (Delworth and Zeng 2016; Delworth et al. 2016; Zhang 2017; Wills et al. 2019). In line with this result, the AMO-related SST-anomaly pattern is similar to the AMOC-related SST-anomaly pattern in the models.

It is known from observations that the NAO plays an important role in North Atlantic SST variability on different time scales, especially on intraseasonal to interannual time scales. In the KCM, we also find a clear link of the extratropical NA SST to the NAO at the multidecadal time scale. The connection between the NAO and the extratropical NA SST in the KCM is through the SPG and the AMOC. The spread among the CMIP5 models is so large that in the ensemble mean, there is only a weak connection between the NAO and the extratropical NA SST at any time scale. In the KCM as well as in the CMIP5 models, SPG and AMOC variability is significantly linked at the multidecadal time scale. An SPG influence on extratropical NA SST on intermediate time scale has been previously suggested in several studies (e.g., Curry and McCartney 2001; Eden and Jung 2001; Sun et al. 2015; Reintges et al. 2016; Nigam et al. 2018; Martin et al. 2019; Wills et al. 2019) and there is some weak evidence for the link in the climate models investigated in this study.

One limitation is the lack of sufficiently long instrumental observations, which inhibits, for example, investigating the influence of the AMOC on NA SST at time scales longer than interannual. Moreover, the SST observations are not long enough to estimate robust statistics and links of the NASST and AMO indices to the SST in different regions of the NA. For this reason, we are heavily relying on climate models that are known to suffer from large SST biases over the NA (e.g., Zhang and Zhao 2015). In particular, most CMIP5 models exhibit a large cold SST bias of several degrees Celsius over the northwest corner region of the NA. We show that the cold bias has a major influence on the origin of multidecadal NA SST variability. CMIP5 models with a small bias exhibit a robust link between the AMOC and extratropical NA SST at the multidecadal time scale, while the relationship is less robust in the models exhibiting a large cold bias.

The cold bias problem is the major reason why we made extensive use of a freshwater flux-corrected version of the KCM that exhibits relatively little SST bias over the tropical and extratropical NA. The corrected KCM simulates enhanced ocean dynamics in the NA in comparison to the uncorrected version exhibiting large SST biases (Park et al. 2016), such as more realistic SPG and deep convection sites. Consistent with the CMIP5 models, the corrected KCM simulates a pronounced link between AMOC and extratropical NA SST on multidecadal time scales, while this link is much weaker in the uncorrected KCM (not shown). One implication of this result could be that relative to the real world, the AMOC influence on extratropical NA SST is strongly underestimated in models exhibiting a large cold SST bias, which would have relevance to decadal predictability of extratropical NA SST and related quantities. By using very large ensembles, Smith et al. (2019) show that decadal climate is more predictable over the NA sector than previously thought. They discuss the signal-to-noise paradox meaning that a climate model can predict the real world better than itself despite being an imperfect representation of the real world and a perfect representation of itself. We hypothesize that the skill of decadal predictions may be maintained at a similar level as in Smith et al. (2019), but with a smaller ensemble size if SST bias over the NA is reduced. We also note that the CMIP5 models exhibit a large spread with respect to the origin of NA SST variability.

One final implication of our study concerns the ongoing debate about the role of ocean dynamics in driving

multidecadal climate variability over the NA sector. One aspect of this debate is around the SST-anomaly pattern associated with the NASST index derived from observations (Fig. 2a), which can be reproduced in simulations in which an atmospheric general circulation model is coupled to a slab ocean model without active ocean dynamics (Clement et al. 2015; Cane et al. 2017; Zhang 2017; Delworth et al. 2017). Clement et al. (2015) interpret the AMO as the response of the upper ocean mixed layer to heat-flux forcing by the atmosphere, which is associated with the NAO. Some of the confusion about the importance of ocean dynamics in NA SST variability may arise from the choice of the SST index. The mechanistic drivers influencing the NASST index can be thermodynamic and dynamic in nature. Furthermore, the different drivers operate on different time scales. Clement et al. (2015) use the NASST index to discuss the role of ocean dynamics in NA SST, which is based on annual SSTs, and this index has been shown here to lump together SST variability of different origin. The climate models used here suggest that the AMO index, which is defined in this study as the low-pass filtered NASST index, may be a better choice to identify ocean dynamical effects on NA SST.

However, when calculated from the short instrumental observations, the SST-anomaly pattern associated with the AMO index still resembles the pattern associated with the NASST index and likely contains large components from atmospheric heat-flux forcing, ocean dynamical heating, and external forcing. The E-NASST (extratropical NA SST) index, which is based on annual data, could be used instead of the AMO index to obtain some hint from instrumental SSTs about the ocean-circulation influence on NA SST. This is because the multidecadal SST variability in many climate models mainly exists over the extratropical NA and is strongly linked to the AMOC and SPG, whereas the NASST index also includes the tropical NA SST variability that is mostly related to atmospheric heat-flux forcing in the models. Thus, on the one hand the E-NASST index strongly reflects the effects of the ocean circulation on multidecadal SST variability and on the other hand avoids the high-frequency tropical NA SST "noise." The E-NASST index therefore avoids the low-pass filter, which can reduce the temporal variability and make statistical tests less stringent (Ebisuzaki 1997). However, a more detailed approach is required instead of simple spatial averaging to clearly separate the different factors influencing NA SST, which would include other variables and more advanced statistical methods such as singular value decomposition (SVD) targeted at investigating the covariance between variables and regions.

Acknowledgments. We acknowledge the World Climate Research Programs Working Group on Coupled Modeling, the individual modeling groups of the Coupled Model Intercomparison Project phase 5 (CMIP5), the U.K. Met Office for providing the SST data, and the National Center for Atmospheric Research for the NAO data. The climate model integrations of the KCM were performed at the Computing Centre of Kiel University and the North-German Supercomputing Alliance (HLRN). This work was supported by the European Union's CLIMPRE InterDec project (01LP1609B) and RACE II Project of BMBF (Grant Agreement 03F0729C) and was also funded in part by a PhD scholarship funded jointly by the China Scholarship Council (CSC). This is a contribution to the Cluster of Excellence "The Future Ocean" at the University of Kiel.

REFERENCES

Amaya, D. J., M. J. DeFlorio, A. J. Miller, and S.-P. Xie, 2017: WES feedback and the Atlantic meridional mode: Observations and CMIP5 comparisons. *Climate Dyn.*, **49**, 1665–1679, https://doi.org/10.1007/s00382-016-3411-1.

Ba, J., and Coauthors, 2014: A multi-model comparison of Atlantic multidecadal variability. *Climate Dyn.*, **43**, 2333–2348, https://doi.org/10.1007/s00382-014-2056-1.

Bellomo, K., L. N. Murphy, M. A. Cane, A. C. Clement, and L. M. Polvani, 2018: Historical forcings as main drivers of the Atlantic multidecadal variability in the CESM large ensemble. *Climate Dyn.*, **50**, 3687–3698, https://doi.org/10.1007/s00382-017-3834-3.

Booth, B. B., N. J. Dunstone, P. R. Halloran, T. Andrews, and N. Bellouin, 2012: Aerosols implicated as a prime driver of twentieth-century North Atlantic climate variability. *Nature*, **484**, 228–232, https://doi.org/10.1038/nature10946.

Brown, P. T., M. S. Lozier, R. Zhang, and W. Li, 2016: The necessity of cloud feedback for a basin-scale Atlantic Multidecadal Oscillation. *Geophys. Res. Lett.*, **43**, 3955–3963, https://doi.org/10.1002/2016GL068303.

Cane, M. A., A. C. Clement, L. N. Murphy, and K. Bellomo, 2017: Low-pass filtering, heat flux, and Atlantic multidecadal variability. *J. Climate*, **30**, 7529–7553, https://doi.org/10.1175/JCLI-D-16-0810.1.

Carton, J. A., X. Cao, B. S. Giese, and A. M. da Silva, 1996: Decadal and interannual SST variability in the tropical Atlantic Ocean. *J. Phys. Oceanogr.*, **26**, 1165–1175, https://doi.org/10.1175/1520-0485(1996)026<1165:DAISVI>2.0.CO;2.

Cayan, D. R., 1992: Latent and sensible heat flux anomalies over the northern oceans: Driving the sea surface temperature. *J. Phys. Oceanogr.*, **22**, 859–881, https://doi.org/10.1175/1520-0485(1992)022<0859:LASHFA>2.0.CO;2.

Clement, A., K. Bellomo, L. N. Murphy, M. A. Cane, T. Mauritsen, G. Rädel, and B. Stevens, 2015: The Atlantic Multidecadal Oscillation without a role for ocean circulation. *Science*, **350**, 320–324, https://doi.org/10.1126/science.aab3980.

Curry, R. G., and M. S. McCartney, 2001: Ocean gyre circulation changes associated with the North Atlantic Oscillation. *J. Phys. Oceanogr.*, **31**, 3374–3400, https://doi.org/10.1175/1520-0485(2001)031<3374:OGCCAW>2.0.CO;2.

Danabasoglu, G., S. G. Yeager, Y. O. Kwon, J. J. Tribbia, A. S. Phillips, and J. W. Hurrell, 2012: Variability of the Atlantic meridional overturning circulation in CCSM4. *J. Climate*, **25**, 5153–5172, https://doi.org/10.1175/JCLI-D-11-00463.1.

Day, J. J., J. C. Hargreaves, J. D. Annan, and A. Abe-Ouchi, 2012: Sources of multi-decadal variability in Arctic sea ice extent. *Environ. Res. Lett.*, **7**, 034011, https://doi.org/10.1088/1748-9326/7/3/034011.

Delworth, T. L., and M. E. Mann, 2000: Observed and simulated multidecadal variability in the Northern Hemisphere. *Climate Dyn.*, **16**, 661–676, https://doi.org/10.1007/s003820000075.

——, and F. Zeng, 2016: The impact of the North Atlantic Oscillation on climate through its influence on the Atlantic meridional overturning circulation. *J. Climate*, **29**, 941–962, https://doi.org/10.1175/JCLI-D-15-0396.1.

——, S. Manabe, and R. Stouffer, 1993: Interdecadal variations of the thermohaline circulation in a coupled ocean–atmosphere model. *J. Climate*, **6**, 1993–2011, https://doi.org/10.1175/1520-0442(1993)006%3C1993:IVOTTC%3E2.0.CO;2.

——, F. Zeng, G. A. Vecchi, X. Yang, L. Zhang, and R. Zhang, 2016: The North Atlantic Oscillation as a driver of rapid climate change in the Northern Hemisphere. *Nat. Geosci.*, **9**, 509–512, https://doi.org/10.1038/ngeo2738.

——, ——, L. Zhang, R. Zhang, G. A. Vecchi, and X. Yang, 2017: The central role of ocean dynamics in connecting the North Atlantic Oscillation to the extratropical component of the Atlantic multidecadal oscillation. *J. Climate*, **30**, 3789–3805, https://doi.org/10.1175/JCLI-D-16-0358.1.

Deser, C., and M. L. Blackmon, 1993: Surface climate variations over the North Atlantic Ocean during winter: 1900–1989. *J. Climate*, **6**, 1743–1753, https://doi.org/10.1175/1520-0442(1993)006<1743:SCVOTN>2.0.CO;2.

Drews, A., and R. J. Greatbatch, 2016: Atlantic multidecadal variability in a model with an improved North Atlantic Current. *Geophys. Res. Lett.*, **43**, 8199–8206, https://doi.org/10.1002/2016GL069815.

——, and ——, 2017: Evolution of the Atlantic multidecadal variability in a model with an improved North Atlantic Current. *J. Climate*, **30**, 5491–5512, https://doi.org/10.1175/JCLI-D-16-0790.1.

Ebisuzaki, W., 1997: A method to estimate the statistical significance of a correlation when the data are serially correlated. *J. Climate*, **10**, 2147–2153, https://doi.org/10.1175/1520-0442(1997)010<2147:AMTETS>2.0.CO;2.

Eden, C., and T. Jung, 2001: North Atlantic interdecadal variability: Oceanic response to the North Atlantic Oscillation (1865–1997). *J. Climate*, **14**, 676–691, https://doi.org/10.1175/1520-0442(2001)014<0676:NAIVOR>2.0.CO;2.

——, and J. Willebrand, 2001: Mechanism of interannual to decadal variability of the North Atlantic circulation. *J. Climate*, **14**, 2266–2280, https://doi.org/10.1175/1520-0442(2001)014<2266:MOITDV>2.0.CO;2.

Enfield, D. B., and D. A. Mayer, 1997: Tropical Atlantic sea surface temperature variability and its relation to El Niño–Southern Oscillation. *J. Geophys. Res.*, **102**, 929–945, https://doi.org/10.1029/96JC03296.

——, A. M. Mestas-Nuñez, and P. J. Trimble, 2001: The Atlantic Multidecadal Oscillation and its relation to rainfall and river flows in the continental U.S. *Geophys. Res. Lett.*, **28**, 2077–2080, https://doi.org/10.1029/2000GL012745.

Folland, C. K., T. N. Palmer, and D. E. Parker, 1986: Sahel rainfall and worldwide sea temperatures, 1901–85. *Nature*, **320**, 602–607, https://doi.org/10.1038/320602a0.

Frankcombe, L. M., and M. H. England, 2015: Separating internal variability from the externally forced climate response. *J. Climate*, **28**, 8184–8202, https://doi.org/10.1175/JCLI-D-15-0069.1.

Frankignoul, C., 1985: Sea surface temperature anomalies, planetary waves, and air–sea feedback in the middle latitudes. *Rev. Geophys.*, **23**, 357–390, https://doi.org/10.1029/RG023i004p00357.

Garuba, O. A., J. Lu, H. A. Singh, F. Liu, and P. Rasch, 2018: On the relative roles of the atmosphere and ocean in the Atlantic multidecadal variability. *Geophys. Res. Lett.*, **45**, 9186–9196, https://doi.org/10.1029/2018GL078882.

Goldenberg, S. B., C. W. Landsea, A. M. Mestas-Nuñez, and W. M. Gray, 2001: The recent increase in Atlantic hurricane activity: Causes and implications. *Science*, **293**, 474–479, https://doi.org/10.1126/science.1060040.

Hodson, D. L., J. I. Robson, and R. T. Sutton, 2014: An anatomy of the cooling of the North Atlantic Ocean in the 1960s and 1970s. *J. Climate*, **27**, 8229–8243, https://doi.org/10.1175/JCLI-D-14-00301.1.

Huang, B., and Coauthors, 2017: Extended Reconstructed Sea Surface Temperature version 5 (ERSSTv5): Upgrades, validations, and intercomparisons. *J. Climate*, **30**, 8179–8205, https://doi.org/10.1175/JCLI-D-16-0836.1.

Hurrell, J. W., Y. Kushnir, G. Ottersen, and M. Visbeck, 2003: An overview of the North Atlantic Oscillation. *The North Atlantic Oscillation: Climatic Significance and Environmental Impact*, *Geophys. Monogr.*, Vol. 134, Amer. Geophys. Union, 1–35, https://doi.org/10.1029/GM134.

Keenlyside, N. S., J. Ba, J. Mecking, N. E. Omrani, M. Latif, R. Zhang, and R. Msadek, 2016: North Atlantic multi-decadal variability—Mechanisms and predictability. *Climate Change: Multidecadal and Beyond*, C.-P. Chang et al., Eds., World Scientific Series on Asia-Pacific Weather and Climate, Vol. 6, World Scientific, 141–157.

Kerr, R. A., 2000: A North Atlantic climate pacemaker for the centuries. *Science*, **288**, 1984–1985, https://doi.org/10.1126/science.288.5473.1984.

Kilbourne, K. H., T. M. Quinn, R. Webb, T. Guilderson, J. Nyberg, and A. Winter, 2008: Paleoclimate proxy perspective on Caribbean climate since the year 1751: Evidence of cooler temperatures and multidecadal variability. *Paleoceanography*, **23**, PA3220, https://doi.org/10.1029/2008PA001598.

Kim, W. M., S. Yeager, P. Chang, and G. Danabasoglu, 2018a: Low-frequency North Atlantic climate variability in the Community Earth System Model large ensemble. *J. Climate*, **31**, 787–813, https://doi.org/10.1175/JCLI-D-17-0193.1.

——, ——, and G. Danabasoglu, 2018b: Key role of internal ocean dynamics in Atlantic multidecadal variability during the last half century. *Geophys. Res. Lett.*, **45**, 13 449–13 457, https://doi.org/10.1029/2018GL080474.

Knight, J. R., R. J. Allan, C. K. Folland, M. Vellinga, and M. E. Mann, 2005: A signature of persistent natural thermohaline circulation cycles in observed climate. *Geophys. Res. Lett.*, **32**, L20708, https://doi.org/10.1029/2005GL024233.

Kushnir, Y., 1994: Interdecadal variations in North Atlantic sea surface temperature and associated atmospheric conditions. *J. Climate*, **7**, 141–157, https://doi.org/10.1175/1520-0442(1994)007%3C0141:IVINAS%3E2.0.CO;2.

——, R. Seager, J. Miller, and J. C. Chiang, 2002: A simple coupled model of tropical Atlantic decadal climate variability. *Geophys. Res. Lett.*, **29**, 2133, https://doi.org/10.1029/2002GL015874.

Latif, M., and N. S. Keenlyside, 2011: A perspective on decadal climate variability and predictability. *Deep-Sea Res. II*, **58**, 1880–1894, https://doi.org/10.1016/j.dsr2.2010.10.066.

——, and Coauthors, 2004: Reconstructing, monitoring, and predicting multidecadal-scale changes in the North Atlantic thermohaline circulation with sea surface temperature. *J. Climate*, **17**, 1605–1614, https://doi.org/10.1175/1520-0442(2004)017<1605:RMAPMC>2.0.CO;2.

Locarnini, R. A., and Coauthors, 2018: *Temperature*. Vol. 1, *World Ocean Atlas 2018*, NOAA Atlas NESDIS 81, 52 pp.

Madec, G., 2008: NEMO ocean engine. Note du Pole de modélisation, Institut Pierre-Simon Laplace (IPSL), 27. Tech. rep. ISSN-1288-1619, 396 pp., https://www.nemo-ocean.eu/wp-content/uploads/NEMO_book.pdf.

Mann, M. E., and K. Emanuel, 2006: Atlantic hurricane trends linked to climate change. *Eos, Trans. Amer. Geophys. Union*, **87**, 233–244, https://doi.org/10.1029/2006EO240001.

Marshall, J., H. Johnson, and J. Goodman, 2001: A study of the interaction of the North Atlantic Oscillation with ocean circulation. *J. Climate*, **14**, 1399–1421, https://doi.org/10.1175/1520-0442(2001)014<1399:ASOTIO>2.0.CO;2.

Martin, T., A. Reintges, and M. Latif, 2019: Coupled North Atlantic sub-decadal variability in CMIP5 models. *J. Geophys. Res. Oceans*, **124**, 2404–2417, https://doi.org/10.1029/2018JC014539.

McCarthy, G. D., I. D. Haigh, J. J.-M. Hirschi, J. P. Grist, and D. A. Smeed, 2015: Ocean impact on decadal Atlantic climate variability revealed by sea-level observations. *Nature*, **521**, 508–510, https://doi.org/10.1038/nature14491.

Msadek, R., W. E. Johns, S. G. Yeager, G. Danabasoglu, T. L. Delworth, and A. Rosati, 2013: The Atlantic meridional heat transport at 26.5°N and its relationship with the MOC in the RAPID array and the GFDL and NCAR coupled models. *J. Climate*, **26**, 4335–4356, https://doi.org/10.1175/JCLI-D-12-00081.1.

Nigam, S., A. Ruiz-Barradas, and L. Chafik, 2018: Gulf Stream excursions and sectional detachments generate the decadal pulses in the Atlantic multidecadal oscillation. *J. Climate*, **31**, 2853–2870, https://doi.org/10.1175/JCLI-D-17-0010.1.

O'Reilly, C. H., M. Huber, T. Woollings, and L. Zanna, 2016: The signature of low-frequency oceanic forcing in the Atlantic Multidecadal Oscillation. *Geophys. Res. Lett.*, **43**, 2810–2818, https://doi.org/10.1002/2016GL067925.

Otterå, O. H., M. Bentsen, H. Drange, and L. Suo, 2010: External forcing as a metronome for Atlantic multidecadal variability. *Nat. Geosci.*, **3**, 688–694, https://doi.org/10.1038/ngeo955.

Park, T., W. Park, and M. Latif, 2016: Correcting North Atlantic sea surface salinity biases in the Kiel Climate Model: Influences on ocean circulation and Atlantic Multidecadal Variability. *Climate Dyn.*, **47**, 2543–2560, https://doi.org/10.1007/s00382-016-2982-1.

Park, W., N. Keenlyside, M. Latif, A. Ströh, R. Redler, E. Roeckner, and G. Madec, 2009: Tropical Pacific climate and its response to global warming in the Kiel Climate Model. *J. Climate*, **22**, 71–92, https://doi.org/10.1175/2008JCLI2261.1.

Pearson, K., 1895: Notes on regression and inheritance in the case of two parents. *Proc. Roy. Soc. London*, **58**, 240–242, https://doi.org/10.1098/rspl.1895.0041.

Reintges, A., M. Latif, and W. Park, 2016: Sub-decadal North Atlantic Oscillation variability in observations and the Kiel Climate Model. *Climate Dyn.*, **48**, 3475–3487, https://doi.org/10.1007/s00382-016-3279-0.

Robson, J., R. Sutton, K. Lohmann, D. Smith, and M. Palmer, 2012: Causes of the rapid warming of the North Atlantic Ocean in the mid-1990s. *J. Climate*, **25**, 4116–4134, https://doi.org/10.1175/JCLI-D-11-00443.1.

——, ——, and D. Smith, 2014: Decadal predictions of the cooling and freshening of the North Atlantic in the 1960s and the role of ocean circulation. *Climate Dyn.*, **42**, 2353–2365, https://doi.org/10.1007/s00382-014-2115-7.

Roeckner, E., and Coauthors, 2003: The atmospheric general circulation model ECHAM 5: Part I: Max-Planck-Institut für Meteorlogie Rep. 349, 140 pp.

Rowell, D. P., C. K. Folland, K. Maskell, and M. N. Ward, 1995: Variability of summer rainfall over tropical North Africa (1906–92): Observations and modelling. *Quart. J. Roy. Meteor. Soc.*, **121**, 669–704, https://doi.org/10.1002/QJ.49712152311.

Ruprich-Robert, Y., R. Msadek, F. Castruccio, S. Yeager, T. Delworth, and G. Danabasoglu, 2017: Assessing the climate impacts of the observed Atlantic multidecadal variability using the GFDL CM2.1 and NCAR CESM1 global coupled models. *J. Climate*, **30**, 2785–2810, https://doi.org/10.1175/JCLI-D-16-0127.1.

Smith, D. M., and Coauthors, 2019: Robust skill of decadal climate predictions. *npj Climate Atmos. Sci.*, **2**, 13, https://doi.org/10.1038/s41612-019-0071-y.

Sun, C., J. Li, and F.-F. Jin, 2015: A delayed oscillator model for the quasi-periodic multidecadal variability of the NAO. *Climate Dyn.*, **45**, 2083–2099, https://doi.org/10.1007/s00382-014-2459-z.

Sutton, R. T., and D. L. Hodson, 2005: Atlantic Ocean forcing of North American and European summer climate. *Science*, **309**, 115–118, https://doi.org/10.1126/science.1109496.

Swart, N. C., J. C. Fyfe, E. Hawkins, J. E. Kay, and A. Jahn, 2015: Influence of internal variability on Arctic sea-ice trends. *Nat. Climate Change*, **5**, 86–89, https://doi.org/10.1038/nclimate2483.

Taylor, K. E., R. J. Stouffer, and G. A. Meehl, 2012: An overview of CMIP5 and the experiment design. *Bull. Amer. Meteor. Soc.*, **93**, 485–498, https://doi.org/10.1175/BAMS-D-11-00094.1.

Thompson, R. O., 1979: Coherence significance levels. *J. Atmos. Sci.*, **36**, 2020–2021, https://doi.org/10.1175/1520-0469(1979)036<2020:CSL>2.0.CO;2.

Timmermann, A., M. Latif, R. Voss, and A. Grötzner, 1998: Northern Hemispheric interdecadal variability: A coupled air–sea mode. *J. Climate*, **11**, 1906–1931, https://doi.org/10.1175/1520-0442-11.8.1906.

Ting, M., Y. Kushnir, R. Seager, and C. Li, 2009: Forced and internal twentieth-century SST trends in the North Atlantic. *J. Climate*, **22**, 1469–1481, https://doi.org/10.1175/2008JCLI2561.1.

——, ——, and C. Li, 2014: North Atlantic multidecadal SST oscillation: External forcing versus internal variability. *J. Mar. Syst.*, **133**, 27–38, https://doi.org/10.1016/j.jmarsys.2013.07.006.

Trenberth, K. E., and D. J. Shea, 2006: Atlantic hurricanes and natural variability in 2005. *Geophys. Res. Lett.*, **33**, L12704, https://doi.org/10.1029/2006GL026894.

Valcke, S., E. Guilyardi, and C. Larsson, 2006: PRISM and ENES: A European approach to Earth system modelling. *Concurr. Comput.: Pract. Exper.*, **18**, 247–262, https://doi.org/10.1002/cpe.915.

Venzke, S., M. R. Allen, R. T. Sutton, and D. P. Rowell, 1999: The atmospheric response over the North Atlantic to decadal changes in sea surface temperature. *J. Climate*, **12**, 2562–2584, https://doi.org/10.1175/1520-0442(1999)012<2562:TAROTN>2.0.CO;2.

von Storch, H., and F. W. Zwiers, 2001: *Statistical Analysis in Climate Research*. Cambridge University Press, 484 pp.

Wang, C., and L. Zhang, 2013: Multidecadal ocean temperature and salinity variability in the tropical North Atlantic: Linking with the AMO, AMOC, and subtropical cell. *J. Climate*, **26**, 6137–6162, https://doi.org/10.1175/JCLI-D-12-00721.1.

——, S. Dong, and E. Munoz, 2010: Seawater density variations in the North Atlantic and the Atlantic meridional overturning circulation. *Climate Dyn.*, **34**, 953–968, https://doi.org/10.1007/s00382-009-0560-5.

Welch, P. D., 1967: The use of fast Fourier transform for the estimation of power spectra: A method based on time averaging over short, modified periodograms. *IEEE Trans. Audio Electroacoust.*, **15**, 70–73, https://doi.org/10.1109/TAU.1967.1161901.

Wills, R. C., K. C. Armour, D. S. Battisti, and D. L. Hartmann, 2019: Ocean–atmosphere dynamical coupling fundamental to the Atlantic multidecadal oscillation. *J. Climate*, **32**, 251–272, https://doi.org/10.1175/JCLI-D-18-0269.1.

Xie, S.-P., and S. G. H. Philander, 1994: A coupled ocean–atmosphere model of relevance to the ITCZ in the eastern Pacific. *Tellus*, **46A**, 340–350, https://doi.org/10.3402/tellusa.v46i4.15484.

——, and J. A. Carton, 2004: Tropical Atlantic variability: Patterns, mechanisms, and impacts. *The Ocean–Atmosphere Interaction*, *Geophys. Monogr.*, Vol. 147, Amer. Geophys. Union, 121–142.

Yan, X., R. Zhang, and T. R. Knutson, 2019: A multivariate AMV index and associated discrepancies between observed and CMIP5 externally forced AMV. *Geophys. Res. Lett.*, **46**, 4421–4431, https://doi.org/10.1029/2019GL082787.

Yuan, T., L. Oreopoulos, M. Zelinka, H. Yu, J. R. Norris, M. Chin, S. Platnick, and K. Meyer, 2016: Positive low cloud and dust feedbacks amplify tropical North Atlantic Multidecadal Oscillation. *Geophys. Res. Lett.*, **43**, 1349–1356, https://doi.org/10.1002/2016GL067679.

Zhang, J., and R. Zhang, 2015: On the evolution of Atlantic Meridional Overturning Circulation fingerprint and implications for decadal predictability in the North Atlantic. *Geophys. Res. Lett.*, **42**, 5419–5426, https://doi.org/10.1002/2015GL064596.

Zhang, L., and C. Wang, 2013: Multidecadal North Atlantic sea surface temperature and Atlantic meridional overturning circulation variability in CMIP5 historical simulations. *J. Geophys. Res. Oceans*, **118**, 5772–5791, https://doi.org/10.1002/jgrc.20390.

——, and C. Zhao, 2015: Processes and mechanisms for the model SST biases in the North Atlantic and North Pacific: A link with the Atlantic meridional overturning circulation. *J. Adv. Model. Earth Syst.*, **7**, 739–758, https://doi.org/10.1002/2014MS000415.

Zhang, R., 2007: Anticorrelated multidecadal variations between surface and subsurface tropical North Atlantic. *Geophys. Res. Lett.*, **34**, L12713, https://doi.org/10.1029/2007GL030225.

——, 2010: Latitudinal dependence of Atlantic meridional overturning circulation (AMOC) variations. *Geophys. Res. Lett.*, **37**, L16703, https://doi.org/10.1029/2010GL044474.

——, 2017: On the persistence and coherence of subpolar sea surface temperature and salinity anomalies associated with the Atlantic multidecadal variability. *Geophys. Res. Lett.*, **44**, 7865–7875, https://doi.org/10.1002/2017GL074342.

——, and T. L. Delworth, 2005: Simulated tropical response to a substantial weakening of the Atlantic thermohaline circulation. *J. Climate*, **18**, 1853–1860, https://doi.org/10.1175/JCLI3460.1.

——, and Coauthors, 2013: Have aerosols caused the observed Atlantic multidecadal variability? *J. Atmos. Sci.*, **70**, 1135–1144, https://doi.org/10.1175/JAS-D-12-0331.1.

——, R. Sutton, G. Danabasoglu, T. L. Delworth, W. M. Kim, J. Robson, and S. G. Yeager, 2016: Comment on "The Atlantic Multidecadal Oscillation without a role for ocean circulation." *Science*, **352**, 1527, https://doi.org/10.1126/science.aaf1660.

——, ——, ——, Y. O. Kwon, R. Marsh, S. G. Yeager, D. E. Amrhein, and C. M. Little, 2019: A review of the role of the Atlantic Meridional Overturning Circulation in Atlantic multidecadal variability and associated climate impacts. *Rev. Geophys.*, **57**, 316–375, https://doi.org/10.1029/2019RG000644.

Chapter 4 Subpolar Gyre – AMOC – Atmosphere Interactions on Multidecadal Timescales in a version of the Kiel Climate Model

This chapter is a reprint of paper *"Subpolar Gyre – AMOC – Atmosphere Interactions on Multidecadal Timescales in a version of the Kiel Climate Model"* published in Journal of Climate.

Citation: Jing Sun, Mojib Latif, and Wonsun Park (2021). " Subpolar Gyre – AMOC – Atmosphere Interactions on Multidecadal Timescales in a version of the Kiel Climate Model ", *Journal of Climate*, 34(16): 6583-6602, https://doi.org/10.1175/JCLI-D-20-0725.1.

Jing Sun's contributions to this publication:

She did the analysis, produced 14 out of 15 figures and modified the remaining figure. She wrote the first draft of the manuscript and revised the manuscript together with her co-authors.

Subpolar Gyre–AMOC–Atmosphere Interactions on Multidecadal Timescales in a Version of the Kiel Climate Model

JING SUN,[a,b] MOJIB LATIF,[a,c] AND WONSUN PARK[a]

[a] *GEOMAR Helmholtz Centre for Ocean Research Kiel, Kiel, Germany*
[b] *Ocean University of China, Qingdao, China*
[c] *Faculty of Mathematics and Natural Sciences, Christian Albrechts University of Kiel, Kiel, Germany*

(Manuscript received 17 September 2020, in final form 8 May 2021)

ABSTRACT: There is a controversy about the nature of multidecadal climate variability in the North Atlantic (NA) region, concerning the roles of ocean circulation and atmosphere–ocean coupling. Here we describe NA multidecadal variability from a version of the Kiel Climate Model, in which both subpolar gyre (SPG)–Atlantic meridional overturning circulation (AMOC) coupling and atmosphere–ocean coupling are essential. The oceanic barotropic and meridional overturning streamfunctions and the sea level pressure are jointly analyzed to derive the leading mode of Atlantic sector variability. This mode accounting for 23.7% of the total combined variance is oscillatory with an irregular periodicity of 25–50 years and an *e*-folding time of about a decade. SPG and AMOC mutually influence each other and together provide the delayed negative feedback necessary for maintaining the oscillation. An anomalously strong SPG, for example, drives higher surface salinity and density in the NA's sinking region. In response, oceanic deep convection and AMOC intensify, which, with a time delay of about a decade, reduces SPG strength by enhancing upper-ocean heat content. The weaker gyre leads to lower surface salinity and density in the sinking region, which reduces deep convection and eventually AMOC strength. There is a positive ocean–atmosphere feedback between the sea surface temperature and low-level atmospheric circulation over the southern Greenland area, with related wind stress changes reinforcing SPG changes, thereby maintaining the (damped) multidecadal oscillation against dissipation. Stochastic surface heat flux forcing associated with the North Atlantic Oscillation drives the eigenmode.

KEYWORDS: Ocean circulation; Atmosphere-ocean interaction; Stochastic models; Multidecadal variability; Meridional overturning circulation

1. Introduction

The North Atlantic (NA) region exhibits pronounced multidecadal variability such as that in sea surface temperature (SST) (Folland et al. 1986; Kushnir 1994; Knight et al. 2005; Álvarez-García et al. 2008), hurricane activity (Goldenberg et al. 2001), or Sahel rainfall (Folland et al. 1986; Zhang and Delworth 2006). There is an ongoing debate about the mechanisms underlying the multidecadal variability in the NA region, and external and internal factors have been proposed to explain the variability (e.g., Latif and Keenlyside 2011; Ting et al. 2014; Bellomo et al. 2018; Zhang et al. 2019). Unfortunately, instrumental data are limited, hindering understanding the origin of the multidecadal variability. For example, instrumental SSTs with relatively good spatial coverage or station-based sea level pressure (SLP) data only are available for about the last 150 years, which is too short to investigate in detail the causes and characteristics of multidecadal climate variability. Records of other quantities such as subsurface ocean temperatures or ocean circulation parameters are even shorter. Observations of the Atlantic meridional overturning circulation (AMOC) at 26.5°N (Cunningham et al. 2007; Kanzow et al. 2007) or moored observations of the deep western boundary current (DWBC) in the northwest Atlantic (Toole et al. 2017), for example, only had started in 2004. At 53°N, the western boundary current system of the Labrador Sea has been measured by moorings since 1997 (Zantopp et al. 2017), allowing us to merely resolve multiyear to decadal changes. Some insight into the nature of the multidecadal variability in the NA, however, was obtained from long-term surface observations, and these suggest that ocean circulation is the major factor influencing NA SST variability at decadal to multidecadal time scales whereas the atmosphere drives the NA SST variability on shorter time scales (Bjerknes 1964; Latif et al. 2006; Gulev et al. 2013; Bryden et al. 2020). This picture is supported by ocean–sea ice general circulation models that have been forced by time-dependent atmospheric surface observations. Álvarez-García et al. (2008), for example, report that the observed multidecadal SST variability during 1958–2000 exhibits a close link to the ocean model's AMOC.

The limited observations are the reason why heavy use is being made of multicentennial to millennial control integrations of climate models to explore the nature of internal multidecadal variability in the Atlantic. Additional insight into the mechanisms of multidecadal variability is obtained from historical simulations with climate models, in which estimates of observed external forcing 1850–2014 is specified (Taylor et al. 2012; Zhang and Wang 2013; Weyer et al. 2020). However, climate models have generally been unable to simulate atmospheric anomalies in the extratropics as strong as the observed such as that in the North Atlantic Oscillation (NAO) in either coupled (Gillett 2005) or in forced mode with specified observed boundary conditions (Scaife et al. 2009). Moreover, climate

Corresponding author: Jing Sun, jsun@geomar.de

DOI: 10.1175/JCLI-D-20-0725.1

models suffer from biases that are particularly prominent in the subpolar NA, with large errors in mean-state SST and sea surface salinity (SSS), which in turn may bias decadal variability (Menary et al. 2015). In fact, climate models disagree with regard to the origin of the multidecadal variability in the NA, its periodicity, and its spatial structure.

In many climate models, midlatitude and subpolar multidecadal SST variations are significantly correlated with fluctuations in the AMOC (e.g., Ba et al. 2014; Sun et al. 2020), suggesting a link to northward heat transport changes, consistent with the early studies of Delworth et al. (1993); Timmermann et al. (1998) and Latif et al. (2004). Some studies link interdecadal AMOC variability in a variety of models to westward propagating baroclinic Rossby waves (te Raa and Dijkstra 2002; Frankcombe et al. 2008; Sévellec and Fedorov 2013). Besides, a coupled upper ocean–atmosphere–sea ice mode (Escudier et al. 2013) may interact with the westward propagating anomalies (Ortega et al. 2015). However, all these mechanisms might be model dependent.

The subpolar gyre (SPG), also in line with Delworth et al. (1993), interacts with the AMOC (Zhang 2008; Lohmann et al. 2009) and plays an important role in preconditioning the density structure in the NA sinking region in a number of climate models. Meanwhile, some observational and modeling studies suggest that specific SST anomalies in the NA can induce a winter NAO response, which will influence the AMOC by affecting oceanic deep convection (Sutton et al. 2018). Therefore, there may be important dynamical ocean–atmosphere interactions operating in the multidecadal variability over the NA region (Grossmann and Klotzbach 2009; Sun et al. 2019).

Comparisons between slab ocean and fully coupled general circulation model simulations are commonly used for understanding the relative roles of atmospheric forcing and ocean dynamics on SST. The role of the ocean circulation in driving multidecadal SST variability in the Atlantic, which is termed Atlantic multidecadal oscillation (AMO) or Atlantic multidecadal variability (AMV), has been challenged by Clement et al. (2015), arguing that the main features of the observed AMO are reproduced in models where the ocean heat transport is prescribed. Allowing the ocean circulation to interact with the atmosphere does not significantly alter the characteristics of the AMO in the analyzed climate models. The results of Clement et al. (2015) suggest that the AMO is the response to stochastic forcing from the midlatitude atmospheric circulation. Finally, external forcing, natural and anthropogenic, also has been suggested to explain some of the multidecadal climate variability observed in the NA region (e.g., Otterå et al. 2010; Booth et al. 2012; Muthers et al. 2016).

Here we present a control integration of a version of the Kiel Climate Model (KCM), in which variability of the ocean circulation *and* dynamical ocean–atmosphere coupling are crucial in producing a quasi-oscillatory multidecadal mode with an irregular period of 25–50 years over the NA region that clearly sticks out above red noise, where the multidecadal time scale is set by the ocean circulation. The atmosphere locally responds to the SST anomalies in the SPG region, thereby reinforcing ocean circulation change and lengthening the time scale.

The multidecadal mode can be understood within the stochastic climate model framework that can be considered as null hypothesis for the generation of internal climate variability. This conceptual model has been originally formulated in a rather general manner by Hasselmann (1976), and different versions of the model have been applied to explain some aspects of the variability in the NA on a variety of time scales (Frankignoul 1985; Saravanan and McWilliams 1997). Mecking et al. (2014) studied an ocean–sea ice general circulation model (NEMO) that was driven using white noise forcing associated with the NAO. The AMOC and SPG strength in that simulation both exhibit enhanced power at low frequencies but no dominant time scale, and thus provide no evidence for an oscillatory ocean-only mode of variability. Here we study the variability in a control integration of a coupled atmosphere–ocean–sea ice general circulation model, the KCM, that employs an ocean–sea ice component of the NEMO family. Therefore, our coupled simulation, in some way, can be understood as an extension of the uncoupled study by Mecking et al. (2014).

We address the following questions in this study: first, what is the role of the Atlantic Ocean circulation, wind-driven and buoyancy-driven, in the multidecadal variability? Second, how do the SPG and AMOC interact? Third, what is the role of dynamical ocean–atmosphere coupling in the multidecadal variability? Finally, is the multidecadal variability consistent with the stochastic climate model framework? And if so, what stochastic model applies to the multidecadal variability simulated by the KCM, what is the stochastic forcing, and what spectral characteristics does it exhibit?

The paper is organized as follows. Section 2 gives an overview of the data and methods used in this study. The results are presented in section 3. The major findings of this study are summarized and discussed in section 4.

2. Material and methods

a. Data

Observations are used to calculate long-term climatologies for model comparison (Fig. 1). The SST climatology for 1955–64 is from the *World Ocean Atlas 2018* (*WOA18*) with 1° × 1° resolution (Locarnini et al. 2018; https://www.nodc.noaa.gov/OC5/woa18/). Observed SLPs during 1900–2012 with 5° × 5° resolution are from the Hadley Centre Sea Level Pressure dataset (HadSLP2r; Allan and Ansell 2006).

We analyze a multimillennial, 3000-yr-long, preindustrial control integration of a version of the Kiel Climate Model using a CO_2 concentration of 286 ppm. A list of references of published studies employing different versions of the KCM, originally described in Park et al. (2009), can be obtained from https://www.geomar.de/kcms. The KCM version that is used here employs ECHAM5 (Roeckner et al. 2003) as atmospheric component, with a horizontal resolution of T42 (2.8° × 2.8°) and 19 vertical levels. The ocean–sea ice component is NEMO (Madec 2008) on a 2° Mercator mesh (ORCA2) horizontally, with increased meridional resolution of 0.5° near the equator and 31 vertical levels. The atmosphere model is coupled to the

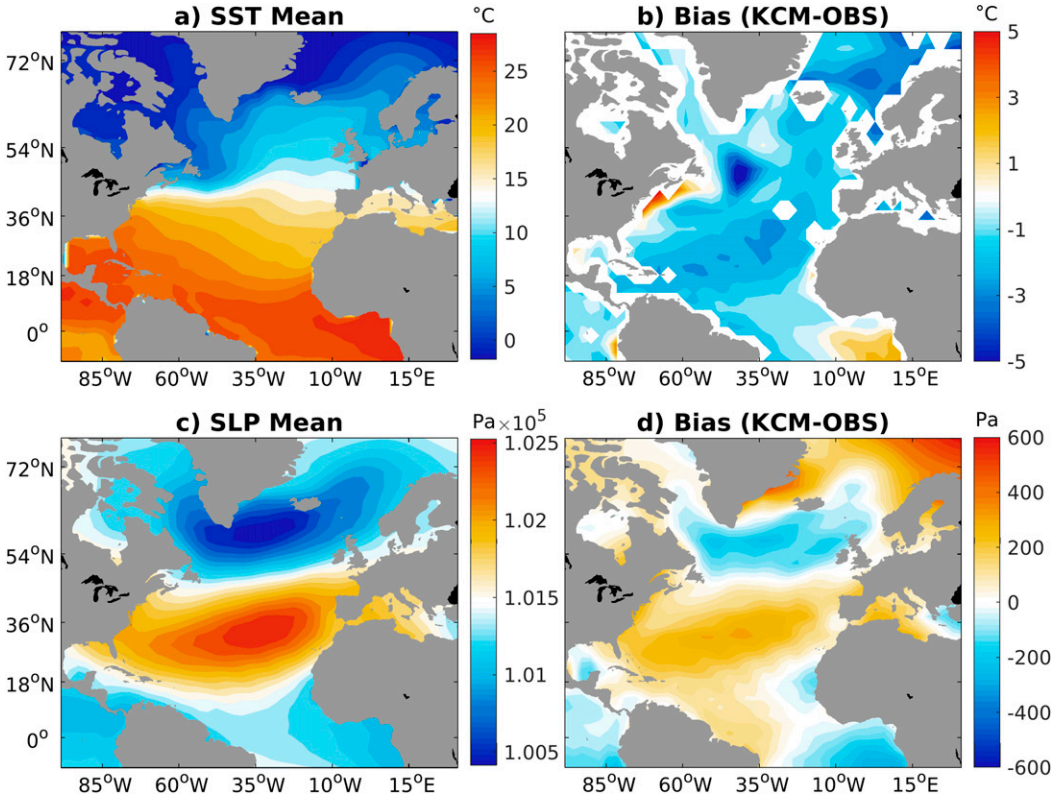

FIG. 1. (a) Long-term annual-mean SST (°C) in the KCM. (b) SST bias relative to the long-term annual-mean SST derived from observations 1955–64 provided by *WOA18*. (c) Long-term annual-mean SLP (Pa) in the KCM. (d) SLP bias relative to the long-term annual-mean SLP observations 1900–2012 calculated from HadiSLP2r. The observations have been linearly detrended. All 3000 years of the control run were used in computing the means of the KCM.

ocean–sea ice model via OASIS (Valcke et al. 2006). A surface freshwater flux correction (FWC) is applied to the model over the NA (10°–80°N), which not only largely eliminates upper-ocean salinity biases over that region but also considerably reduces the cold SST and upper-ocean temperature biases over the NA (Park et al. 2016).

The simulated long-term annual mean SSTs (SLPs) over the NA and the biases relative to the long-term climatologies from observations are shown in Figs. 1a and 1b (Figs. 1c,d). There is still an obvious cold SST bias over the NA (Fig. 1b), indicating that the FWC, although removing sea surface salinity biases, does not completely eliminate the cold SST bias. The remaining cold SST bias is comparable to the multimodel ensemble-mean cold SST bias calculated from models participating in phases 3, 5, and 6 of the Coupled Model Intercomparison Project (CMIP3, CMIP5, and CMIP6) (see Fig. 3 in Bock et al. 2020). The SLP climatology is an indicator of the mean low-level atmospheric circulation, and the KCM's SLP climatology clearly depicts the Icelandic low and the Azores high (Fig. 1c). SLP biases are on the order of several hectopascals in the pressure centers (Fig. 1d).

Additionally, a 700-yr-long sensitivity experiment is conducted with the KCM, in which daily wind stress is randomly chosen from a 700-yr-long chunk of the control run, but obeying the seasonal cycle, and specified over the global ocean (W_{random} hereafter). Annual anomalies are used for the analyses throughout the paper unless otherwise stated.

b. *POP analysis*

The principal oscillation pattern (POP) analysis (Hasselmann 1988; von Storch et al. 1988, 1995) is a multivariate statistical technique designed to infer simultaneously the characteristic patterns and time scales of a vector time series. POPs are defined as the normal modes of a linear dynamical representation of the data in terms of a first-order autoregressive vector process with residual noise forcing. Let $X(t)$ represent an n-dimensional stochastic process. For practical purposes, the original process is usually reduced into the subspace of leading empirical orthogonal function (EOFs; Lorenz 1956). Hence, X is composed of the leading principal components (PCs). The evolution of X is represented as a first-order multivariate Markov process: $X(t+1) = \mathbf{A}X(t) + \text{noise}$. It can be shown that in order to minimize the noise, the system matrix $\mathbf{A}$ has to be chosen as $\mathbf{A} = \mathbf{C}_1\mathbf{C}_0^{-1}$, where $\mathbf{C}_1$ denotes the lag-1 covariance matrix of $X(t)$ and $\mathbf{C}_0$ the lag-0 covariance matrix. To perform a POP analysis is to solve the eigenproblem for $\mathbf{A}$ and

to find the temporal variation (POP coefficients) of each eigenvector or POP [see, e.g., von Storch et al. (1995) for further details].

POPs associated with real eigenvalues represent nonpropagating, nonoscillatory patterns that decay exponentially. POPs associated with complex eigenvalues occur in complex conjugate pairs and can represent standing wave structures (if one pattern is much stronger than the other), propagating waves (if both patterns are periodic and have the same structure except for a quarter-wavelength shift) or, in general, an arbitrary amphidromic oscillation. Complex POPs have a rotation period and a time scale for exponential decay that are estimated as part of the eigenproblem. The evolution associated with a (complex) POP mode can be described as a (damped) cyclic sequence of patterns:

$$\ldots \rightarrow p_{\text{imag}} \rightarrow p_{\text{real}} \rightarrow -p_{\text{imag}} \rightarrow -p_{\text{real}} \rightarrow p_{\text{imag}} \rightarrow \ldots . \quad (1)$$

In this study, we calculate the POPs from a joint dataset comprised of the Atlantic barotropic streamfunction (PSI), meridional overturning streamfunction (MOC), and sea level pressure (SLP). The former two quantities are intended to represent the horizontal and vertical ocean circulations, respectively, whereas the SLP can be treated as the component representing the low-level atmospheric circulation. The three variables are transformed into one data matrix after dividing by their respective sum of the spatial standard deviations [28.3 Sv ($1\,\text{Sv} \equiv 10^6\,\text{m}^3\,\text{s}^{-1}$) for PSI, 25.1 Sv for MOC, and 21.5 hPa for SLP], so that each variable has the same total variance in the POP analysis. The region 0°–70°N, 80°W–0°E is chosen for the POP analysis. Here we use the PCs of the first 15 EOFs in the POP analysis, which account for 88.8% of the joint data variability. Results are stable when using at least the PCs of the first 12 EOFs. Because annual values have been used in the POP analysis, the time step in the estimation of the lag-1 covariance matrix $\mathbf{C}_1$ is 1 year. No time filtering is applied prior to the POP analysis.

We link the variability associated with the leading POP mode, which we have derived from PSI, MOC, and SLP, to other variables over the NA by means of lag regression analysis.

c. Statistical methods and definition of climate indices

We depict maps of linear regression coefficients of different variables on selected indices, calculated at different time lags, where the indices have been normalized by their respective standard deviation σ. An F test is used to test the significance of the regression coefficients. The Student's t test and Monte Carlo simulation based on nonparametric random phase (Ebisuzaki 1997) are applied to test the significance of the correlation coefficients. Cross-spectral analysis is used to investigate the relationship between two time series in the frequency domain. Sun et al. (2020) used the method to investigate the links of area-averaged North Atlantic SST indices to some of their mechanistic drivers. For the computation of cross-spectra, we use the Hamming window and set the window length to 200 samples with an overlap of 120 samples (e.g., von Storch and Zwiers 2001). Welch's method of overlapped averaged periodogram is applied (Welch 1967). The power spectrum estimate is obtained by applying the Daniell window with length m to smooth the raw periodogram (Bloomfield 2004). The upper 90% and 95% confidence levels of the power spectra are calculated according to the chi-squared distribution of the variance of the background noise. If the lag-1 autocorrelation coefficient is negative or close to zero, white noise is chosen as the background spectrum; otherwise red noise is chosen [see details in Gilman et al. (1963)].

Several indices are used in this study. We primarily make use of the coefficient time series of the real part of the leading POP mode to obtain regression patterns of selected variables at different phases of the POP cycle. We note that theoretically the real and imaginary part time series of a (complex) POP mode are in quadrature. Further, we use an NAO index defined as the PC of the leading EOF of the SLP anomalies in winter [December–March (DJFM)] over the North Atlantic region (20°–80°N, 90°W–40°E), following Hurrell et al. (2013), which accounts for 52.7% of the variance. We additionally define a Greenland SLP index (GI), which is the area mean of the SLP anomalies over the southern Greenland region (54.4°–68.4°N, 60°–22.5°W), where only ocean grid points are used in the calculation of the index. The reason for defining the GI is given in section 3 when discussing the atmospheric response to the SST anomalies south of Greenland. An SST index is defined as the PC of the leading EOF of the SST anomalies over the extratropical NA (20°–70°N, 80°W–0°E), which is termed PC1_{SST} and accounts for 21.4% of the total variance (the regression pattern shown in Fig. 6e is very similar to the leading EOF). In W_{random}, the leading SST EOF is very similar to that in the control run and accounts for 19.5% of the variance. An AMOC index is defined as the maximum of the overturning streamfunction at 40°N (Zhang 2008). Finally, an SPG index is defined as the inverted area average of the barotropic streamfunction anomalies over the subpolar NA (50°–58°N, 42°–26°W), similar to a previous study (Lohmann et al. 2009).

3. Results

a. Power spectra

As shown in Park et al. (2016), the Atlantic Ocean circulation simulated in the control run exhibits strong multidecadal variability. The power spectrum of the SPG index (Fig. 2a) and that of the AMOC index (Fig. 2b) are red with increasing variance toward longer time scales. Both spectra exhibit a statistically significant peak above the 95% confidence level (relative to red noise) at periods of 25–50 years. We note that the spectrum of the AMOC index is characterized by a steeper increase than the SPG spectrum, which is in line with the findings of Mecking et al. (2014). The spectrum of the GI (Fig. 2c) exhibits an almost even variance distribution across time scales, which is largely consistent with a white-noise type spectrum. There is, however, enhanced power at multidecadal time scales (relative to red noise) above the 95% confidence level in the spectrum of the GI, consistent with the spectra of the two ocean circulation indices. The spectrum of PC1_{SST} (Fig. 2d) also exhibits significantly enhanced variability in the range 25–50 years.

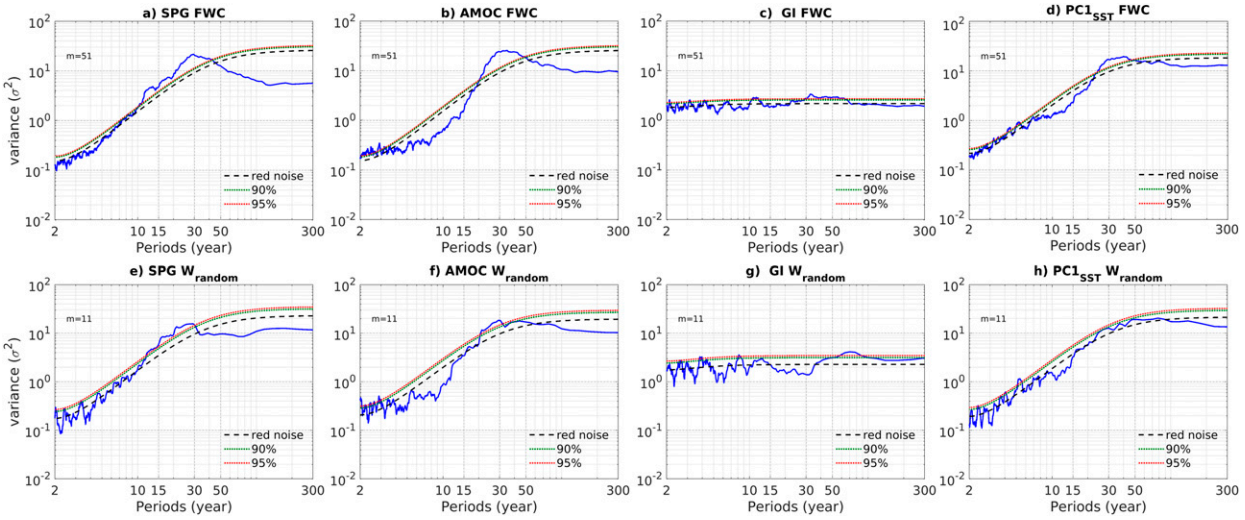

FIG. 2. (a)–(d) Power spectrum of indices from the KCM's control run. The window length m for smoothing is 51 points. (a) SPG index spectrum (blue solid curve), and the 90% confidence level (green dotted curve) and 95% confidence level (red dotted curve) with reference to a fitted red-noise process (black dashed curve). (b) As in (a), but for the AMOC index. (c) As in (a), but for the Greenland SLP index (GI). (d) As in (a), but for $PC1_{SST}$. Also shown are power spectra of the indices from the KCM's random wind stress experiment (W_{random}): (e) SPG index, (f) AMOC index, (g) GI, and (h) $PC1_{SST}$. The window length m for smoothing is 11 points. The indices have been normalized by their respective standard deviations prior to computing the spectra. All 3000 years of the control run were used in (a)–(d), and all 700 years of W_{random} in (e)–(h).

Spectra of the same indices are shown from the sensitivity experiment W_{random} in Figs. 2e–h. In this experiment, the wind stress feedback on the ocean is inhibited. To resolve the multidecadal variability a different window length m is applied in calculating the spectra from W_{random} than in the control run, as the choice of m depends on the length of the time series. The power over the multidecadal time scale (25–50 years) in the spectra of the SPG index (Fig. 2e) and AMOC index (Fig. 2f) is strongly reduced compared to the control run with less prominent peaks, whereas the spectra of the GI index (Fig. 2g) and of $PC1_{SST}$ (Fig. 2h) do not exhibit any significant peaks exceeding the 95% confidence level in the range 25–50 years. The differences between the spectra indicate robust dynamical ocean–atmosphere interactions in the control run but not in the experiment W_{random}. We conclude that the multidecadal ocean circulation variability in W_{random} can be understood as an ocean-only mode that is strongly damped and merely sticks out above red noise. It is the dynamical coupling between the ocean and the atmosphere through the SST–wind stress feedback, which enhances the multidecadal variability and extends the variability toward longer time scales in the fully coupled run.

b. *Combined principal oscillation pattern analysis*

POP analysis is applied jointly to the barotropic streamfunction (PSI), the meridional overturning streamfunction (MOC), and the sea level pressure (SLP), where all 3000 years are used in the analysis. The leading POP mode (POP1) is complex and accounts for 23.7% of total joint variability. POP1 has a rotation period of 38 years and decay time (e-folding time) of 11 years. The second most energetic POP mode (POP2) accounts for 15% of the total variance. POP2 has a rotation period of 18.9 years and decay time of 6 years. Here we concentrate on the multidecadal variability and only discuss the variability associated with POP1.

We note that a POP analysis also has been performed jointly only on PSI and MOC (not shown). In that analysis, the leading POP mode accounts for 40.1% of the joint variability; it has a rotation period of 40.7 years and an e-folding time of 9.3 years, and the PSI and MOC patterns are very similar to those shown below from the POP analysis with the SLP included. Finally, a POP analysis of PSI, MOC, and SLP from W_{random} has been conducted. Overall, the leading POP mode calculated from W_{random} is similar to that derived from the control run. The most important difference between the leading POP modes calculated from the two simulations is the e-folding time amounting to only 5.7 years in W_{random}, which is about half of that in the control run. This further supports the important role of the wind stress–SST feedback for maintaining the multidecadal oscillation.

Only the last 300 years of the (complex) coefficient time series (PC) of POP1 are shown in Fig. 3a. However, both the real-part (PC1r) and imaginary-part (PC1i) exhibit marked multidecadal variability throughout the 3000-yr-long integration, as exemplified by the power spectra of PC1r and PC1i, which were calculated over all 3000 years and both exhibit statistically significant peaks near the rotation period of 38 years (Figs. 3b,c). The power drops but remains large at centennial time scales in both spectra. PC1i clearly leads PC1r (Fig. 3a). However, the phase difference at the rotation period slightly deviates from $\pi/2$, which is expected from the POP concept, as derived from cross-spectral analysis of the two time series (Fig. 3d), indicating some asymmetry in the POP cycle.

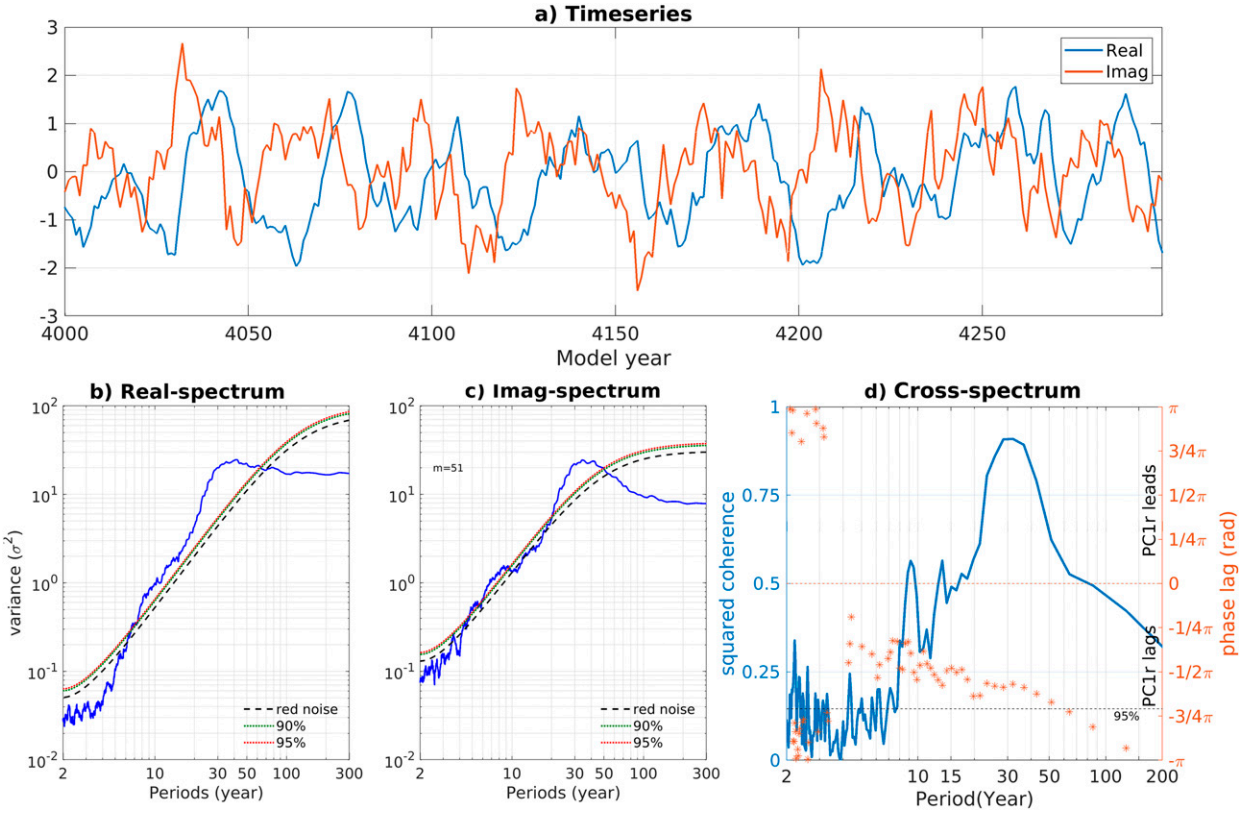

FIG. 3. (a) Last 300 years of the real-part (PC1r) and imaginary-part coefficient time series (PC1i) of the leading POP mode (POP1) derived from the control run. (b) Power spectrum of PC1r. (c) Power spectrum of PC1i. The window length m for smoothing is 51 points. The time series have been normalized by their respective standard deviations prior to computing the spectra. The 90% confidence level, 95% confidence level, and fitted red noise process are labeled as in Fig. 2. (d) Squared coherence (blue) and phase spectrum (orange stars) between PC1r and PC1i. The phase only is shown when the squared coherence exceeds the 95% confidence level (black dotted line). A phase lag of zero indicates that the two time series vary in phase (orange dotted line), while a positive (negative) phase lag indicates that PC1r leads (lags). All 3000 years of the control run were used in (b)–(d).

Finally, there is highly significant squared coherence between PC1r and PC1i at multidecadal time scales (Fig. 3d).

The real and imaginary part patterns of POP1—POP1r and POP1i—are shown in Fig. 4, where the normalization has been changed back. POP1r exhibits quite large loadings in MOC, PSI, and SLP (Figs. 4a–c, respectively). This phase can be considered as the extreme phase of the POP cycle with respect to MOC. The MOC anomalies linked to POP1r (color shading in Fig. 4a) represent an anomalously strong AMOC with a basinwide positive overturning streamfunction anomaly (see also Fig. 5e) similar to that described in the context of the Atlantic multidecadal variability simulated in the original KCM version (Park and Latif 2008). Explained variances (contours in Fig. 4a) amount to about 80% in the center of the overturning anomalies and 30% near the equator. Moreover, PC1r is strongly correlated with the AMOC index (defined at 40°N). The correlation coefficient between the two time series is largest at zero lag and amounts to 0.8, which is significant at 95% confidence level.

The pattern of PSI linked to POP1r (Fig. 4b) exhibits large negative anomalies in the center of the SPG, describing an anomalously strong SPG. The largest explained variances are located in the Labrador Sea where they amount to about 60%. The correlation coefficient between PC1r and the SPG index amounts to 0.34 at zero lag and 0.44 when the SPG index leads by 5 years where the correlation is largest, both significant at the 95% confidence level. We additionally computed the correlation function between the SPG index and the AMOC index, which also yields a time lag of 5 years at the correlation maximum with the SPG index leading (not shown). South of the negative barotropic streamfunction anomalies, positive anomalies along the western boundary are observed (Fig. 4b), which will be addressed below when discussing the mechanism of the multidecadal variability.

The salient feature of the SLP anomalies linked to POP1r is the localized low pressure system over the southern Greenland area (Fig. 4c). PC1r accounts for a rather small fraction of the variance in the SLP (less than 10%), which is not surprising given the chaotic nature of the atmospheric variability. The atmosphere in the middle and high latitudes contains many chaotic subsystems spanning many different time scales, ranging from days to centuries, which is demonstrated by the spectrum of the GI exhibiting nearly white-noise shape

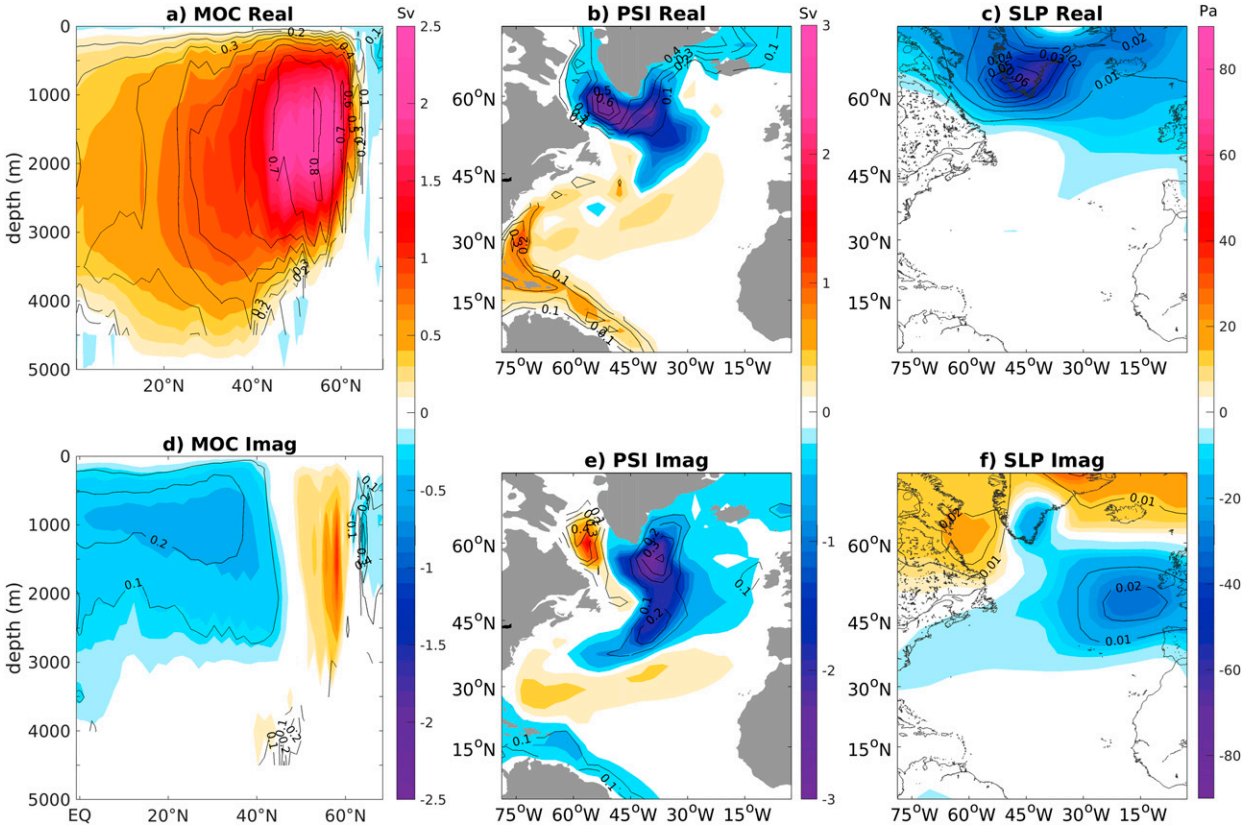

FIG. 4. Spatial patterns of POP1: (left) MOC (meridional overturning circulation streamfunction; Sv), (center) PSI (barotropic streamfunction; Sv), and (right) SLP (sea level pressure; Pa). Shown are the (a) real part pattern of MOC, (b) real part pattern of PSI, (c) real part pattern of SLP, (d) imaginary part pattern of MOC, (e) imaginary part pattern of PSI, and (f) imaginary part pattern of SLP. Color indicates loadings and contours explained variances. Explained variance is shown with a contour interval of 0.1 for MOC and PSI, and 0.01 for SLP.

(Fig. 2c). Therefore, the contour interval for the explained variance has been chosen as 0.01 in Fig. 4c (and Fig. 4f).

The imaginary part patterns of POP1 (i.e., the MOC, PSI, and SLP anomalies related to POP1i) are shown in Figs. 4d–f, respectively. PC1i leads PC1r by a quarter of the rotation period [Eq. (1)] (i.e., by about a decade), so that the patterns given by POP1i can be considered as precursor patterns with respect to the patterns given by POP1r. MOC exhibits large-scale negative anomalies south of about 40°N with explained variances on the order of 20% and relatively small positive anomalies in the region 50°–60°N (Fig. 4d). With respect to PSI (Fig. 4e), POP1i exhibits relatively large anomalies in the subpolar NA that account for a substantial fraction of the variance in the barotropic streamfunction. In particular, there is a dipole anomaly in PSI around the southern tip of Greenland, with positive anomalies in the west and negative anomalies in the east. Explained variances amount to about 30% in the two poles. The negative PSI anomalies bend in a southwestern direction. The transition from POP1i to POP1r thus describes southward propagating overturning anomalies and an intensifying SPG.

The SLP pattern linked to POP1i (Fig. 4f) exhibits low pressure anomalies over the midlatitude NA, centered over the eastern part, and high pressure anomalies to the north, centered over the Labrador Sea and Nordic seas. The magnitude of the SLP anomalies, however, is much smaller than that in POP1r (Fig. 4c), so that the evolution of the SLP anomalies to first order can be understood as a standing oscillation. Overall, the anomalies related to POP1 exhibit rather complex propagation characteristics with regard to MOC and PSI and interactions between them, and also suggests an atmospheric role in the multidecadal oscillation. These aspects will be discussed in more detail in the following subsections.

To understand the mechanisms behind the multidecadal variability described by POP1, we address the following questions: first, how do the oceanic overturning and gyre circulations change? Second, in which way do the ocean circulation changes influence the SST? Third, is the atmosphere sensitive to the SST changes? Fourth, if so, how does the atmosphere feed back onto the ocean? Fifth, how do the SPG and AMOC interact with each other? Sixth, what is the role of stochastic forcing in the multidecadal cycle? To address these questions, we primarily calculate maps of local regression coefficients of selected variables on PC1r at different time lags, ranging from lag = −8 years to lag = +8 years with a time step of 2 years, representing approximately half a cycle (Figs. 5–12).

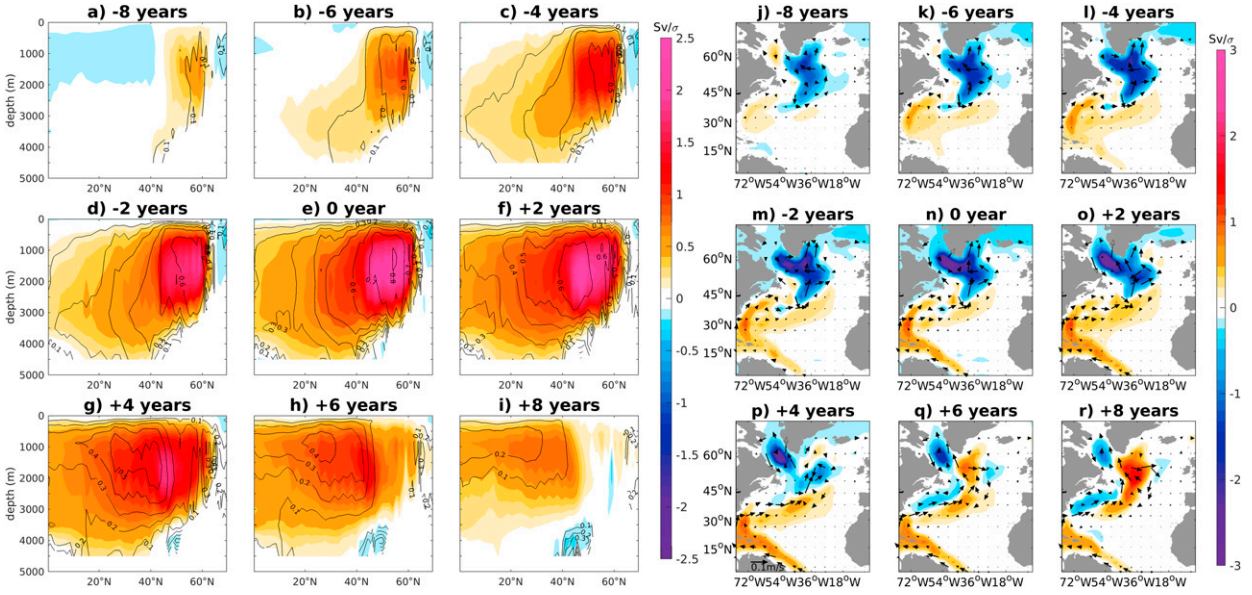

FIG. 5. (a)–(i) Regression maps of the meridional overturning streamfunction (MOC) upon PC1r, and (j)–(r) of the barotropic streamfunction (PSI; color) with depth-integrated (50–500 m) ocean currents superimposed (arrows) from lag = −8 to lag = +8 years (at 2-yr intervals). Regression coefficients are calculated based on one standard deviation (σ) of PC1r. Color indicates the regressions; contours in (a)–(i) indicate explained variances shown with a contour interval (CI) of 0.1.

The regressions are based on a one standard deviation change (σ) in PC1r.

c. Ocean circulation change

Lag = 0 years represents the conditions associated with the real-part phase of POP1, namely POP1r, when MOC, PSI, and SLP are well developed and explain the most variance in the respective fields over the subpolar NA (Figs. 4a–c). As a consistency check, we first calculate the regression patterns of MOC (Figs. 5a–i) and PSI (Figs. 5j–r). The MOC and PSI regression patterns at lag = 0 years (Figs. 5e and 5n, respectively) well reproduce the POP1r patterns (Figs. 4a,b), and the regression patterns at lag = −8 years (Figs. 5a,j) are very similar to the POP1i patterns (Figs. 4d,e). Thus, the lag regression method appears to be well suited to investigate the space–time structure of oceanic and atmospheric anomalies that are associated with POP1, irrespective of whether or not the considered variable has been part of the POP analysis.

A small positive MOC anomaly first develops at lag = −8 years in the region 50°–60°N (Fig. 5a), which does not account for much variance at this time. The positive MOC anomaly strengthens in place and accounts there for most of the variance in the overturning streamfunction at lag = 0 years with values of about 80% (Fig. 5e). Furthermore, the positive MOC anomaly expands southward and remains relatively strong south of 40°N until lag = +8 years (Fig. 5i). At this time, first signs of a negative MOC anomaly develop in the subpolar NA. Overall, the MOC anomalies at lag = +8 years are similar to those at lag = −8 years but with opposite signs. In summary, the regressions of the overturning streamfunction anomalies on PC1r from lag = −8 to lag = +8 years illustrate the development of an anomalously strong AMOC and its subsequent weakening.

The regression maps of the PSI anomalies associated with PC1r have the anomalous depth-integrated (50–500 m) ocean currents superimposed as arrows (Figs. 5j–r). At lag = −8 years, there is a cyclonic (negative) barotropic streamfunction anomaly centered south of Greenland, which reaches southward to about 40°N. The cyclonic PSI anomaly in the SPG region subsequently intensifies and remains relatively strong without changing shape until lag = +2 years (Figs. 5j–o). Explained variances are not shown in Figs. 5j–r. As indicated by the two POP patterns (Figs. 4b,e), the explained variances in PSI are large in the subpolar NA throughout the POP cycle, amounting to up to 60% in localized regions. The small positive barotropic streamfunction anomalies off the coast of North America to the southwest of the large negative anomalies at lag = −8 years (Fig. 5j) strengthen during the subsequent years. There are two parts of the positive PSI anomalies that can be distinguished. The part close to the western boundary propagates southward along the western boundary (Figs. 5k–o), whereas the zonally elongated part propagates eastward and then northward east of the negative PSI anomaly (Figs. 5k–o). The meridional dipole structure in PSI from lag = +2 to lag = +6 years (Figs. 5o–q) represents an anomalously strong Gulf Stream/North Atlantic Current (NAC) system, consistent with the study of Koul et al. (2020) analyzing observations and a simulation with another global climate model. At lag = +8 years (Fig. 5r), positive PSI anomalies have replaced the negative PSI anomalies in the SPG region observed at lag = −8 years (Fig. 5j), indicating that the SPG has now weakened relative to its climatological mean state.

d. Influence of ocean circulation on SST

We next address the SST and net surface heat flux variability associated with POP1r. Major SST anomalies (Figs. 6a–i) go

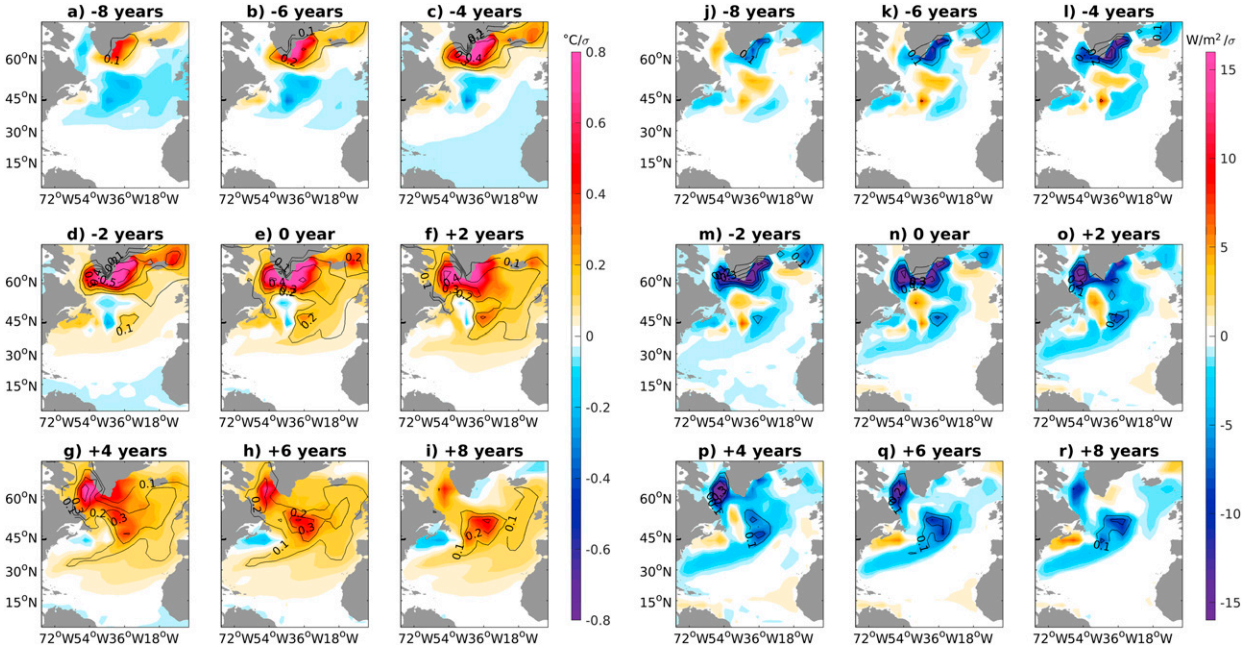

FIG. 6. (a)–(i) Regression maps of sea surface temperature (SST) upon PC1r, and (j)–(r) of the net surface-heat flux (color) from lag = −8 to lag = +8 years (at 2-yr intervals). Regression coefficients are calculated based on one standard deviation (σ) of PC1r. Color indicates the regressions and contours indicate explained variances (CI is 0.1).

along with negative net heat-flux anomalies during all phases (Figs. 6j–r), indicating that the SST anomalies are driven by ocean dynamics as the atmosphere acts as a damping; that is, the ocean releases (takes up) heat when the SST anomalies are positive (negative). We conjecture that the warm SST anomalies observed in the subpolar NA from lag = −8 to lag = −2 years are mostly due to the anomalously strong gyre circulation (Figs. 4j–m). The strengthening AMOC (and associated heat transport) is suggested by the SST anomalies developing in the southwestern subtropical NA around lag = −2 years that subsequently propagate eastward and northward (Figs. 6d–i). At lag = +4 and lag = +6 years, the SST anomaly pattern is very similar to that when regressing the SST anomalies on an AMOC index (Sun et al. 2020, their Fig. 2g).

e. Sensitivity of the atmosphere to SST anomalies

The atmospheric response to extratropical SST anomalies is still controversial (Czaja et al. 2019). Two types of response can be distinguished in atmospheric general circulation models, a linear baroclinic and a nonlinear barotropic response (Kushnir et al. 2002). Here, the linear atmospheric response appears to apply, which operates without synoptic eddy involvement. The linear response to surface heating is characterized by low-level wind convergence, with an associated cyclonic circulation, and an upper-level wind divergence, with an associated anticyclonic circulation (Thomson and Vallis 2018). At lag = −8 years, there is a positive SST anomaly east of the southern tip of Greenland (Fig. 6a). The positive SST anomaly grows and expands to the northeast and to the west during the following years (Figs. 6b–d). As the SST anomalies grow, atmospheric heating (negative heat flux anomalies) also becomes larger (Figs. 6k–m). We assume that the surface heating is linearly related to the SST anomaly south of Greenland. The cross-correlation function between PC1r, which is correlated with $PC1_{SST}$ at about 0.8 when PC1r leads by 1 year, and a near-surface (10 m) wind divergence index, defined as the area average over the southern Greenland region (57.2°–73.9°N, 56.25°–22.5°W), recovers the multidecadal periodicity and exhibits the largest negative correlation amounting to −0.3 (the 95% confidence level is 0.037) when PC1r leads by two years (not shown). At lag = 0 years, the magnitude of the correlation only is slightly smaller. The peak correlation increases to about 0.6 when applying an 11-yr running mean filter to the time series, whereby the structure of the cross-correlation function does not change. Thus, the SST anomaly south of Greenland goes along with low-level wind convergence over the southern Greenland area, supporting the notion of a linear atmospheric response.

We note the strong meridional gradient at the southern flank of the SST anomaly south of Greenland at lag = 0 years (Fig. 6e). Therefore, we also attempt to obtain insight into the role of surface baroclinicity changes in the atmospheric response. For this purpose, we only use winter averages (DJFM), as synoptic eddy activity is strongest during this part of the year. The correlation of the GI with the meridional gradient at the southern flank of the SST anomaly (evaluated over the region 51.6°–60°N, 53.4°–30.9°W), which serves as a measure of surface baroclinicity change, is insignificant. The result remains virtually unchanged when moving the box, over which the meridional gradient of the SST anomaly is calculated, by ±2° latitude. We finally note that the vertical structure of the atmospheric pressure changes is baroclinic

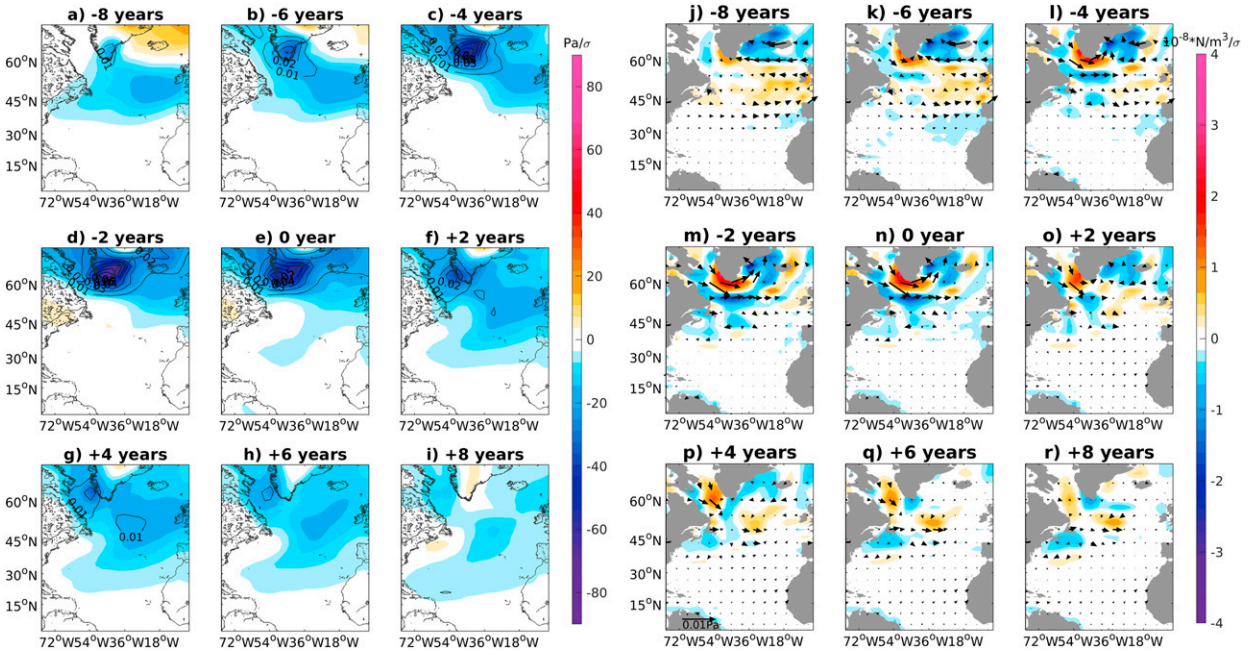

FIG. 7. (a)–(i) Regression maps of sea level pressure (SLP; only shown over ocean points) upon PC1r, and (j)–(r) of the wind stress curl (color) with wind stress vectors superimposed (arrows) from lag = −8 to lag = +8 years (at 2-yr intervals). Regression coefficients are calculated based on one standard deviation (σ) of PC1r. Color indicates the regressions and contours in (a)–(i) indicate explained variances (CI is 0.01).

(not shown), with anomalously high pressure aloft, also indicating that the atmospheric response is dominated by the linear regime.

f. Low-level atmospheric variability and its feedback on the ocean

We now investigate in more detail the low-level atmospheric changes and their feedback on the ocean. Regression maps of the SLP anomalies upon PC1r are shown in Figs. 7a–i, and regression maps of the wind stress (arrows) and wind stress curl anomalies (color shading) in Figs. 7j–r. Explained variances are small with values typically less than 10%, as discussed above. This is why the contour interval for the explained variance in the SLP regression maps is set to 0.01 in Figs. 7a–i, while it is 0.1 otherwise. The SLP regression map at lag = 0 years well reproduces the POP1r pattern (Fig. 4c), and the regression map at lag = −8 years is similar to the POP1i pattern (Fig. 4f). The salient feature in the SLP regression maps is the anomalously low pressure over large regions of the NA. This pattern is not the NAO pattern, but it projects on it. Most important to our discussion concerning the mechanism underlying the variability linked to POP1 is the deepening of the low pressure anomaly over the southern Greenland area from lag = −8 years to lag = −2 years (Figs. 7a–d). The low pressure anomaly starts weakening after lag = −2 years and has disappeared at lag = +8 years (Fig. 7i), when SLP anomalies are small over the entire NA. Anomalous surface westerlies are observed on the southern flank of the low pressure anomaly center, which are particularly well developed from lag = −4 years to lag = 0 years (Figs. 7l–n). The associated wind stress curl (color shading) is positive south of the southern tip of Greenland and provides cyclonic vorticity to the ocean, which explains the strengthening of the barotropic streamfunction during this time (Figs. 5l–n). In the experiment W_{random} in which the wind stress feedback is inhibited, the PSI and SLP regressions upon PC1r (from the POP analysis of W_{random}) are similar in structure from lag = −6 to lag= −2 years but weaker by about 40%–50%. This again demonstrates the importance of the positive wind stress (curl) feedback on the SPG in the control run.

At this stage of the analysis, the following points can be made about the multidecadal variability described by POP1 (Figs. 5–7): first, there are major changes in the ocean circulation, horizontal and vertical (Fig. 5), with the SPG leading the AMOC. Second, it is the changes in the ocean circulation that drive the major SST changes, as the surface heat fluxes act as a damping (Fig. 6). Third, the atmosphere responds to the SST anomalies south of Greenland in the form of a rather localized low pressure anomaly (Figs. 7a–i) centered over southern Greenland. Fourth, the associated changes in the wind stress curl (Figs. 7j–r) add cyclonic vorticity to the ocean, which intensifies the SPG. Fifth, the stronger SPG reinforces the SST anomaly south of Greenland, which in turn further deepens the low pressure anomaly. Thus, there is a positive feedback loop between the SST, SLP, wind stress (curl), and SPG, as already indicated by the spectral analyses (Fig. 2), through which anomalies in these quantities grow from about lag = −6 to lag = −2 years. Sixth, the AMOC (Figs. 5a–i) intensifies over the years, with very first signs in the subpolar NA at lag = −8 years, and the AMOC is suggested to drive the surface warming over

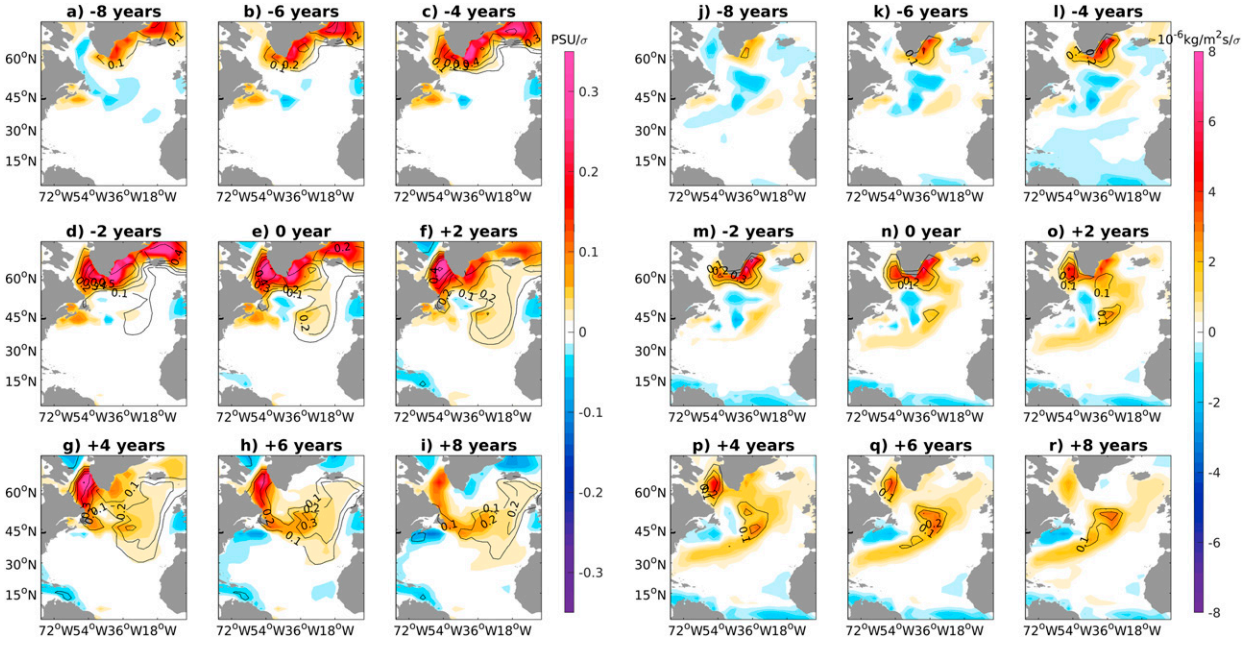

FIG. 8. (a)–(i) Regression maps of sea surface salinity (SSS) upon PC1r, and (j)–(r) of the freshwater flux from lag = −8 to lag = +8 years (at 2-yr intervals). Regression coefficients are calculated based on one standard deviation (σ) of PC1r. Color indicates the regressions and contours indicate explained variances (CI is 0.1).

most of the NA beyond lag = 0 years (Figs. 6a–i), keeping in mind that the surface heat fluxes act as a damping on the SST anomalies throughout the POP cycle.

g. *SPG–AMOC interaction*

How do the gyre and the overturning circulation interact with each other? We calculate the regression maps of sea surface salinity (SSS) and freshwater flux (FW) anomalies upon PC1r (Fig. 8). The major SSS anomalies must be due to ocean circulation changes, because the SSS and FW anomalies generally have the same sign (i.e., anomalously high SSS goes along with anomalously high freshwater input and vice versa). We note that sea ice variability cannot explain the size of the SSS anomalies (not shown). Further, the anomaly patterns of the net heat flux (Figs. 6j–r) and of the freshwater flux (Figs. 8j–r) bear some resemblance, suggesting that both fluxes are part of the atmospheric response to the SST anomalies south of Greenland. Positive SSS anomalies first appear at lag = −8 years in the Greenland Sea and in the Irminger Sea. The SSS anomalies expand thereafter and at lag = −4 years positive SSS anomalies are observed in all three deep convection sites of the NA (Fig. 8c), in the Labrador Sea, Irminger Sea, and Greenland Sea [see Park et al. (2016) for the deep convection sites in the KCM version used here]. The SSS anomalies intensify until about lag = −2 years (Fig. 8d), along with the strengthening SPG. We therefore attribute the positive SSS anomalies during this time to the enhanced gyre transporting more salinity into the NA's sinking region. From lag = 0 years onward (Figs. 8e–i), positive SSS anomalies also appear in the midlatitudes, which is likely due to the strengthening AMOC (Figs. 5e–i) through enhanced meridional transport, keeping in mind that the FW anomalies (Figs. 8n–r) cannot account for the increasing SSS. Farther south, near the western boundary, negative SSS anomalies are observed that propagate northward along the boundary (Figs. 8e–i). The origin of these negative SSS anomalies is unclear. As the local FW anomalies are negative, as well as the rainfall anomalies (not shown), direct atmospheric forcing can be excluded. One plausible explanation for the negative SSS anomalies could be the stronger upper ocean currents (Figs. 5o–r) associated with the stronger AMOC, which reduce the time over which the surface waters are exposed to the net evaporation prevailing in this region, which will show up as negative SSS anomalies.

We next investigate the surface density and mixed layer depth (MLD) anomalies (Fig. 9). The regression patterns of the surface density anomalies (Figs. 9a–i) are similar to that of the SSS anomalies (Figs. 8a–i). Large positive surface density anomalies in the regions of oceanic deep convection are simulated from lag = −4 to lag = 0 years (Figs. 9c–e), which also are the regions of large SSS anomalies (Figs. 8c–e). Because the positive SST anomalies observed in these regions reduce the surface density, the higher surface density must be due to the anomalously high SSSs. In response to the enhanced density, the MLD increases in the deep convection sites of the NA (Figs. 8k–m). Larger MLD implies intensified deep convection, which in turn strengthens the AMOC (Figs. 5a–i). After lag = 0 years, the surface density begins to decline in the sinking region (Figs. 9f–i), which is presumably due to the weakening SPG (Figs. 5o–r), and MLD anomalies begin to reduce (Figs. 9o–r). The MLD anomalies south of Greenland become negative at lag = +4 years (Fig. 9p), which will slow the AMOC.

To assess the relative importance of the different deep convection sites on the ocean circulation two MLD indices are

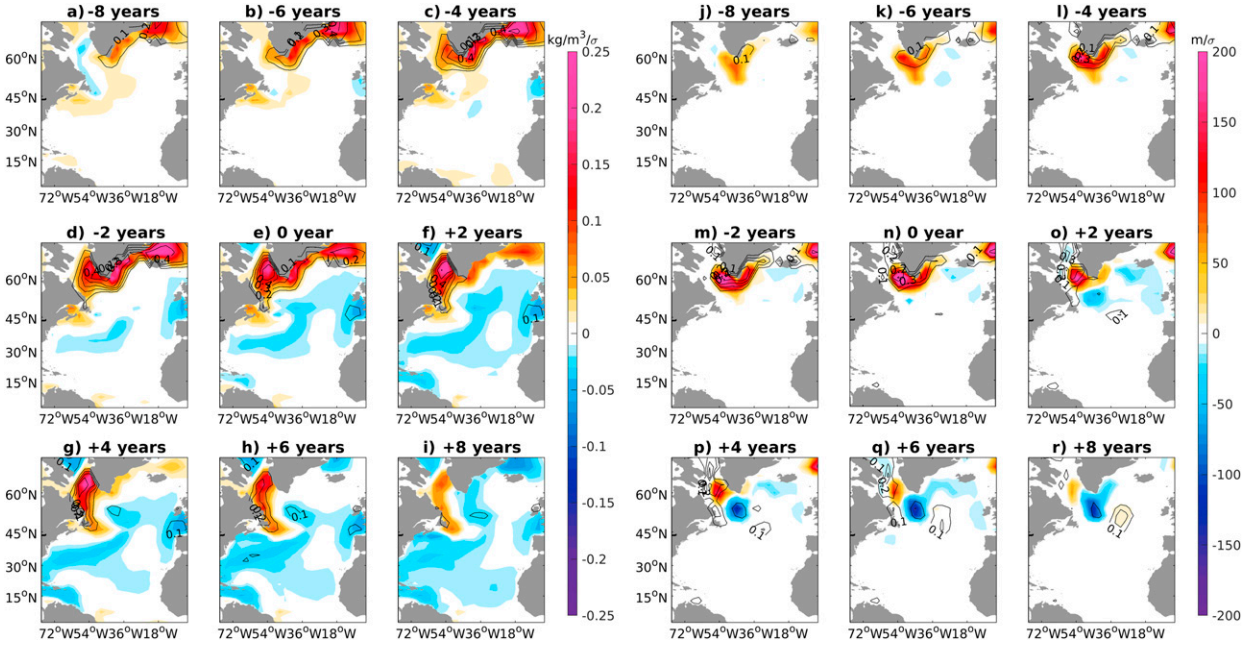

FIG. 9. (a)–(i) Regression maps of sea surface density upon PC1r, and (j)–(r) of the mixed layer depth (MLD) from lag = −8 to lag = +8 years (at 2-yr intervals). Regression coefficients are calculated based on one standard deviation (σ) of PC1r. Color indicates the regressions and contours indicate explained variances (CI is 0.1).

defined, whereby the definition is guided by regressing the MLD upon PC1r (Fig. 10a). A south Greenland index (S-GI) is defined as the area average of the MLD over the Irminger Sea and Labrador Sea (box A) and a Greenland Sea index (GSI) as the area average of the MLD over the Greenland Sea (box B). The SPG index and the AMOC index are regressed upon the two MLD indices (Figs. 10b and 10c, respectively). Both ocean circulation indices are significantly related to the MLD in the two regions, consistent with the MLD regressions upon PC1r (Fig. 9). We conclude that both deep convection regions are important in driving the SPG and the AMOC, whereby the S-GI region (box A) appears to have a stronger influence on the multidecadal ocean circulation variability. The SPG index approximately varies in phase with whereas the AMOC index lags the MLD anomalies in the two deep convection regions, where the time lags between the MLD indices and the AMOC index are consistent with previous modeling studies (Msadek and Frankignoul 2009; Danabasoglu 2008).

A stronger AMOC transports more heat from the subtropics northward into the upper midlatitude and subpolar NA (Msadek et al. 2013). Specifically, the NAC component of the AMOC advects more warm and salty water from the subtropical gyre into the eastern part of the SPG, as already suggested by the SST and SSS (Figs. 6a–i and 8a–i, respectively). The top 700-m ocean heat content (OHC) regression maps depict a slow transition from negative (Fig. 11a) to positive

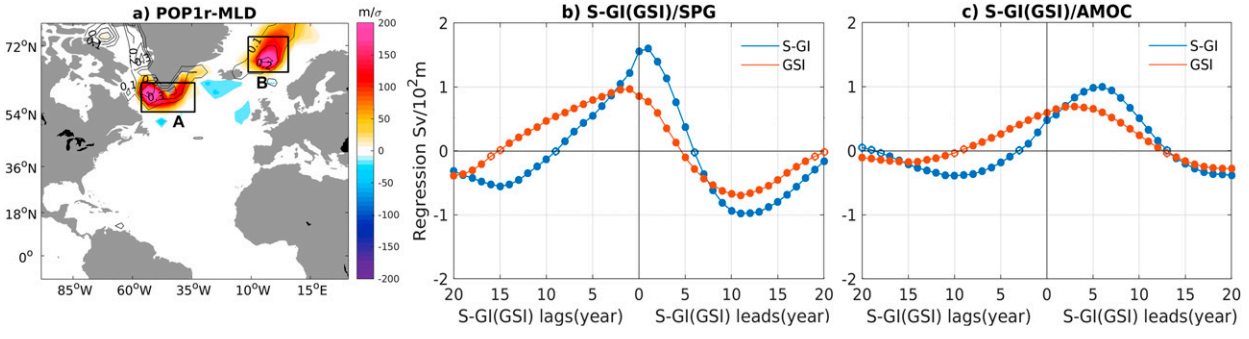

FIG. 10. (a) Regression map of MLD upon PC1r at lag = 0 years. Regression coefficients are calculated based on one standard deviation (σ) of PC1r. Color indicates the regressions and contours indicate explained variances (CI is 0.1). The South Greenland MLD index (S-GI) is defined as the area average over box A and the Greenland Sea MLD index (GSI) as the area average over box B. (b) Lag-regression functions between the SPG index and S-GI (blue curve) and GSI (orange curve). Filled dots indicate that the correlations are significant at the 95% level. (c) As in (b), but for the AMOC index.

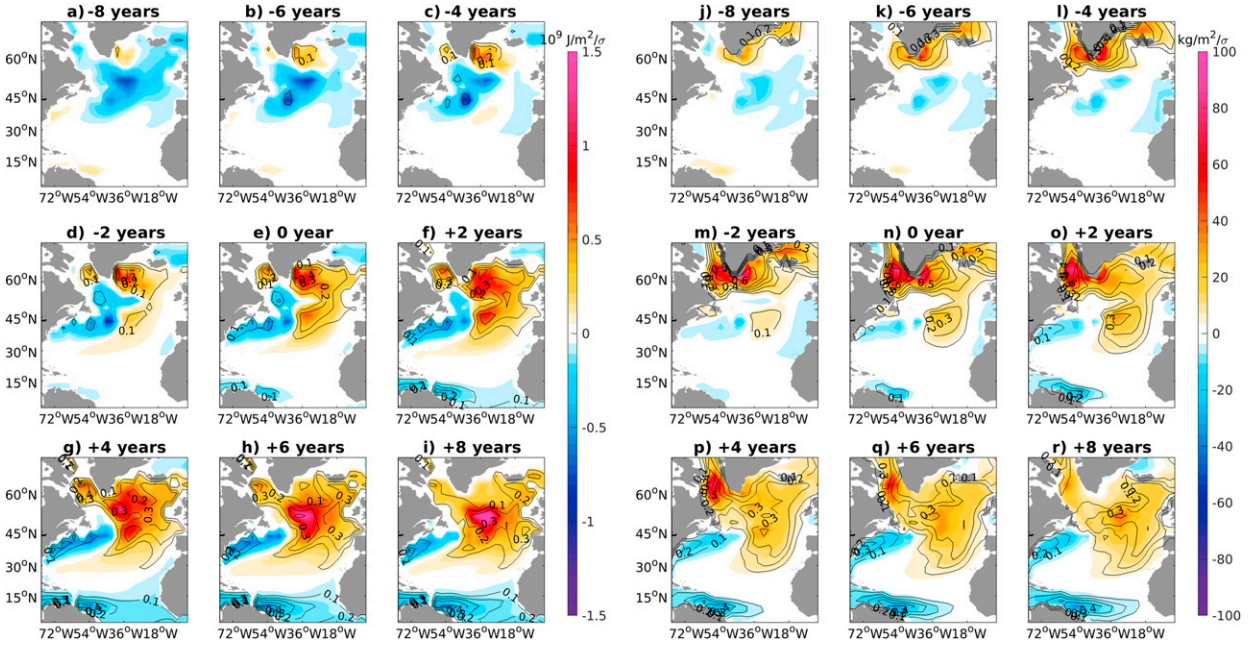

FIG. 11. (a)–(i) Regression maps of upper-ocean (0–700 m) heat content (OHC) upon PC1r, and (j)–(r) of the upper-ocean (0–700 m) salt content (OSC) from lag = −8 to lag = +8 years (at 2-yr intervals). Regression coefficients are calculated based on one standard deviation (σ) of PC1r. Color indicates the regressions and contours indicate explained variances (CI is 0.1).

anomalies (Fig. 11i) in the eastern part of the midlatitude and subpolar NA. This transition is due to the strengthening AMOC. We note that the dipole OHC anomalies, with negative anomalies in the southwest and positive anomalies in the northeast, observed from lag = 0 to lag = +8 years (Figs. 11e–i), are also typical of an anomalously strong AMOC in another climate model (Zhang 2008). The reverse pattern would be characteristic of an AMOC slowing, as suggested by a set of climate models (Saba et al. 2016). This relationship between weak AMOC and reduced OHC also exists in the KCM version used here, as described by Latif et al. (2019), who discuss fast decadal AMOC-slowing events.

The top 700-m ocean salt content (OSC) exhibits large positive anomalies in the deep convection sites of the NA from lag = −4 to lag = 0 years (Figs. 11l–n). These OSC anomalies are instrumental in driving the stronger AMOC given the opposing influence of the positive OHC anomalies on upper-ocean density (Figs. 11c–e).

In Fig. 12, we depict the regression maps of the sea surface height (SSH; Figs. 12a–i) and top 700-m ocean dynamic height (ODH; Figs. 12j–r) anomalies. Although SSH is an ocean surface parameter, it integrates ocean variability from bottom to surface and is connected to the ocean interior changes (e.g., three-dimensional large-scale ocean circulation). From lag = −4 to lag = 0 years, the SSH anomalies are strongly negative in the sinking region of the NA (Figs. 12c–e). The changes in the SSH can result either from changes in the mass or mean density of the water column. As mass change by the FW is small, the negative SSH anomalies represent the increased formation of North Atlantic Deep Water (NADW), consistent with the MLD anomalies (Figs. 9l–n). The NADW is exported southward along the western boundary, as seen by the negative SSH anomalies off the coast of North America, and eventually reaches the tropical Atlantic exhibiting negative SSH anomalies from lag = +2 years onward (Figs. 12f–i). To the east of the negative SSH anomalies, positive SSH anomalies start to develop around lag = 0 (Fig. 12e). While the negative SSH anomalies are associated with the southward flowing deep cold water branch of the AMOC, the positive SSH anomalies are linked to the upper northward flowing warm water branch of the AMOC. The upper AMOC branch is emphasized by the top 700-m depth-integrated ODH anomalies that were calculated directly from the hydrostatic balance with referenced pressure level of 2000 dbar (Figs. 12n–r). Because the ODH is determined by the dynamical balance associated with ocean density distribution, it can show the temperature and salinity variations impacts. The ODH anomalies here must be due to the OHC anomalies (Figs. 11e–i), which exhibit a great resemblance regarding the spatial pattern. Moreover, the OSC anomalies are positive, as pointed out above (Figs. 11n–r), and thus cannot explain the ODH anomalies.

At lag = +8 years, the phase reversal is almost completed: the positive ODH anomalies in the north give rise to a weaker SPG. At this time, the SLP and wind stress anomalies over the SPG region are relatively small (Figs. 7i,r), as they are at lag = −8 years. The weaker SPG reduces the salinity transport into the sinking region of the NA, which lowers the SSS and surface density, and in turn the MLD (Fig. 9). Finally, as reduced MLD is an indicator of less intense oceanic deep convection, the AMOC will slow with a time delay.

The important processes and time scales involved in the multidecadal variability over the NA, as described by POP1, are summarized schematically in Fig. 13. First, there is a fast

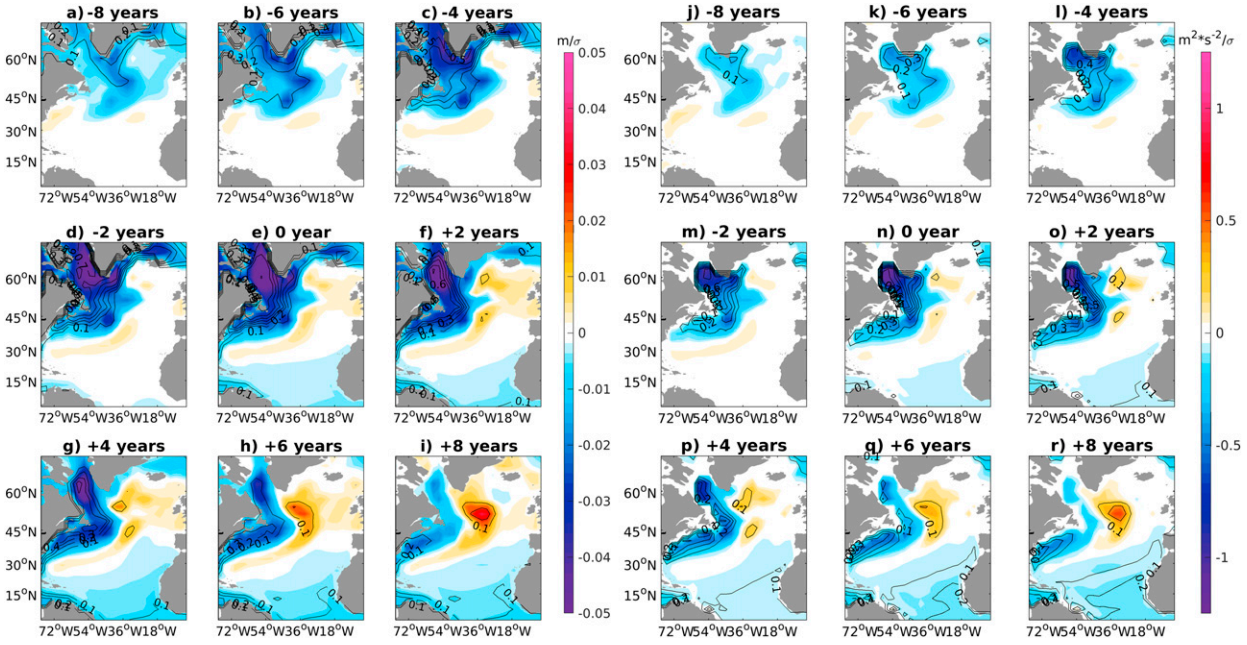

FIG. 12. (a)–(i) Regression maps of sea surface height (SSH) upon PC1r, and (j)–(r) of the upper-ocean (0–700 m) dynamic height referenced to 2000 dbar (ODH) from lag = −8 to lag = +8 years (at 2-yr intervals). Regression coefficients are calculated based on one standard deviation (σ) of the PC1r. Color indicates the regressions, and contours indicate explained variances (CI is 0.1).

positive ocean–atmosphere feedback involving the SPG, SST, SLP, and wind stress (curl). We infer from the regression maps that the positive feedback operates for about 4 years, from lag = −6 to lag = −2 years. The sequence of processes associated with the positive ocean–atmosphere feedback can be described as follows: the enhanced SPG drives positive SST anomalies south of Greenland through increased oceanic heat advection from the south, noting that the surface heat fluxes act as a damping on the SST anomalies. The positive SST anomalies drive a low pressure SLP anomaly that is centered over southern Greenland. The rather persistent and localized low pressure anomaly goes along with positive wind stress curl anomalies that add cyclonic vorticity to the ocean, thereby further intensifying the SPG.

Second, there is a slow adjustment of the AMOC to the density changes in the NA's sinking region that provides the delayed negative feedback necessary for the oscillation. We note, however, that there is some overlap of the fast and slow feedback processes. The change in the AMOC influences the SPG in a way eventually bringing about the phase reversal by enhancing the upper ocean heat content in the subpolar NA, which weakens the SPG. In response, the upper ocean salinity transport into the NA's sinking region diminishes and upper ocean density reduces. According to the POP clock (1), the evolution from an anomalously strong AMOC to a "normal" AMOC is described by the transition from POP1r (lag = 0 years in the regressions) to the negative of POP1i, which takes a quarter of the rotation period (i.e., about a decade). It is the SPG that connects AMOC change with oceanic deep convection, whereby the latter drives the AMOC that in turn influences the SPG. We infer from cross-correlation analysis that the SPG index leads the AMOC index by about 5 years (not shown), which together with the AMOC's adjustment time scale of about a decade gives rise to the multidecadal periodicity. Additionally, the coupled ocean–atmosphere feedback between the SST and wind stress (curl) extends the multidecadal variability into longer time scales.

h. Stochastic forcing of the multidecadal oscillation

On the one hand, the atmosphere responds to the SST changes south of Greenland as part of the multidecadal variability linked to POP1, as indicated, for example, by the near-surface wind divergence anomalies over southern Greenland that are significantly correlated with the SST anomalies. The atmospheric response acts as a damping on the multidecadal SST anomalies, as shown by the corresponding surface heat flux anomalies. In the following, we show that on the other hand, the stochastic heat flux forcing by the atmosphere over the subpolar NA is driver of the multidecadal variability and essential to continuously exciting POP1 exhibiting a decay time of about a decade that is considerably smaller than the rotation period of 38 years.

Previous studies suggested that the NAO, which is the dominant mode of atmospheric variability over the NA sector in winter, is an important driver of low-frequency ocean circulation variability through associated heat flux variability (e.g., Eden and Jung 2001; Mecking et al. 2014; Delworth and Zeng 2016). We apply an EOF analysis to the KCM's winter-mean (DJFM) net surface-heat flux anomalies over the extratropical NA (20°–70°N, 90°W–40°E). The first EOF ($EOF1_{Qnet}$; Fig. 14a) accounting for 24.8% of the total variance is closely related to the model's winter NAO,

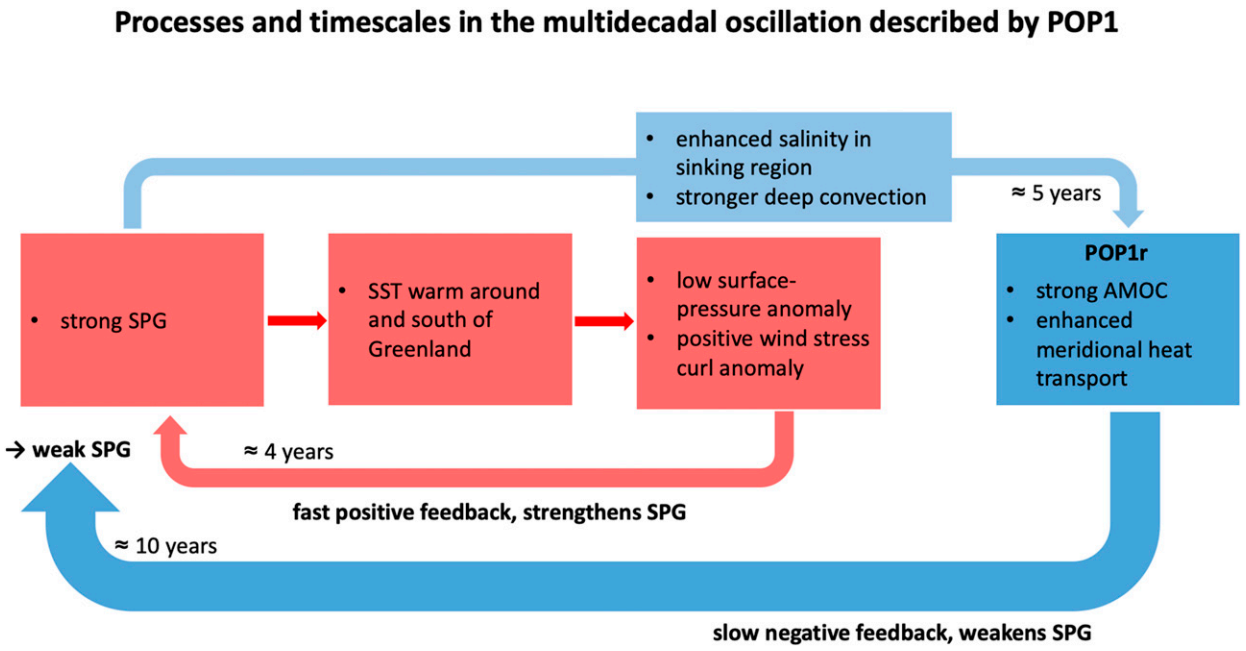

FIG. 13. Schematic diagram of the processes and time scales involved in the multidecadal oscillation described by the leading POP mode (POP1). The fast positive ocean–atmosphere feedback (red color) involving the SPG, SST, SLP, and wind stress (curl) operates for about 4 years. Enhanced SPG drives positive SST anomalies around south of Greenland through increased oceanic heat advection from the south, in turn driving a low pressure SLP anomaly centered over southern Greenland. The positive wind stress curl anomaly associated with the low pressure anomaly adds cyclonic vorticity to the ocean, thereby further intensifying the SPG. The delayed negative feedback is shown in the blue color. The SPG leads AMOC by about 5 years due to the density changes in the sinking region that are forced by the SPG. Anomalously strong AMOC influences the SPG by enhancing the upper-ocean heat content in the subpolar NA, which weakens the SPG. In response, the upper-ocean salinity transport into the sinking region diminishes and upper-ocean density reduces. According to the POP clock (1), the evolution from an anomalously strong AMOC to a "normal" AMOC is described by the transition from POP1r (lag = 0 years in the regressions) to the negative of POP1i (approximately lag = +8 years).

with a correlation coefficient of the corresponding principal component ($PC1_{Qnet}$) with the wintertime NAO index amounting to 0.83. Further, a cross-spectral analysis between the two time series reveals highly significant squared coherence over a broad range of time scales with zero phase difference (Fig. 15a). $EOF1_{Qnet}$ exhibits a tripolar pattern, which is consistent with observations when the heat fluxes are caused by the positive phase of the NAO (Czaja and Marshall 2001). The negative heat flux anomalies (enhanced oceanic heat loss) over the Labrador Sea are most important here, as they were shown to drive the AMOC in a number of climate models and also in the KCM (Park et al. 2016). The power spectrum of $PC1_{Qnet}$ is consistent with white noise, exhibiting almost the same level of variance across time scales (Fig. 14b). We note the statistically significant multidecadal peak (relative to white noise) in the spectrum of $PC1_{Qnet}$, which indicates that the atmospheric response to the multidecadal SST variability projects on the NAO. However, the major SLP response is a more localized pattern over the southern Greenland area, as described above (Fig. 7).

Next, cross-spectral analysis is performed between $PC1_{Qnet}$ and the AMOC index (Fig. 15b). The two indices only exhibit large squared coherence near the rotation period of POP1 with a phase difference close to zero, indicating an equilibrium response of the AMOC at this time scale. At the other frequencies, the squared coherence is relatively small. Thus, the AMOC only responds to the heat flux variability associated with $EOF1_{Qnet}$ in a narrow frequency range. Such behavior is consistent with the stochastic excitation of a multidecadal eigenmode by the nearly white noise heat flux forcing linked to $EOF1_{Qnet}$ that is related to the NAO. The results of the cross-spectral analysis are similar when replacing the AMOC index by PC1r (Fig. 15c), the POP coefficient time series of POP1r, which, as noted above, is closely related to the AMOC index with a correlation coefficient of 0.8 at zero lag. The cross-spectral analysis between $PC1_{Qnet}$ and the SPG index (Fig. 15d) also exhibits a squared-coherence peak near the rotation period but with a phase shift in the range of $\pi/4$ and $\pi/2$ (i.e., 4–8 years), with the SPG leading. This is consistent with the SPG leading the AMOC by several years and the atmosphere quickly responding to the SST anomalies south of Greenland, as shown above.

4. Summary and discussion

In this study, we investigate a multimillennial preindustrial control integration of a version of the Kiel Climate Model (KCM) and describe the mechanism underlying the simulated multidecadal climate variability in the North Atlantic (NA)

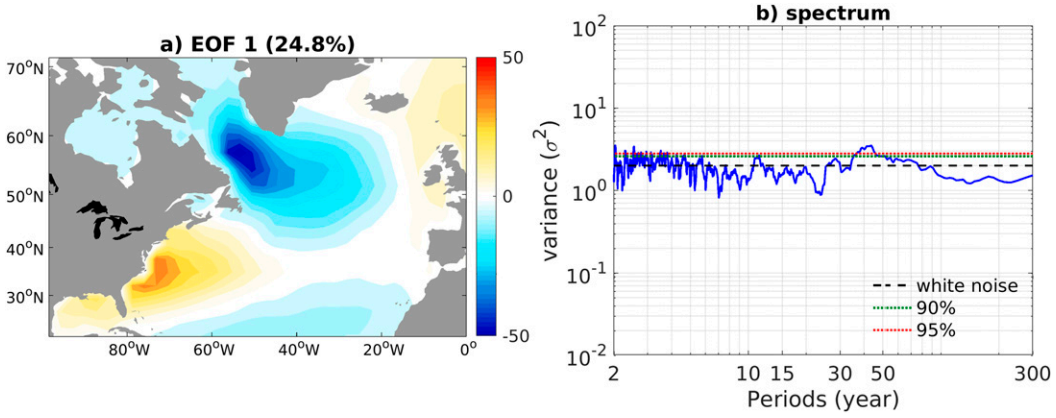

FIG. 14. (a) Pattern of the leading EOF of winter-mean (DJFM) net surface-heat flux anomalies from the KCM's control run. (b) Power spectrum (σ^2) of the corresponding PC1 (blue curve), 90% confidence level (green dotted curve), and 95% confidence level (red dotted curve) with reference to a fitted white-noise process (black dashed curve). The time series has been normalized by its standard deviation prior to computing the spectrum.

sector. Specifically, we address the interactions between the subpolar gyre (SPG), the Atlantic meridional overturning circulation (AMOC), and the atmosphere. A principal oscillation pattern (POP) analysis is applied jointly to the barotropic streamfunction (PSI), meridional overturning streamfunction (MOC), and sea level pressure (SLP) to derive the leading modes of coupled variability in the NA sector. The leading POP mode accounting for 23.7% of the joint variance, which only is described in this study, is multidecadal with a rotation period (cycle length) of 38 years and a damping time of about a decade. We find that in the KCM, the interactions among the SPG, AMOC, and atmosphere are essential to understanding the nature of the multidecadal climate variability in the NA region. In principle, the eigenmode can be understood as an ''ocean-only'' mode, but the atmosphere plays an essential role by considerably enhancing the multidecadal variability.

The SPG is important in linking the AMOC to the atmosphere. Changes in SPG strength have two effects. First, they drive SST changes south of Greenland and second, they control the salinity transport into the sinking region of the NA. The SST change influences the atmosphere, where the atmospheric response primarily consists of a localized SLP anomaly centered over the southern Greenland area. The wind stress curl anomaly associated with the SLP change reinforces the SPG change. Thus, the SPG, SST, SLP, and wind stress form a positive feedback loop, and this amplifying feedback is important in enhancing and maintaining the multidecadal variability, as shown by a sensitivity experiment in which the wind stress feedback is inhibited.

Second, the change in the salinity transport in response to the altered SPG influences the upper-ocean density and in turn oceanic deep convection and, with a time delay, the AMOC. The adjustment of the AMOC provides the delayed negative feedback, which drives the phase reversal from one phase of the oscillation to the other by influencing the SPG in a manner that the resulting change is opposite to the initial SPG change. Some of the elements of the multidecadal variability observed in the KCM have also been described from a version of the Hadley Centre climate model by Dong and Sutton (2005) and in other climate models. To our knowledge, however, the three-way interaction between the SPG, the AMOC, and the atmosphere, which operates in the KCM, has not been previously described.

The mechanism in this study is different to that described in previous studies in which the AMOC variability is related to westward propagating baroclinic Rossby waves (e.g., Sévellec and Fedorov 2013). When the density anomalies associated with the Rossby waves reach the western boundary, the resulting zonal density gradient will lead to an AMOC anomaly according to the thermal wind balance. This relationship, however, cannot be established in observations, and climate models suggest it operates on shorter time scales than multidecadal. In our study, although a similar pattern is observed, for example in the OHC (Fig. 11), the dipole is not related to westward propagating density anomalies. The density gradient may influence the AMOC, but it is not the main driver of the AMOC.

This study supports the interpretation of the KCM's multidecadal variability in the NA region as a stochastically forced eigenmode. Latif et al. (2002) introduced a concept composed of three stochastic models: the simple first-order model, in which the ocean mixed layer is stochastically forced by the surface fluxes; the stochastic excitation of an eigenmode of the ocean circulation; and the stochastic excitation of an eigenmode of the coupled ocean–atmosphere system. The multidecadal variability described here seems to belong to the second category, where the stochastic forcing, exhibiting nearly white-noise character, is provided by heat flux variability linked to the NAO. However, ocean–atmosphere coupling over the southern Greenland area is key to enhancing the level of multidecadal variability, especially in SST, and extending the variability to longer time scales.

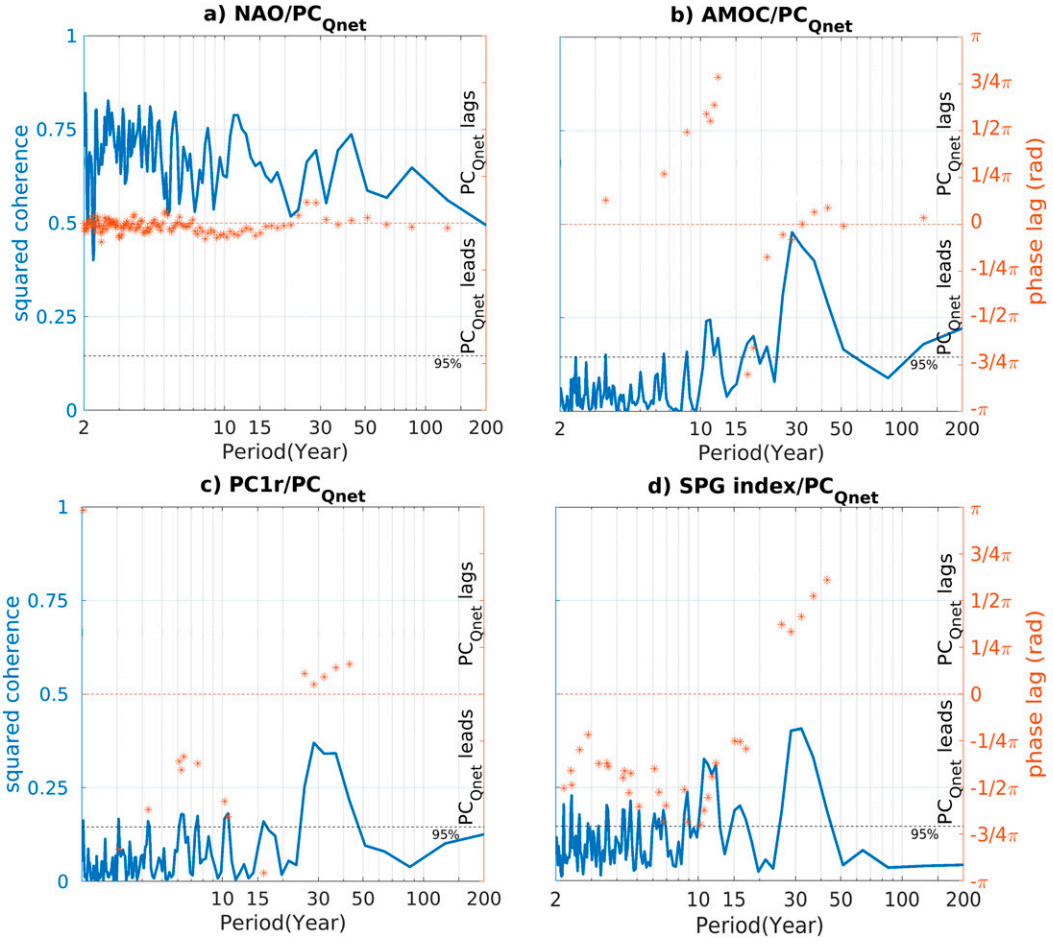

FIG. 15. (a) Squared coherence (blue curve) and phase spectrum (orange stars) between the winter-NAO index (DJFM) and the PC of the leading net surface-heat flux EOF (DJFM), labeled PC_{Qnet}. The phase only is shown when the squared coherence exceeds the 95% confidence level (black dotted line). A phase lag of 0 indicates that the two time series vary in phase (orange dotted line), while a positive (negative) phase lag indicates that PC_{Qnet} lags (leads). (b) As in (a), but with the AMOC index. (c) As in (a), but with the real-part POP coefficient time series, PC1r. (d) As in (a), but with the SPG index.

This study supports previous studies (e.g., Delworth et al. 2017; Sun et al. 2018; Zhang et al. 2019), suggesting that the ocean circulation is crucial in the generation of the multidecadal variability in the NA region. However, climate models simulate a wide range of multidecadal variability with varying spatial patterns, time scales, and mechanisms. Since instrumental observations are limited, in the ocean and in the atmosphere, it is not possible to verify by data the existence of a multidecadal eigenmode in the NA sector and its underling mechanism as simulated by the KCM, specifically the three-way interaction between the SPG, AMOC, and atmosphere.

Acknowledgments. This work was supported by a Ph.D. scholarship funded jointly by the China Scholarship Council (CSC). Support from the InterDec Project (Grant Agreement 01LP1609B) and the project RACE (Grant Agreement 03F0651B) funded by the German Ministry of Education and Research (BMBF) is acknowledged. We thank to Dr. Taewook Park at Korea Polar Research Institute for conducting the model experiments and providing the data. We thank the three anonymous reviewers for their valuable comments on our manuscript.

REFERENCES

Allan, R., and T. Ansell, 2006: A new globally complete monthly historical gridded mean sea level pressure dataset (HadSLP2): 1850–2004. *J. Climate*, **19**, 5816–5842, https://doi.org/10.1175/JCLI3937.1.

Álvarez-García, F., M. Latif, and A. Biastoch, 2008: On multidecadal and quasi-decadal North Atlantic variability. *J. Climate*, **21**, 3433–3452, https://doi.org/10.1175/2007JCLI1800.1.

Ba, J., and Coauthors, 2014: A multi-model comparison of Atlantic multidecadal variability. *Climate Dyn.*, **43**, 2333–2348, https://doi.org/10.1007/s00382-014-2056-1.

Bellomo, K., L. N. Murphy, M. A. Cane, A. C. Clement, and L. M. Polvani, 2018: Historical forcings as main drivers of the Atlantic multidecadal variability in the CESM large ensemble.

Climate Dyn., **50**, 3687–3698, https://doi.org/10.1007/s00382-017-3834-3.

Bjerknes, J., 1964: Atlantic air–sea interaction. *Advances in Geophysics*, Vol. 10, Academic Press, 1–82, https://doi.org/10.1016/S0065-2687(08)60005-9.

Bloomfield, P., 2004: *Fourier Analysis of Time Series: An Introduction*. John Wiley & Sons, 288 pp.

Bock, L., and Coauthors, 2020: Quantifying progress across different CMIP phases with the ESMValTool. *J. Geophys. Res. Atmos.*, 125, e2019JD032321, https://doi.org/10.1029/2019JD032321.

Booth, B. B., N. J. Dunstone, P. R. Halloran, T. Andrews, and N. Bellouin, 2012: Aerosols implicated as a prime driver of twentieth-century North Atlantic climate variability. *Nature*, **484**, 228–232, https://doi.org/10.1038/nature10946.

Bryden, H. L., W. E. Johns, B. A. King, G. McCarthy, E. L. McDonagh, B. I. Moat, and D. A. Smeed, 2020: Reduction in ocean heat transport at 26°N since 2008 cools the eastern subpolar gyre of the North Atlantic Ocean. *J. Climate*, **33**, 1677–1689, https://doi.org/10.1175/JCLI-D-19-0323.1.

Clement, A., K. Bellomo, L. N. Murphy, M. A. Cane, T. Mauritsen, G. Rädel, and B. Stevens, 2015: The Atlantic Multidecadal Oscillation without a role for ocean circulation. *Science*, **350**, 320–324, https://doi.org/10.1126/science.aab3980.

Cunningham, S. A., and Coauthors, 2007: Temporal variability of the Atlantic meridional overturning circulation at 26.5°N. *Science*, **317**, 935–938, https://doi.org/10.1126/science.1141304.

Czaja, A., and J. Marshall, 2001: Observations of atmosphere–ocean coupling in the North Atlantic. *Quart. J. Roy. Meteor. Soc.*, **127**, 1893–1916, https://doi.org/10.1002/qj.49712757603.

——, C. Frankignoul, S. Minobe, and B. Vannière, 2019: Simulating the midlatitude atmospheric circulation: What might we gain from high-resolution modeling of air–sea interactions? *Curr. Climate Change Rep.*, **5**, 390–406, https://doi.org/10.1007/s40641-019-00148-5.

Danabasoglu, G., 2008: On multidecadal variability of the Atlantic meridional overturning circulation in the Community Climate System Model version 3. *J. Climate*, **21**, 5524–5544, https://doi.org/10.1175/2008JCLI2019.1.

Delworth, T., and F. Zeng, 2016: The impact of the North Atlantic Oscillation on climate through its influence on the Atlantic meridional overturning circulation. *J. Climate*, **29**, 941–962, https://doi.org/10.1175/JCLI-D-15-0396.1.

——, S. Manabe, and R. Stouffer, 1993: Interdecadal variations of the thermohaline circulation in a coupled ocean–atmosphere model. *J. Climate*, **6**, 1993–2011, https://doi.org/10.1175/1520-0442(1993)006<1993:IVOTTC>2.0.CO;2.

——, F. Zeng, L. Zhang, R. Zhang, G. A. Vecchi, and X. Yang, 2017: The central role of ocean dynamics in connecting the North Atlantic Oscillation to the extratropical component of the Atlantic multidecadal oscillation. *J. Climate*, **30**, 3789–3805, https://doi.org/10.1175/JCLI-D-16-0358.1.

Dong, B., and R. Sutton, 2005: Mechanism of interdecadal thermohaline circulation variability in a coupled ocean–atmosphere GCM. *J. Climate*, **18**, 1117–1135, https://doi.org/10.1175/JCLI3328.1.

Ebisuzaki, W., 1997: A method to estimate the statistical significance of a correlation when the data are serially correlated. *J. Climate*, **10**, 2147–2153, https://doi.org/10.1175/1520-0442(1997)010<2147:AMTETS>2.0.CO;2.

Eden, C., and T. Jung, 2001: North Atlantic interdecadal variability: Oceanic response to the North Atlantic Oscillation (1865–1997). *J. Climate*, **14**, 676–691, https://doi.org/10.1175/1520-0442(2001)014<0676:NAIVOR>2.0.CO;2.

Escudier, R., J. Mignot, and D. Swingedouw, 2013: A 20-year coupled ocean–sea ice–atmosphere variability mode in the North Atlantic in an AOGCM. *Climate Dyn.*, **40**, 619–636, https://doi.org/10.1007/s00382-012-1402-4.

Folland, C. K., T. N. Palmer, and D. E. Parker, 1986: Sahel rainfall and worldwide sea temperatures, 1901–85. *Nature*, **320**, 602–607, https://doi.org/10.1038/320602a0.

Frankcombe, L. M., H. A. Dijkstra, and A. von der Heydt, 2008: Sub-surface signatures of the Atlantic Multidecadal Oscillation. *Geophys. Res. Lett.*, **35**, L19602, https://doi.org/10.1029/2008GL034989.

Frankignoul, C., 1985: Sea surface temperature anomalies, planetary waves, and air–sea feedback in the middle latitudes. *Rev. Geophys.*, **23**, 357–390, https://doi.org/10.1029/RG023i004p00357.

Gillett, N., 2005: Northern Hemisphere circulation. *Nature*, **437**, 496, https://doi.org/10.1038/437496a.

Gilman, D. L., F. J. Fuglister, and J. M. Mitchell, 1963: On the power spectrum of "red noise". *J. Atmos. Sci.*, **20**, 182–184, https://doi.org/10.1175/1520-0469(1963)020<0182:OTPSON>2.0.CO;2.

Goldenberg, S. B., C. W. Landsea, A. M. Mestas-Nuñez, and W. M. Gray, 2001: The recent increase in Atlantic hurricane activity: Causes and implications. *Science*, **293**, 474–479, https://doi.org/10.1126/science.1060040.

Grossmann, I., and P. J. Klotzbach, 2009: A review of North Atlantic modes of natural variability and their driving mechanisms. *J. Geophys. Res.*, **114**, D24107, https://doi.org/10.1029/2009JD012728.

Gulev, S. K., M. Latif, N. Keenlyside, W. Park, and K. P. Koltermann, 2013: North Atlantic Ocean control on surface heat flux on multidecadal timescales. *Nature*, **499**, 464–467, https://doi.org/10.1038/nature12268.

Hasselmann, K., 1976: Stochastic climate models Part I. Theory. *Tellus*, **28**, 473–485, https://doi.org/10.1111/j.2153-3490.1976.tb00696.x.

——, 1988: PIPs and POPs: The reduction of complex dynamical systems using principal interaction and oscillation patterns. *J. Geophys. Res.*, **93**, 11015–11 021, https://doi.org/10.1029/JD093iD09p11015.

Hurrell, J. W., Y. Kushnir, G. Ottersen, and M. Visbeck, 2013: An overview of the North Atlantic Oscillation. *The North Atlantic Oscillation. Geophys. Monogr.*, Vol. 134, Amer. Geophys. Union, 1–35, https://doi.org/10.1029/GM134.

Kanzow, T., and Coauthors, 2007: Observed flow compensation associated with the MOC at 26.5°N in the Atlantic. *Science*, **317**, 938–941, https://doi.org/10.1126/science.1141293.

Knight, J. R., R. J. Allan, C. K. Folland, M. Vellinga, and M. E. Mann, 2005: A signature of persistent natural thermohaline circulation cycles in observed climate. *Geophys. Res. Lett.*, **32**, L20708, https://doi.org/10.1029/2005GL024233.

Koul, V., and Coauthors, 2020: Unraveling the choice of the North Atlantic subpolar gyre index. *Sci. Rep.*, **10** (1), 1–12, https://doi.org/10.1038/s41598-020-57790-5.

Kushnir, Y., 1994: Interdecadal variations in North Atlantic sea surface temperature and associated atmospheric conditions. *J. Climate*, **7**, 141–157, https://doi.org/10.1175/1520-0442(1994)007<0141:IVINAS>2.0.CO;2.

——, W. A. Robinson, I. Bladé, N. M. J. Hall, S. Peng, and R. Sutton, 2002: Atmospheric GCM response to extratropical SST anomalies: Synthesis and evaluation. *J. Climate*, **15**, 2233–2256, https://doi.org/10.1175/1520-0442(2002)015<2233:AGRTES>2.0.CO;2.

Latif, M., and N. S. Keenlyside, 2011: A perspective on decadal climate variability and predictability. *Deep-Sea Res. II*, **58**, 1880–1894, https://doi.org/10.1016/j.dsr2.2010.10.066.

——, A. Timmermann, A. Grötzner, C. Eckert, and R. Voss, 2002: On North Atlantic interdecadal variability: A stochastic view. *Ocean Forecasting,* N. Pinardi, and J. Woods, Eds., Springer, 149–177.

——, and Coauthors, 2004: Reconstructing, monitoring, and predicting multidecadal-scale changes in the North Atlantic thermohaline circulation with sea surface temperature. *J. Climate*, **17**, 1605–1614, https://doi.org/10.1175/1520-0442(2004)017<1605:RMAPMC>2.0.CO;2.

——, M. Collins, H. Pohlmann, and N. Keenlyside, 2006: A review of predictability studies of the Atlantic sector climate on decadal time scales. *J. Climate*, **19**, 5971–5987, https://doi.org/10.1175/JCLI3945.1.

——, T. Park, and W. Park, 2019: Decadal Atlantic meridional overturning circulation slowing events in a climate model. *Climate Dyn.*, **53**, 1111–1124, https://doi.org/10.1007/s00382-019-04772-7.

Locarnini, R. A., and Coauthors, 2018: *Temperature*. Vol. 1, *World Ocean Atlas 2018*, A. Mishonov, Technical Ed., NOAA Atlas NESDIS 81, 52 pp.

Lohmann, K., H. Drange, and M. Bentsen, 2009: Response of the North Atlantic subpolar gyre to persistent North Atlantic oscillation like forcing. *Climate Dyn.*, **32**, 273–285, https://doi.org/10.1007/s00382-008-0467-6.

Lorenz, E. N., 1956: Empirical orthogonal functions and statistical weather prediction. Statistical Forecast Project Rep. 1, Dept. of Meteorology, Massachusetts Institute of Technology, 49 pp.

Madec, G., 2008: NEMO ocean engine. Note du Pole de modélisation, Institut Pierre-Simon Laplace (IPSL), Tech. Rep. 27, 209 pp.

Mecking, J. V., N. S. Keenlyside, and R. J. Greatbatch, 2014: Stochastically-forced multidecadal variability in the North Atlantic: A model study. *Climate Dyn.*, **43**, 271–288, https://doi.org/10.1007/s00382-013-1930-6.

Menary, M. B., D. L. Hodson, J. I. Robson, R. T. Sutton, R. A. Wood, and J. A. Hunt, 2015: Exploring the impact of CMIP5 model biases on the simulation of North Atlantic decadal variability. *Geophys. Res. Lett.*, **42**, 5926–5934, https://doi.org/10.1002/2015GL064360.

Msadek, R., and C. Frankignoul, 2009: Atlantic multidecadal oceanic variability and its influence on the atmosphere in a climate model. *Climate Dyn.*, **33**, 45–62, https://doi.org/10.1007/s00382-008-0452-0.

——, W. E. Johns, S. G. Yeager, G. Danabasoglu, T. L. Delworth, and A. Rosati, 2013: The Atlantic meridional heat transport at 26.5°N and its relationship with the MOC in the RAPID array and the GFDL and NCAR coupled models. *J. Climate*, **26**, 4335–4356, https://doi.org/10.1175/JCLI-D-12-00081.1.

Muthers, S., C. Raible, E. Rozanov, and T. Stocker, 2016: Response of the AMOC to reduced solar radiation—The modulating role of atmospheric chemistry. *Earth Syst. Dyn.*, **7**, 877–892, https://doi.org/10.5194/esd-7-877-2016.

Ortega, P., J. Mignot, D. Swingedouw, F. Sévellec, and E. Guilyardi, 2015: Reconciling two alternative mechanisms behind bidecadal variability in the North Atlantic. *Prog. Oceanogr.*, **137**, 237–249, https://doi.org/10.1016/j.pocean.2015.06.009.

Otterå, O. H., M. Bentsen, H. Drange, and L. Suo, 2010: External forcing as a metronome for Atlantic multidecadal variability. *Nat. Geosci.*, **3**, 688–694, https://doi.org/10.1038/ngeo955.

Park, T., W. Park, and M. Latif, 2016: Correcting North Atlantic sea surface salinity biases in the Kiel Climate Model: Influences on ocean circulation and Atlantic multidecadal variability. *Climate Dyn.*, **47**, 2543–2560, https://doi.org/10.1007/s00382-016-2982-1.

Park, W., and M. Latif, 2008: Multidecadal and multicentennial variability of the meridional overturning circulation. *Geophys. Res. Lett.*, **35**, L22703, https://doi.org/10.1029/2008GL035779.

——, N. Keenlyside, M. Latif, A. Ströh, R. Redler, E. Roeckner, and G. Madec, 2009: Tropical Pacific climate and its response to global warming in the Kiel Climate Model. *J. Climate*, **22**, 71–92, https://doi.org/10.1175/2008JCLI2261.1.

Roeckner, E., and Coauthors, 2003: The atmospheric general circulation model ECHAM 5. Part I: Model description. MPI-Rep. 349, 127 pp.

Saba, V. S., and Coauthors, 2016: Enhanced warming of the northwest Atlantic Ocean under climate change. *J. Geophys. Res. Oceans*, **121**, 118–132, https://doi.org/10.1002/2015JC011346.

Saravanan, R., and J. C. McWilliams, 1997: Stochasticity and spatial resonance in interdecadal climate fluctuations. *J. Climate*, **10**, 2299–2320, https://doi.org/10.1175/1520-0442(1997)010<2299:SASRII>2.0.CO;2.

Scaife, A. A., and Coauthors, 2009: The CLIVAR C20C project: Selected twentieth century climate events. *Climate Dyn.*, **33**, 603–614, https://doi.org/10.1007/s00382-008-0451-1.

Sévellec, F., and A. V. Fedorov, 2013: The leading, interdecadal eigenmode of the Atlantic meridional overturning circulation in a realistic ocean model. *J. Climate*, **26**, 2160–2183, https://doi.org/10.1175/JCLI-D-11-00023.1.

Sun, C., J. Li, X. Li, J. Xue, R. Ding, F. Xie, and Y. Li, 2018: Oceanic forcing of the interhemispheric SST dipole associated with the Atlantic multidecadal oscillation. *Environ. Res. Lett.*, **13**, 074026, https://doi.org/10.1088/1748-9326/aacf66.

——, ——, F. Kucharski, J. Xue, and X. Li, 2019: Contrasting spatial structures of Atlantic multidecadal oscillation between observations and slab ocean model simulations. *Climate Dyn.*, **52**, 1395–1411, https://doi.org/10.1007/s00382-018-4201-8.

Sun, J., M. Latif, W. Park, and T. Park, 2020: On the interpretation of the North Atlantic averaged sea surface temperature. *J. Climate*, **33**, 6025–6045, https://doi.org/10.1175/JCLI-D-19-0158.1.

Sutton, R. T., G. D. McCarthy, J. Robson, B. Sinha, A. T. Archibald, and L. J. Gray, 2018: Atlantic multidecadal variability and the UK ACSIS program. *Bull. Amer. Meteor. Soc.*, **99**, 415–425, https://doi.org/10.1175/BAMS-D-16-0266.1.

Taylor, K. E., R. J. Stouffer, and G. A. Meehl, 2012: An overview of CMIP5 and the experiment design. *Bull. Amer. Meteor. Soc.*, **93**, 485–498, https://doi.org/10.1175/BAMS-D-11-00094.1.

te Raa, L. A., and H. A. Dijkstra, 2002: Instability of the thermohaline ocean circulation on interdecadal timescales. *J. Phys. Oceanogr.*, **32**, 138–160, https://doi.org/10.1175/1520-0485(2002)032<0138:IOTTOC>2.0.CO;2.

Thomson, S. I., and G. K. Vallis, 2018: Atmospheric response to SST anomalies. Part I: Background-state dependence, teleconnections, and local effects in winter. *J. Atmos. Sci.*, **75**, 4107–4124, https://doi.org/10.1175/JAS-D-17-0297.1.

Timmermann, A., M. Latif, R. Voss, and A. Grötzner, 1998: Northern hemispheric interdecadal variability: A coupled air–sea mode. *J. Climate*, **11**, 1906–1931, https://doi.org/10.1175/1520-0442-11.8.1906.

Ting, M., Y. Kushnir, and C. Li, 2014: North Atlantic multidecadal SST oscillation: External forcing versus internal variability. *J. Mar. Syst.*, **133**, 27–38, https://doi.org/10.1016/j.jmarsys.2013.07.006.

Toole, J. M., M. Andres, I. A. Le Bras, T. M. Joyce, and M. S. McCartney, 2017: Moored observations of the Deep Western Boundary Current in the NW Atlantic: 2004–2014. *J. Geophys. Res. Oceans*, **122**, 7488–7505, https://doi.org/10.1002/2017JC012984.

Valcke, S., E. Guilyardi, and C. Larsson, 2006: PRISM and ENES: A European approach to Earth system modelling. *Concurr. Comput.: Pract. Exper.*, **18**, 247–262, https://doi.org/10.1002/cpe.915.

von Storch, H., and F. W. Zwiers, 2001: *Statistical Analysis in Climate Research*. Cambridge University Press, 484 pp.

——, T. Bruns, I. Fischer-Bruns, and K. Hasselmann, 1988: Principal oscillation pattern analysis of the 30- to 60-day oscillation in general circulation model equatorial troposphere. *J. Geophys. Res.*, **93**, 11 022–11 036, https://doi.org/10.1029/JD093iD09p11022.

——, G. Bürger, R. Schnur, and J. S. von Storch, 1995: Principal oscillation patterns: A review. *J. Climate*, **8**, 377–400, https://doi.org/10.1175/1520-0442(1995)008<0377:POPAR>2.0.CO;2.

Welch, P. D., 1967: The use of fast Fourier transform for the estimation of power spectra: A method based on time averaging over short, modified periodograms. *IEEE Trans. Audio Electroacoust.*, **15**, 70–73, https://doi.org/10.1109/TAU.1967.1161901.

Weyer, W. and Coauthors, 2020: CMIP6 models predict significant 21st century decline of the Atlantic meridional overturning circulation. *Geophys. Res. Lett.*, **47**, e2019GL086075, https://doi.org/10.1029/2019GL086075.

Zantopp, R., J. Fischer, M. Visbeck, and J. Karstensen, 2017: From interannual to decadal: 17 years of boundary current transports at the exit of the Labrador Sea. *J. Geophys. Res. Oceans*, **122**, 1724–1748, https://doi.org/10.1002/2016JC012271.

Zhang, L., and C. Wang, 2013: Multidecadal North Atlantic sea surface temperature and Atlantic meridional overturning circulation variability in CMIP5 historical simulations. *J. Geophys. Res. Oceans*, **118**, 5772–5791, https://doi.org/10.1002/jgrc.20390.

Zhang, R., 2008: Coherent surface–subsurface fingerprint of the Atlantic meridional overturning circulation. *Geophys. Res. Lett.*, **35**, L20705, https://doi.org/10.1029/2008GL035463.

——, and T. L. Delworth, 2006: Impact of Atlantic multidecadal oscillations on India/Sahel rainfall and Atlantic hurricanes. *Geophys. Res. Lett.*, **33**, L17712, https://doi.org/10.1029/2006GL026267.

——, R. Sutton, G. Danabasoglu, Y. O. Kwon, R. Marsh, S. G. Yeager, D. E. Amrhein, and C. M. Little, 2019: A review of the role of the Atlantic meridional overturning circulation in Atlantic multidecadal variability and associated climate impacts. *Rev. Geophys.*, **57**, 316–375, https://doi.org/10.1029/2019RG000644.

Chapter 5 Natural variability prevalence in Atlantic Meridional Overturning since 1900

This chapter is a reprint of paper "*Natural variability prevalence in Atlantic Meridional Overturning since 1900*" submitted to Nature Climate Change.

Citation: Mojib Latif, Jing Sun, Martin Visbeck, and M. Hadi Bordbar (2021) " Natural variability prevalence in Atlantic Meridional Overturning since 1900 ", *Nature Climate Change*, under review.

Jing Sun's contributions to this publication:

She did the analysis, produced 6 out of 7 figures and 2 subfigures in the remaining figure. She wrote the manuscript together with her co-authors.

Natural variability prevalence in Atlantic Meridional Overturning since 1900

Mojib Latif*[1, 2], Jing Sun[1], Martin Visbeck[1, 2], and M. Hadi Bordbar[3]

[1]Geomar Helmholtz Centre for Ocean Research Kiel, Kiel, Germany

[2]Christian-Albrechts University Kiel, Kiel Germany

[3]Leibniz-Institut für Ostseeforschung Warnemünde – IOW, Rostock, Germany

*correspondence to mlatif@geomar.de

There is a debate about slowing of the Atlantic Meridional Overturning Circulation (AMOC), a key component of the global climate system. Some of the debate is around the sea surface temperature (SST) in parts of the subpolar North Atlantic that slightly cooled despite by far the largest part of the global surface ocean warmed. The cooling may reflect diminishing AMOC-related heat transport, projected by climate models should atmospheric greenhouse-gas concentrations continue to rise unabatedly. Ocean-transport observations indicating stable AMOC only started 25 years ago. SST is influenced by the AMOC on decadal timescales and beyond, and measured for more than a century. Here we show that Atlantic SST suggests prevalence of natural AMOC variability, and this is consistent with historical climate-model simulations predicting minor AMOC slowing. This study demonstrates the importance of systematic and sustained in-situ monitoring systems that can detect and attribute with high confidence an anthropogenic AMOC signal.

Global warming and AMOC

Anthropogenic global surface warming (global warming hereafter) is unequivocal and the humans are the main cause (IPCC, 2013; IPCC, 2014). The oceans are slowing global warming with adverse consequences for the marine ecosystems. For example, the oceans have taken up about one third of the total anthropogenic carbon dioxide (CO_2) emissions since the start of industrialization, causing ocean acidification (Dupont and Pörtner, 2013).

Moreover, the oceans have stored more than 90% of the heat trapped in the global climate system by the accumulation of greenhouse gases (GHGs) in the atmosphere, leading to more frequent and longer lasting marine heat waves (Oliver et al., 2018). Some of the global warming impacts, however, only slowly unfold in the ocean due to its large thermal and dynamical inertia. This concerns, for example, sea level rise and the response of the AMOC, a three-dimensional system of currents in the Atlantic Ocean with global climatic relevance (Broecker, 1991; Srokosz et al. 2012, R. Zhang et al. 2019).

The vast majority of climate models predict significant future AMOC slowing, if anthropogenic GHG-emissions continue to rise unabatedly (Schmittner et al., 2005; IPCC, 2013; Reintges et al., 2017; Menary and Wood, 2018; Weyer et al., 2020). Significant AMOC slowing would drive major climatic impacts such as shifting rainfall patterns on land (Liu et al., 2010), accelerated regional sea level rise (Levermann et al., 2005; Landerer et al., 2013), or reduction in oceanic CO_2-uptake. However, it remains unclear as to whether a sustained anthropogenic AMOC slowing already is underway (Bryden et al., 2005; Latif et al., 2006; Rahmstorf et al., 2015; Caesar et al., 2018; Fu et al., 2020). Direct ocean-circulation observation in the North Atlantic (NA) is limited (Cunningham et al., 2007; Toole et al., 2017; Handmann et al., 2018; Lobelle et al., 2020). Inferences drawn about the AMOC's history from proxy data (Caesar et al., 2021) or indices derived from other variables, which may provide information about the circulation's variability, for example SST (Latif et al., 2004; Dima and Lohmann, 2010), salinity (Zhu and Liu, 2020) or Labrador Sea convection (Thornalley et al., 2018) are subject to large uncertainties.

Atlantic sea surface temperature

Pronounced decadal and longer timescale (long-term hereafter) natural variability (Delworth and Mann, 2000) complicates the detection of anthropogenic signals over the NA sector. An example is the large long-term variability in the SST of the NA (Fig. 1a-c). Further, the drivers of long-term natural climate variability are not well understood, for example the causes of the Atlantic Multidecadal Oscillation/Variability (AMO/V), the leading mode of long-term NA-SST

variability (Knight et al., 2005; Sutton and Hodson, 2005; Zhang and Delworth, 2006). Internal (Collins et al., 2006; Ting et al., 2009) as well as external mechanisms (Otterå et al., 2010; Booth et al., 2012) were proposed to influence the AMO/V, and the mechanisms also greatly differ among climate models (Park and Latif, 2008; Delworth and Zeng, 2012; Booth et al, 2012; Ba et al., 2014; Clement et al., 2015). Observations suggest that the SST contrast between the North Atlantic and South Atlantic, termed interhemispheric dipole (Folland et al., 1986), could be linked to the AMOC (Latif et al., 2006) which in turn is forced by the low-frequency portion of the North Atlantic Oscillation (NAO, Fig. 1d), the leading mode of atmospheric winter-circulation variability (Hurrell, 1995). This relationship is supported by a number of climate models (e.g. Delworth et al., 2017). However, the relationships between AMO/V, AMOC and NAO are obscured by variable external forcing (Klavans et al., 2019; Mann et al., 2021a and 2021b), and remote forcing, e.g. from the Southern Ocean (Martin et al., 2013), also may influence variability over the Atlantic region.

Ocean-circulation changes most prominently influence the SST on sub-basin scale. The SST cooling in parts of the subpolar NA, which is referred to as the North Atlantic warming hole (NAWH, Fig. S1a) may be an example and the consequence of GHG-induced AMOC slowing and diminishing associated northward ocean-heat transport (Drijfhout et al., 2012; Sevellec et al., 2017; Gervais et al., 2018). Other causes for the NAWH also have been discussed, for example increased ocean-heat transport out of the subpolar NA into higher latitudes (Keil et al., 2020). Moreover, the deep mixed layers in the NAWH (Fig. S1b), indicating strong vertical heat exchange, would delay externally forced surface warming. Finally, anthropogenic aerosols reducing net surface-solar radiation could have counteracted the surface warming by the increasing atmospheric GHG-concentrations.

The SST 1900-2019 averaged over the NAWH (boxes in Figs. 2a, 3a, 4a) and obtained from two datasets (Methods) exhibits strong long-term variability (Fig. 1a). This SST index is virtually identical to a previously defined SST index that was suggested as a fingerprint for AMOC variability (Caesar et al., 2018). Two other indices (Fig. 1 b, c), averaging the SST

over larger areas of the NA (Methods), exhibit similar long-term variability. A major multidecadal SST cooling is observed in all three SST indices during 1930-1980, where the later part of the cooling was discussed in Hodson et al. (2014). After this cooling phase, the SST in the NAWH (Fig. 1a) stayed anomalously cold for about a decade, underwent a fast and strong increase during the 1990s, and featured pronounced multiannual variability after 2000 without an obvious trend. Thus, the SST in the NAWH was relatively stable after 1980, when the atmospheric CO_2-concentration (Fig. 1d) and net top-of-the-atmosphere radiative forcing (RF; Figs. 2b, 3b) exhibited the largest increases. We note the strong year-to-year variability in the NAWH, which is largely due to atmospheric heat-flux forcing linked to the winter-NAO (Cayan, 1992). This short-term variability is not addressed here, as the focus of this study is on long-term variability.

Principal Oscillation Pattern (POP) analysis is applied to the annual Atlantic SSTs (Methods), which is a multivariate statistical technique designed to simultaneously inferring the characteristic spatial patterns and timescales of a vector time series (Storch et al., 1995). The two leading modes, POP1 and POP2, are governed by long-term variability and of interest here. POP1, accounting for 44.3% of the total Atlantic-SST variability, is a real mode and has an e-folding time of 10.7 years. This mode exhibits positive anomalies over the Atlantic basin, with the exception of the NAWH (Fig. 2a). POP1 accounts for up to 80% of the SST variability in the subtropical Northwest Atlantic but hardly any in the NAWH. In the other regions of the Atlantic, the explained variances amount to at least 40%. The time evolution of POP1, PC1 (Fig. 2b), is governed by an accelerating upward trend with substantial superimposed variability. PC1 well follows the long-term evolution of RF, with a correlation coefficient amounting to 0.86. The prominent short-lived downward spikes in RF during the second half of the 20th century are not captured by PC1 and due to explosive volcanic eruptions (Myhre et al., 2013). We conjecture that POP1 describes the externally forced Atlantic SST variability, in particular the effects of global warming.

The global map of local regression coefficients upon PC1 (Fig. 2c) reproduces in large parts the global SST-trend pattern 1900-2019 (Fig. S1a). POP1 accounts for a relatively large fraction of the SST variability over most of the global ocean outside of the NAWH. Over the subpolar Southern Ocean, in the region 160° E – 40° W, another warming hole is observed in the regression pattern (Fig. 2c), which also is present in the map of linear SST trends (Fig. S1a). Compensating external effects, such as stronger surface westerly winds in response to stratospheric ozone loss (Thompson and Solomon, 2002; Fogt and Garreth, 2020) or meltwater input from the Antarctic ice sheet to the Southern Ocean (Park and Latif, 2018), could have offset the GHG-induced surface warming and may explain the warming hole in the Southern Ocean. There, as in the NAWH, relatively deep mixed layers (Fig. S1b) also may have contributed to the lack of surface warming. In the warming-hole regions of the NA and Southern Ocean, internal long-term variability is particularly strong in climate models (Boer and Lambert, 2008) and contributes a larger share to decadal forecast skill than external forcing (Boer et al., 2013). This especially concerns the Southern Ocean exhibiting strong internal multidecadal to centennial variability in climate models (Menary et al., 2013; Martin et al., 2013; Latif et al., 2013; L. Zhang et al., 2019).

The second most energetic mode of Atlantic SST variability, POP2, also is real, accounts for about 20% of the total Atlantic SST variability and has an e-folding time of 6.2 years. POP2 is the interhemispheric dipole, which is linked to long-term AMOC variability in climate models (Latif et al., 2004; Park and Latif, 2008; Dima and Lohmann, 2010; Roberts et al., 2013; Drijfhout, 2015; Sun et al., 2020). Centers with opposite sign are observed in the subpolar NA and subtropical South Atlantic (Fig. 3a), where POP2 accounts for up to 40% and 50% of the SST variability, respectively. POP2 explains considerably less variance in the tropical Atlantic where POP1 explains the most. The corresponding time series PC2 (Fig. 3b) is correlated with RF at -0.48 and 0.22 after linear-trend removal. We conjecture that POP2 describes the internal AMOC-related SST variability in the Atlantic.

The salient feature of PC2 (Fig. 3b) is the decline during 1930-1980, which, when multiplying with the POP2 pattern (Fig. 3a), translates into SST warming over most ocean regions and cooling south of Greenland (Fig. 3c). In this respect, POP2 in consistent with the linear SST trends 1930-1980 (not shown), also exhibiting cooling south of Greenland and SST warming in the global average. The latter, depending on dataset, amounts to 0.09° C – 0.17° C during this period. We note that the mid-20th century decline in PC2 was preceded by a long-term decline in the winter-NAO index (Fig. S2), which is consistent with an ocean-model study addressing the AMOC's response to surface-heat flux variability associated with the NAO (Eden and Jung, 2001). However, correlations between PC2 and the winter-NAO index (Fig. S3) are small and subject to large uncertainties due to the short instrumental records.

After 1980, when RF and globally averaged SST exhibited the largest increases, PC2 hardly depicts any trend (Fig. 3b), supporting that POP2 mainly describes internal variability. POP2, though only derived from Atlantic SST, is strongly related to the SST in the Southern-Ocean. In fact, POP2 accounts for the most variance in the Atlantic sector of the Southern Ocean with values up to 60%, and explained variances amount still to about 40% in the Indian Ocean and Western Pacific sectors of the Southern Ocean (Fig. 3c).

Historical climate model simulations

The observed NA SST variability is within the range of historical simulations with state-of-the-art climate models (Fig. 1a-c), employing estimates of external forcing 1900-2014 (Taylor et al., 2012; Eyring et al., 2016). A measure of the externally forced variability is given by the ensemble-mean, i.e. by averaging over all models. The ensemble-mean SST variability is much weaker than the observed variability in the NAWH (Fig. 1a) and subpolar NA (Fig. 1b), suggesting prevalence of internal SST variability in these two regions. The observed SST variability is reasonably well reproduced by the ensemble mean when averaging over the whole NA (Fig. 1c), suggesting a major role of external forcing in driving tropical and subtropical Atlantic SST. This is consistent with POP1, which is closely linked to RF (Fig. 2a), explaining the most variance in the tropics and subtropics. The ensemble-mean NA SSTs,

however, lead the observed SSTs by about a decade in all the three index regions (Fig. 1a-c). We note in this context that historical external forcing is subject to considerable uncertainties. Aerosol-cloud interaction is the largest source of uncertainty in estimating historical anthropogenic radiative forcing and representing this interaction in climate models poses a major challenge (Randall et al., 2013; Ghan et al., 2016).

A variance-maximizing statistical method (EOF analysis, Methods) is applied jointly to the ensemble-mean Atlantic SST and meridional overturning stream function (MOC). The SST pattern (Fig. 4a) of the leading mode, EOF1, accounting for 47.8% of the joint variance, is similar to POP1 (Fig. 2a) with major warming over most of the Atlantic and a warming hole in the subpolar NA south of Greenland. Variances explained in SST by EOF1 are generally large, exhibiting a maximum in the subtropical NA, with values in localized regions exceeding 90%, and a minimum south of Greenland, with values of less than 10% (Fig. 4a). The MOC pattern exhibits negative loadings north of the equator, indicating weaker overturning, which are centered near 40° N in the depth range 1,000 m – 2,000 m (Fig. 4b). Positive loadings are observed south of the equator. With regard to MOC, the explained variances are largest in the center of the negative loadings where they amount to about 80% (Fig. 4b). Regions of large explained variances indicate a high model consistency.

In climate models, MOC anomalies associated with changes in the North Atlantic Deep Water (NADW) formation first appear in the subpolar NA and then propagate southward (Zhang and Zhang, 2015). Major AMOC slowing due to global warming is characterized by basin-wide negative stream function anomalies (Reintges et al., 2017). EOF1 is thus consistent with the initial stage of AMOC slowing forced by global warming. Because EOF1 is a measure of the externally forced signal in SST and MOC, the corresponding principal component PC1 (Fig. 4c) is expected to be significantly correlated with RF; the correlation coefficient between the two time series amounts to 0.79. PC1 is governed by multidecadal variability until about 1980, and it exhibits a sustained upward trend thereafter. Since 1980,

the reduction in the negative MOC center amounts to about 1 Sv (10^6 $m^3 \cdot s^{-1}$), which generally is assumed to be within the range of natural variability.

Discussion

Observed SSTs and a large ensemble of historical simulations with state-of-the-art climate models suggest prevalence of internal AMOC and associated heat transport variability since the beginning of the 20th century. This notion is supported, for example, by the relationship between RF and subpolar NA SST, where the latter is strongly influenced by AMOC-related upper-ocean heat transport. Most of the SST cooling in the subpolar NA, which has been attributed to anthropogenic AMOC slowing (Caesar et al., 2018), occurred during 1930-1980 when RF did not exhibit a long-term trend. On the other hand, slight SST warming was observed in the subpolar NA after 1980 when RF rapidly increased primarily due to rising anthropogenic CO_2-emissions. A relatively stable AMOC and associated heat transport during the last decades also is supported by ocean syntheses combining ocean general circulation models (OGCMs) and data (Köhl, 2015; Jackson et al., 2019), hindcasts with OGGMs forced by observed atmospheric boundary conditions (Danabasoglu et al., 2016), and instrumental measurements of key AMOC components (Fu et al., 2020; Moat et al., 2020). Neither of these datasets suggest major AMOC slowing during the last decades.

The historical simulations with the CMIP5/6 models yield sustained AMOC slowing of only about 1 Sv during the last decades. This is consistent with Weyer at al. (2020), analyzing an ensemble of CMIP6 models and reporting that linear trends over the entire historical period 1850–2014 are generally neutral. A major factor causing anthropogenic AMOC slowing is thought to be Greenland ice melt. Meltwater forcing, however, is not considered in the historical simulations, which may cause underestimation of AMOC slowing. A high-resolution OGCM study finds that the present meltwater forcing from the West Greenland ice sheet is not large enough to drive significant reductions in NADW formation and thus AMOC strength (Böning et al., 2016). Climate-model sensitivity to forcing, however, is a long-standing issue, especially with regard to the AMOC's sensitivity to freshwater forcing (Gent, 2018).

Finally, sea levels may provide clues about ocean-circulation change. Satellite altimetry sea levels starting in 1993 feature a globally averaged increase of about 9 cm, but with large regional variation and virtually no trend in the NAWH. Assuming mass flux is small in comparison to vertically integrated density change, the absence of significant sea-level trends in the NAWH could have resulted from the competing effects of oceanic heat uptake, enhancing upper-ocean heat content and sea level, and reduced AMOC-related heat transport into the region, decreasing upper-ocean heat content and sea level. The leading EOF mode of sea-level variability 1993-2019 (EOF1, Fig. S1c), accounting for 36.3% of the total variability, is the global-warming signal in sea level, as suggested by the steady upward trend in the corresponding principal component (PC1, Fig. S1d). Ocean-circulation change is emphasized by dynamic sea level, the departure from the global average. When removing the global average from EOF1 (Fig. S1e), negative anomalies appear along the path of the North Atlantic Current and southeast of Greenland. The marked decadal AMOC-slowing event around 2010, which went along with a reduction in northward ocean-heat transport (Bryden et al., 2020), coincides with the drop in EOF1-related dynamic sea level (Fig. S1f) southeast of Greenland (box in Fig. S1e). This slowing event could well have been a realization of internal AMOC variability (Latif et al., 2019), without excluding it being part of a long-term trend, reinforcing the need for systematic and sustained in-situ AMOC-observation systems to detect with high confidence externally forced AMOC slowing.

Methods

Observed SST during 1900-2019 with 2°×2° resolution is used here and obtained from Extended Reconstructed Sea Surface Temperature Version 5 (ERSST.v5; Huang et al., 2017). SSTs from Kaplan Extended SST V2 during 1900-2019 with 5°×5° resolution also are analyzed (Kaplan et al., 1998). We use the station-based NAO index from 1865 to 2010 retrieved from https://climatedataguide.ucar.edu/climate-data/hurrell-north-atlantic-oscillation-nao-index-station-based. This NAO index is based on the difference of normalized winter (December-March, DJFM) sea level pressure (SLP) between Lisbon, Portugal and Stykkisholmur/Reykjavik, Iceland since 1864. The radiative forcing of four Representative Concentration Pathways (RCPs) scenarios (van Vuuren et al., 2011) is used in Figs. 1, 2, and 3. In Fig. 1d, the historical CO_2-concentration is shown with RCP8.5 at the end.

The warming-hole SST index is defined as the annual-mean SST anomalies over the North Atlantic region 46°N-62°N and 46°W-20°W. A North Atlantic SST (NASST) is defined as the annual-mean SST anomalies averaged over the region 40°N-60°N and 80°W-0°E. An Atlantic Multidecadal Oscillation/Variability (AMO/V) index is defined as low-pass filtered (11-year running mean) annual-mean SST anomalies averaged over the region 0°-65°N and 80°W-0°E. All SST indices are calculated as area-weighted means.

Mixed Layer depth climatology with 2°×2° resolution (de Boyer Montégut et al., 2004) is based on a density threshold of 0.03 $kg \cdot m^{-3}$.

Annual sea level data 1993-2019 are obtained from Copernicus https://cds.climate.copernicus.eu. For the EOF analysis (see below), the Sea Level Anomaly (SLA) product was used, which is defined relative to the mean of 1993-2012 (Clementi et al., 2019).

An ensemble of 36 historical Coupled Model Intercomparison Project runs are used. 12 phase 5 (CMIP5) models (ACCESS1-3,CanESM2,CCSM4,CESM1-BGC,CESM1-CAM5,CNRM-CM5,FGOALS-g2,MIROC5,MPI-ESM-MR,MRI-CGCM3,NorESM1-M, NorESM1-ME) integrated for the period 1900-2005; and 24 phase 6 (CMIP6) models (ACCESS-CM2,ACCESS-ESM1-5,CanESM5,CESM2,CESM2-WACCM,CESM2-WACCM-FV2,CIESM,CMCC-CM2-HR4,E3SM-1-0,E3SM-1-1,E3SM-1-1-ECA,FGOALS-f3-L,FGOALS-g3,INM-CM4-8,INM-CM5-0,MIROC6,MPI-ESM-1-2-HAM,MPI-ESM1-2-HR,MPI-ESM1-2-LR,MRI-ESM2-0,NorCPM1,NorESM2-LM,NorESM2-MM,SAM0-UNICON) integrated for the period1900-2014. SST fields have been linearly interpolated to 1°×1° resolution.

The Principal Oscillation Patterns (POPs) are defined as the normal modes of a linear dynamical representation of the data in terms of a first-order autoregressive-vector process with residual noise forcing (Hasselmann, 1988; Storch et al., 1988; von Storch et al., 1995). Let X(t) represent an n-dimensional stochastic process. For practical purposes, the original process is usually reduced into the subspace of leading Empirical Orthogonal Function (EOFs). Hence, X is the first n leading Principal Components (PCs). The evolution of X is represented as a first-order multivariate Markov process: $X(t + 1) = A \cdot X(t) + \text{noise}$. It can be shown that in order to minimize the noise, the system matrix A has to be chosen as $A = C_1 \cdot C_0^{-1}$, where C_1 denotes the lag-1 covariance matrix of X(t) and C_0 the lag-0 covariance matrix. The time step is 1 year. To perform a POP analysis is to solve the eigenproblem for A and to find the temporal variation (POP coefficients, PCs) of each eigenvector or POP. POPs associated with complex eigenvalues occur in complex conjugate pairs and can represent in general, an arbitrary amphidromic oscillation with a rotation period and a timescale for exponential decay (e-folding time) that are estimated as part of the eigenproblem. POPs associated with real eigenvalues, as those discussed in this study, represent non-propagating, non-oscillatory and damped patterns with an e-folding time for exponential decay.

The POP patterns are shown as maps of local linear regression coefficients of SST upon the POP-coefficient time series, which have been normalized by their respective standard deviation. In the same way, the global regression maps have been calculated. An F test is used to assess the significance of the regression coefficients.

The Student's t-test and Monte Carlo simulation based on nonparametric random phase are applied to assess the significance of the correlation coefficients (Ebisuzaki, 1997).

To analyze the ensemble of historical simulations 1900-2014 with the 36 CMIP models, EOF analysis (Lorenz, 1956) is applied jointly to the Atlantic SST and overturning stream function (MOC), after normalizing each variable by its own mean and standard deviation, making each field has identical total variance. From 2006 to 2014, only the 24 CMIP6 models were available. EOF analysis also is applied to the satellite sea data.

Acknowledgements

This work was supported by a PhD scholarship funded jointly by the China Scholarship Council (CSC). Support from the European Union's Roadmap Project and the project RACE funded by the German Ministry of Education and Research (BMBF) is acknowledged. We acknowledge the World Climate Research Program's Working Group on Coupled Modelling, which is responsible for CMIP, and we thank the climate modeling groups (listed in the Supplementary Material) for producing and making available their model output. For CMIP the U.S. Department of Energy's Program for Climate Model Diagnosis and Intercomparison provides coordinating support and led development of software infrastructure in partnership with the Global Organization for Earth System Science Portals. This study has been conducted using E.U. Copernicus Marine Service Information.

References

Ba J et al (2014) A multi-model comparison for Atlantic multidecadal variability. Climate Dynamics, DOI: 10.1007/s00382-014-2056-1.

Boer GJ and SJ Lambert (2008) Multi-model decadal potential predictability of precipitation and temperature. Geophys. Res. Lett., 35:L05706. doi:10.1029/2008GL033234.

Boer GJ et al (2013) Decadal predictability and forecast skill. Climate Dynamics, 41, 1817–1833.

Böning CW et al (2016) Emerging impact of Greenland meltwater on deepwater formation in the North Atlantic Ocean, Nat. Geosci., 9, 523-527, doi: 10.1038/ngeo2740.

Booth BB et al (2012) Aerosols implicated as a prime driver of twentieth-century North Atlantic climate variability. Nature, 484(7393):228-32, doi: 10.1038/nature10946.

Broecker WS (1991) The Great Ocean conveyor. Oceanography 4 (2), 79–89.

Bryden H et al (2005) Slowing of the Atlantic meridional overturning circulation at 25°N. Nature, 438, 655–657.

Bryden et al (2020) Reduction in Ocean Heat Transport at 26°N since 2008 Cools the Eastern Subpolar Gyre of the North Atlantic Ocean. J. Climate, 33 (5): 1677–1689.

Caesar L et al (2018) Observed fingerprint of a weakening Atlantic Ocean overturning circulation. Nature, 556, https://doi.org/10.1038/s41586-018-0006-5.

Caesar L et al (2021) Current Atlantic Meridional Overturning Circulation weakest in last millennium. Nature Geoscience, doi.org/10.1038/s41561-021-00699-z.

Cayan D (1992) Latent and Sensible Heat Flux Anomalies over the Northern Oceans: Driving the Sea Surface Temperature. J. Phys. Oceanogr., 22(8), 859-881.

Clement A et al (2015) The Atlantic Multidecadal Oscillation without a role for ocean circulation. Science, 350, 320-324. DOI: 10.1126/science.aab3980.

Clementi E et al (2019) Mediterranean Sea Analysis and Forecast (CMEMS MED-Currents, EAS5 system) [Data set]. Copernicus Marine Environment Monitoring Service (CMEMS). DOI: https://doi.org/10.25423/CMCC/MEDSEA_ANALYSIS_FORECAST_PHY_006_013_EAS5.

Collins M et al (2006) Interannual to Decadal Climate

Predictability in the North Atlantic: A Multimodel-Ensemble Study. J. Climate, 19(7), 1195-1203.

Cunningham SA et al (2007) Temporal variability of the Atlantic Meridional Overturning Circulation at 26°N. Science, 317, 935-938, doi:10.1126/science.1141304.

Danabasoglu G et al (2016) North Atlantic simulations in coordinated ocean-ice reference experiments phase II (CORE-II). Part II: inter-annual to decadal variability. Ocean Model. 97, 65–90. doi: 10.1016/j.ocemod.2015.11.007

de Boyer Montégut et al (2004) Mixed layer depth over the global ocean: An examination of profile data and a profile-based climatology. J. Geophy. Res., Oceans, 109(C12).

Delworth TL and F Zeng (2012) Multicentennial variability of the Atlantic meridional overturning circulation and its climatic influence in a 4000 year simulation of the GFDL CM2.1 climate model. Geophys. Res. Lett., 39(13), doi.org/10.1029/2012GL052107.

Delworth TL and ME Mann (2000) Observed and simulated multidecadal variability in the Northern Hemisphere. Clim. Dyn. 16, 661-676.

Delworth TL et al (2017) The Central Role of Ocean Dynamics in Connecting the North Atlantic Oscillation to the Extratropical Component of the Atlantic Multidecadal Oscillation. J. Climate, 30(10), 3789-3805.

Dima M and G Lohmann (2010) Evidence for Two Distinct Modes of Large-Scale Ocean Circulation Changes over the Last Century. J Climate, 23, 5-16.

Drijfhout S (2015) Competition between global warming and an abrupt collapse of the AMOC in Earth's energy imbalance. Scientific Reports, 5, 14877, 10.1038/srep14877.

Drijfhout S et al (2012) Is a decline of AMOC causing the warming hole above the North Atlantic in observed and modeled warming patterns? J. Climate, 25, 8373–8379, https://doi.org/10.1175/JCLI-D-12-00490.1.

Dupont S and H Pörtner (2013) Get ready for ocean acidification. Nature, 498, 429, doi.org/10.1038/498429a.

Eden C and T Jung (2001) North Atlantic Interdecadal Variability: Oceanic Response to the North Atlantic Oscillation (1865–1997) J. Climate, 14(5), 676-691.

Ebisuzaki W (1997) A method to estimate the statistical significance of a correlation when the data are serially correlated. J. Climate, 10, 2147–2153.

Eyring V et al (2016) Overview of the Coupled Model Intercomparison Project Phase 6 (CMIP6) experimental design and organization, Geosci. Model Dev., 9, 1937-1958, doi:10.5194/gmd-9-1937-2016.

Fogt RL and GJ Garreth (2020) The Southern Annular Mode: Variability, trends, and climate impacts across the Southern Hemisphere. WIREs CLIMATE CHANGE, doi.org/10.1002/wcc.652.

Folland CK et al (1986) Sahel rainfall and worldwide sea temperatures, 1901–85. Nature, 320, 602–607.

Fu Y et al (2020) A stable Atlantic Meridional Overturning Circulation in a changing North Atlantic Ocean since the 1990s. Science Advances, 6, https://doi.org/10.1126/sciadv.abc7836.

Gent PR (2018) A commentary on the Atlantic meridional overturning circulation stability in climate models. Ocean Modelling, 122, 57-66.

Gervais et al (2018) Mechanisms Governing the Development of the North Atlantic Warming Hole in the CESM-LE Future Climate Simulations. J Climate, 31(15), 5927-5946.

Ghan S et al (2016) Challenges in constraining anthropogenic aerosol effects on cloud radiative forcing using present-day spatiotemporal variability. Proceedings of the National Academy of Sciences of the United States of America, 113(21), 5804–5811, doi.org/10.1073/pnas.1514036113.

Handmann P et al (2018) The Deep Western Boundary Current in the Labrador Sea From Observations and a High-Resolution Model. J Geophys Res Oceans, 123 (4), 2829-2850.

Hasselmann, K (1988) PIPs and POPs: The reduction of complex dynamical systems using principal interaction and oscillation patterns. J. Geophy. Res. Atm., 93(D9), 11015-11021.

Hodson DLR et al (2014) An Anatomy of the Cooling of the North Atlantic Ocean in the 1960s and 1970s. J. Climate, 27(21), 8229-8243.

Huang B et al (2017) Extended Reconstructed Sea Surface Temperature version 5 (ERSSTv5), Upgrades, validations, and intercomparisons. J. Climate, 30(20), 8179-8205.

Hurrell JW (1995) Decadal Trends in the North Atlantic Oscillation Regional Temperatures and Precipitation, Science 269, 676–679.

IPCC (2013). Summary for Policymakers. In: Climate Change 2013: The Physical Science Basis. Contribution of Working Group I to the Fifth Assessment Report of the Intergovernmental Panel on Climate Change [Stocker, T.F., D. Qin, G.-K. Plattner, M. Tignor, S.K. Allen, J. Boschung, A. Nauels, Y. Xia, V. Bex and P.M. Midgley (eds.)]. Cambridge University Press, Cambridge, United Kingdom and New York, NY, USA.

IPCC (2014) Climate Change 2014: Synthesis Report. Contribution of Working Groups I, II and III to the Fifth Assessment Report of the Intergovernmental Panel on Climate Change [Core Writing Team, R.K. Pachauri and L.A. Meyer (eds.)]. IPCC, Geneva, Switzerland, 151 pp.

Jackson LC et al (2019) The mean state and variability of the North Atlantic circulation: A perspective from ocean reanalyses. J. Geophys. Res. Ocean 124, 9141–9170.

Kaplan AM et al (1998) Analyses of global sea surface temperature 1856-1991, J. Geophy. Res., Oceans, 103(C9), 18567-18589.

Keil P et al (2020) Multiple drivers of the North Atlantic warming hole. Nature Climate Change, 10, 667–671.

Klavans JM et al (2019) Variable External Forcing Obscures the Weak Relationship between the NAO and North Atlantic Multidecadal SST Variability. J. Climate, 32(13), 3847-3864.

Knight JR et al (2005) A signature of persistent natural thermohaline circulation cycles in observed climate. Geophys. Res. Lett., 32, L20708, doi:10.1029/2005GL024233.

Köhl A (2015) Evaluation of the GECCO2 ocean synthesis: Transports of volume, heat and freshwater in the Atlantic. Q. J. Roy. Meteorol. Soc., 141, 166–181.

Landerer FW et al (2013) Regional Dynamic and Steric Sea Level Change in Response to the IPCC-A1B Scenario. J. Phys. Oceanogr., 37, 296-312.

Latif M et al (2004) Reconstructing, monitoring, and predicting multidecadal-scale changes in the North Atlantic thermohaline circulation with sea surface temperature. J. Climate, 17, 1605–1614.

Latif M et al (2006) Is the thermohaline circulation changing? J. Climate 19 (18): 4631–4637.

Latif M et al (2013) Southern Ocean Sector Centennial Climate Variability and Recent Decadal Trends. J. Climate, 26(19), 7767-7782, doi: 10.1175/JCLI-D-12-00281.1.

Latif M et al (2019) Decadal Atlantic Meridional Overturning Circulation slowing events in a climate model. Climate Dynamics, 53, 1111–1124.

Levermann A et al (2005. Dynamic sea level changes following changes in the thermohaline circulation. Climate Dynamics 24 (4), 347-354.

Liu W et al (2020) Climate impacts of a weakened Atlantic Meridional Overturning Circulation in a warming climate. Science Advances, 6, 26, eaaz4876,DOI: 10.1126/sciadv.aaz4876.

Lobelle D et al (2020) Detectability of an AMOC Decline in Current and Projected Climate Changes. Geophys. Res. Lett., 47, e2020GL089974.

Lorenz EN (1956) Empirical orthogonal functions and statistical weather prediction. Technical report, Statistical Forecast Project Report 1, Dept. of Meteor., MIT, 1956. 49.

Mann ME (2021a) Absence of internal multidecadal and interdecadal oscillations in climate model simulations. Nat Commun 11, 49. https://doi.org/10.1038/s41467-019-13823-w.

Mann ME et al (2021b) Multidecadal climate oscillations during the past millennium driven by volcanic forcing. Science, 371, Issue 6533, pp. 1014-1019. DOI: 10.1126/science.abc5810.

Martin T et al (2013) Multi-centennial variability controlled by Southern Ocean convection in the Kiel Climate Model. Climate Dynamics, 40, 2005–2022.

Menary MB and RA Wood (2018) An anatomy of the projected North Atlantic warming hole in CMIP5 models. Climate Dynamics 50, 3063–3080.

Menary MB et al (2011). A multimodel comparison of centennial Atlantic meridional overturning circulation variability. Climate Dynamics, DOI: 10.1007/s00382-011-1172-4.

Moat BI et al (2020) Pending recovery in the strength of the meridional overturning circulation at 26°N. Ocean Science, doi:10.5194/os-2019-134.

Muir LC and AV Fedorov (2015) How the AMOC affects ocean temperatures on decadal to centennial timescales: the North Atlantic versus an interhemispheric seesaw. Climate Dynamics, 45, 151–160.

Myhre G et al (2013) Anthropogenic and Natural Radiative Forcing. In: Climate Change 2013: The Physical Science Basis. Contribution of Working Group I to the Fifth Assessment Report of the Intergovernmental Panel on Climate Change [Stocker TF et al (eds)]. Cambridge University Press, Cambridge, United Kingdom and New York, NY, USA.

Oliver E et al (2018) Longer and more frequent marine heatwaves over the past century. Nature Communications, 9:1324, doi: 10.1038/s41467-018-03732-9.

Otterå OH et al (2010) External forcing as a metronome for Atlantic multidecadal variability. Nature Geoscience, 3, 688–694.

Park and M Latif (2008) Multidecadal and multicentennial variability of the meridional overturning circulation. Geophy. Res. Lett., 35, L22703, doi:10.1029/2008GL035779.

Park W and M Latif (2018) Ensemble global warming simulations with idealized Antarctic meltwater input. Climate Dynamics, 52, 3223–3239.

Rahmstorf S et al (2015) Exceptional twentieth-century slowdown in Atlantic Ocean overturning circulation. Nat. Climate Change, 5, 475–480, https://doi.org/10.1038/nclimate2554.

Randall D et al (2013) Clouds and aerosols Climate Change 2013 the Physical Science Basis: Working Group I Contribution to the Fifth Assessment Report of the Intergovernmental Panel on Climate Change (Cambridge: Cambridge University Press) 571–658.

Reintges A et al (2017) Uncertainty in twenty-first century projections of the Atlantic Meridional Overturning Circulation in CMIP3 and CMIP5 models. Climate Dynamics 49(5), DOI: 10.1007/s00382-016-3180-x.

Roberts CD et al (2013) A Multimodel Study of Sea Surface Temperature and Subsurface Density Fingerprints of the Atlantic Meridional Overturning Circulation. J. Climate, 26(22), 9155-9174.

Schmittner A et al (2005). Model projections of the North Atlantic thermohaline circulation for the 21st century assessed by observations. Geophys. Res. Lett 32, L23710.

Sevellec F et al (2017). Arctic sea-ice decline weakens the Atlantic Meridional Overturning Circulation. Nature Climate Change, 7, 604–610.

Srokosz M et al (2012) Past, present and future change in the Atlantic meridional overturning circulation. Bulletin of the American Meteorological Society, 93 (11), 1663-1676. ISSN 1520-0477, doi.org/10.1175/BAMS-D-11-00151.1.

Storch H et al (1988) Principal oscillation pattern analysis of the 30-to 60-day oscillation in general circulation model equatorial troposphere. J. Geophys. Res. Atm., 93(D9), 11022-11036.

Storch H et al (1995) Principal oscillation patterns: A review. J. Climate, 8(3), 377-400.

Sun J et al (2020) On the Interpretation of the North Atlantic Averaged Sea Surface Temperature, J. Climate, 33(14), 6025-6045.

Sutton RT and DLR Hodson (2005) North Atlantic forcing of North American and European summer climate. Science, 309, 115–118, https://doi.org/10.1126/science.1109496.

Taylor, KE et al (2012) An overview of CMIP5 and the experimental design. Bull. Am. Meteorol. Soc. 93, 485–498.

Ting M et al (2009) Forced and Internal Twentieth-Century SST Trends in the North Atlantic, J. Climate, 22(6), 1469-1481.

Thompson DWJ and S Solomon (2002) Interpretation of recent Southern Hemisphere climate change, Science, 296, 895–899.

Thornalley DJR et al (2018) Anomalously weak Labrador Sea convection and Atlantic overturning during the past 150 years. Nature, 556, 227-223.

Toole JM et al (2017) Moored observations of the Deep Western Boundary Current in the NW Atlantic: 2004–2014. J Geophys Res Oceans, 122 (9), 7488-7505.

van Vuuren, DP et al (2011) The representative concentration pathways: an overview. Clim. Change, 109, 5–31.

Volkov DL et al (2020) Atlantic meridional overturning circulation and associated heat transport. In “State of the Climate in 2019". Bull. Amer. Meteor. Soc., 101 (8), S163–S169, doi.org/10.1175/BAMS-D-200105.1.

Weyer W et al (2020) CMIP6 Models Predict Significant 21st Century Decline of the Atlantic Meridional Overturning Circulation. Geophys. Res. Lett., 47, e2019GL086075. https://doi.org/10. 1029/2019GL086075.

Zhang J and R Zhang (2015) On the evolution of Atlantic Meridional Overturning Circulation Fingerprint and implications for decadal predictability in the North Atlantic. Geophys. Res. Lett., 42 (13), 5419-5426.

Zhang L et al (2019) Natural variability of Southern Ocean convection as a driver of observed climate trends. Nature Climate Change, 9, 59–65.

Zhang R and TL Delworth (2006) Impact of Atlantic multidecadal oscillations on India/Sahel rainfall and Atlantic hurricanes. Geophys. Res. Lett.,33, DOI:10.1029/2006GL026267.

Zhang R et al (2019) A Review of the Role of the Atlantic Meridional Overturning Circulation in Atlantic Multidecadal Variability and Associated Climate Impacts. Rev. Geophys, 57(2), 316-375.

Zhu C and Liu Z (2020) Weakening Atlantic overturning circulation causes South Atlantic salinity pile-up. Nat. Clim. Chang, 10, 998–1003, https://doi.org/10.1038/s41558-020-0897-7.

Figures

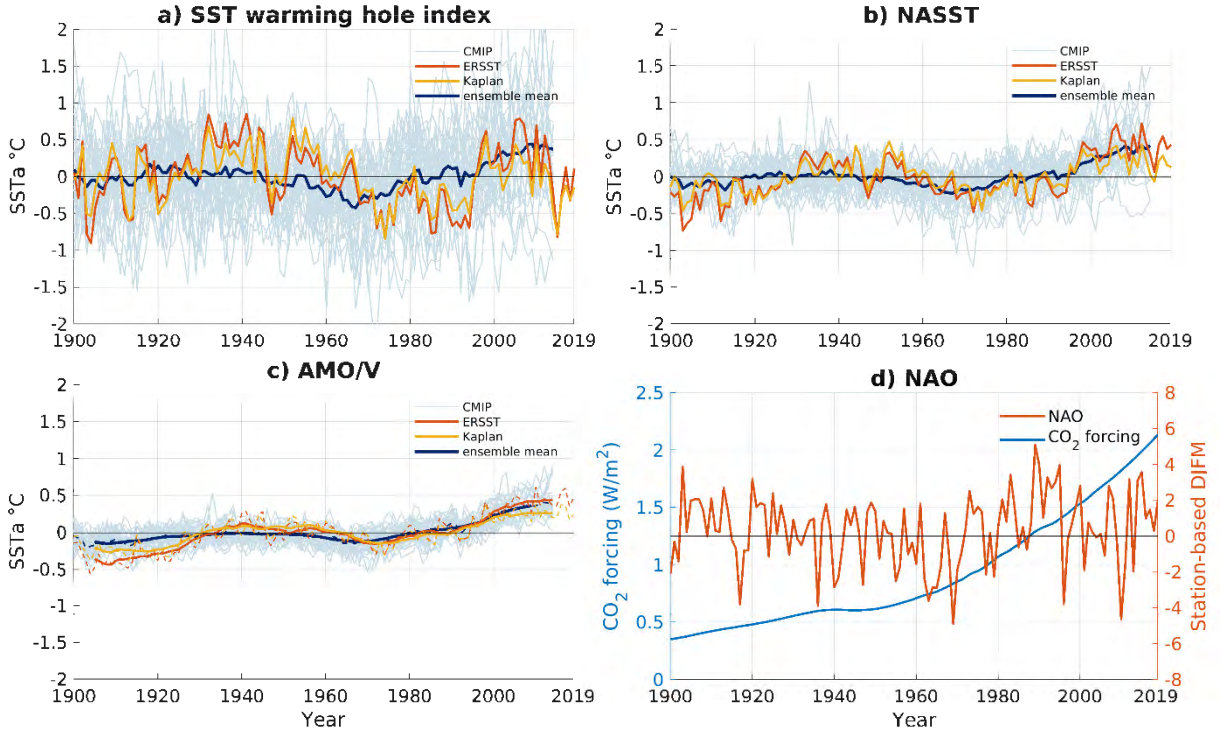

Fig. 1: a) The SST warming hole index (°C) defined as the annual sea surface temperature (SST) anomalies averaged over the region 46°N-62°N and 46°W-20°W. Observations 1900-2019 from ERSST v5 (orange), Kaplan SST v2 (yellow), ensemble-mean SST 1900-2005 (dark blue) of the historical simulations with the CMIP5 and CMIP6 models, and the individual historical simulations with the CMIP5 (1900-2005) and CMIP6 (1900-2014) models (thin grey lines). b) Same as a) but for the NASST index (°C), defined as the annual SST anomalies averaged over the region 40°N-60°N and 80°W-0°E. c) Same as a) but for the Atlantic Multidecadal Oscillation/Variability (AMO/V, °C) index, defined as the 11-year running mean of the annual SST anomalies averaged over the region 0°N-65°N and 80°W-0°E. Dashed thin curves indicate annual indices. d) The North Atlantic Oscillation (NAO) index 1900-2019 (orange), defined as the difference of normalized winter (December-March, DJFM) sea level pressure (SLP) between Lisbon (Portugal) and Stykkisholmur/Reykjavik (Iceland). The blue curve indicates the equivalent-CO_2 radiative forcing (W/m^2) 1900-2005, which is taken from the Representative Concentration Pathway (RCP) 8.5 after 2005.

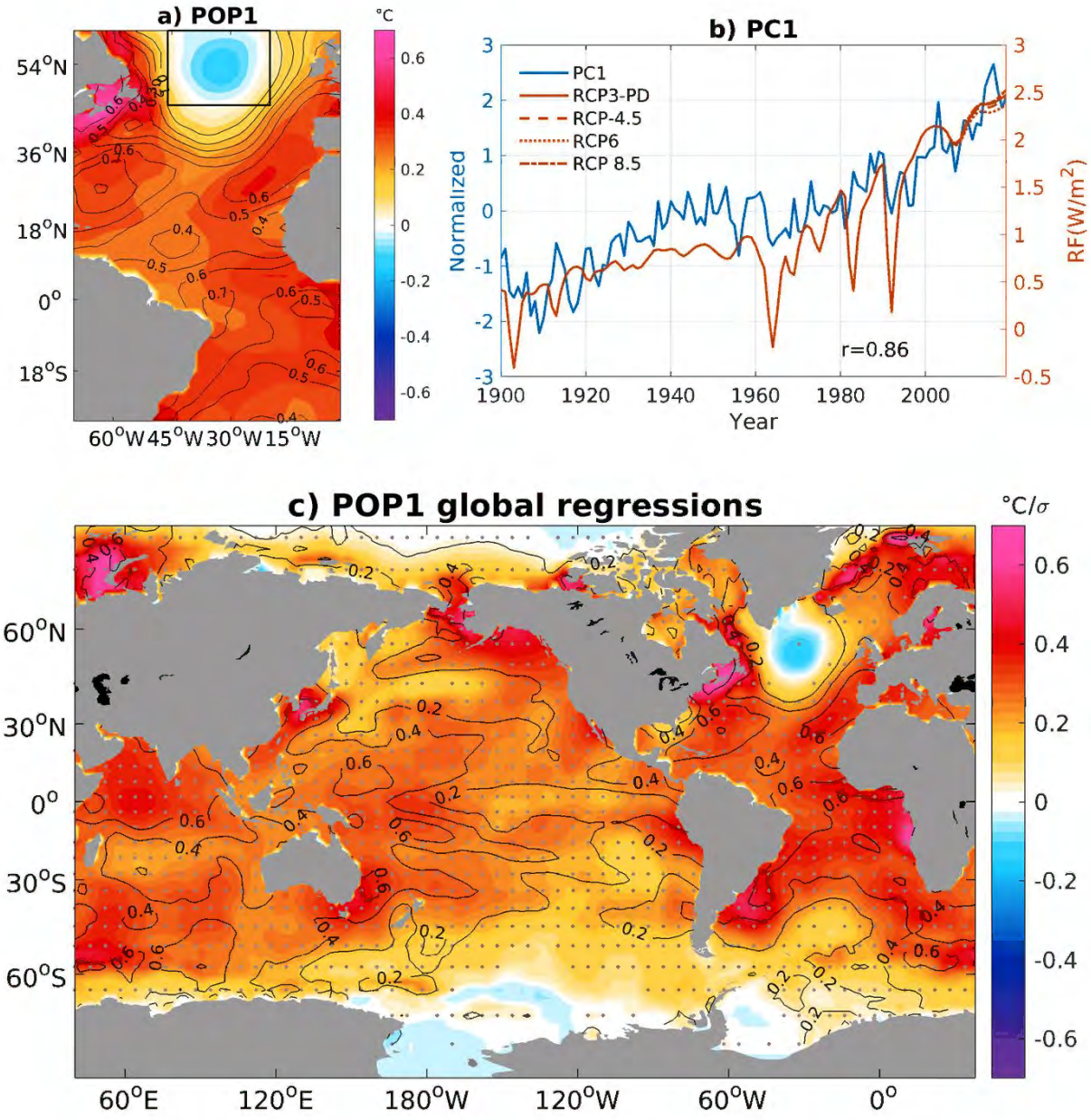

Fig. 2: The leading (most energetic) POP mode (POP1), accounting for 44.3 % of the total Atlantic SST variability. a) Pattern shown by the local regression coefficients (°C) upon the POP coefficient time series PC1 (contours denote explained variance and dots indicate significance at 95% confidence level). b) PC1 (standardized, blue) and the net radiative forcing (W/m^2, orange) with different scenarios after 2005 (RCP4.5, RCP6 and RCP8.5). PC1 and the net radiative forcing with RCP8.5 are correlated at 0.86. c) Global map of local regression coefficients upon PC1.

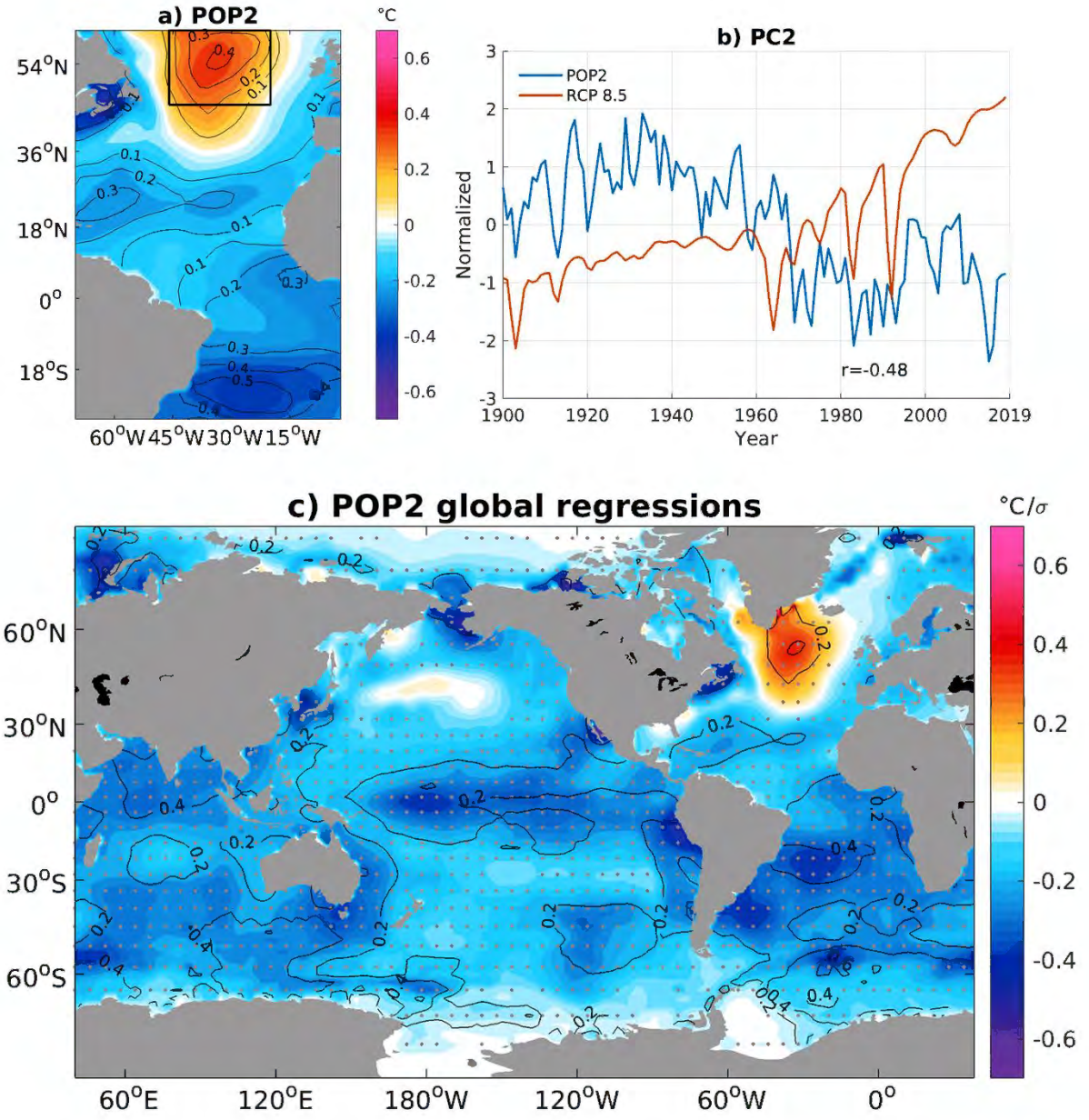

Fig. 3: The second most energetic POP mode (POP2), accounting for 20% of the total Atlantic SST variability. a) Pattern shown by the local regression coefficients (°C) upon the POP coefficient time series PC2 (contours denote explained variance and dots indicate significance at 95% confidence level). b) PC2 (standardized, blue) and the net radiative forcing (standardized, orange) with the RCP8.5 scenario after 2005. PC2 and the net radiative forcing are correlated at -0.48. The correlation amounts to 0.22 after linearly detrending the time series. c) Global map of local regression coefficients upon PC2.

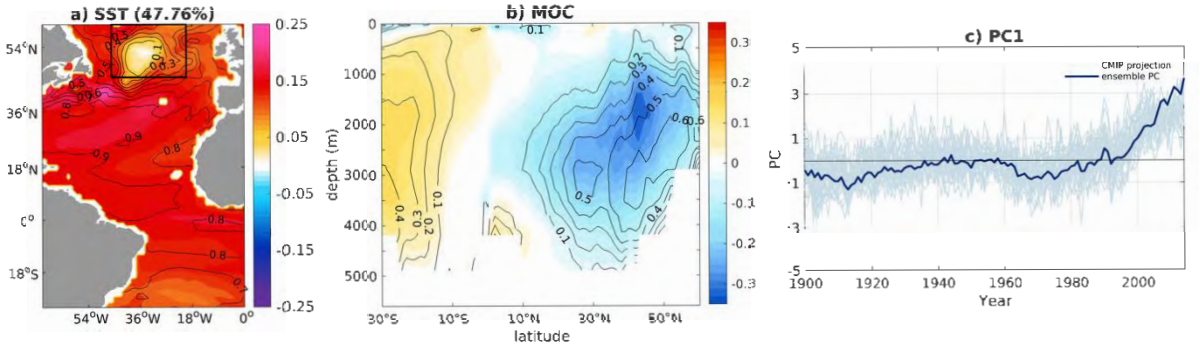

Fig. 4: Leading Empirical Orthogonal Function (EOF1) of the ensemble-mean SST and meridional overturning stream function (MOC) derived from the historical simulations with the CMIP5 and CMIP6 models from 1900-2014. From 2006 to 2014, only CMIP6 models are included. The ensemble-mean is an estimate of the externally forced variability. a) SST pattern (°C), b) MOC pattern (Sv), c) the corresponding time series (principal component) PC1 (thick line), and the projections of the individual climate models onto EOF1 (thin lines). Contours in a) and b) denote explained variance. EOF1 accounts for 47.8% of the joint variance. The unit Sverdrup (Sv) is defined as $10^6\,m^{\cdot 3}s^{-1}$.

Supplementary Figures

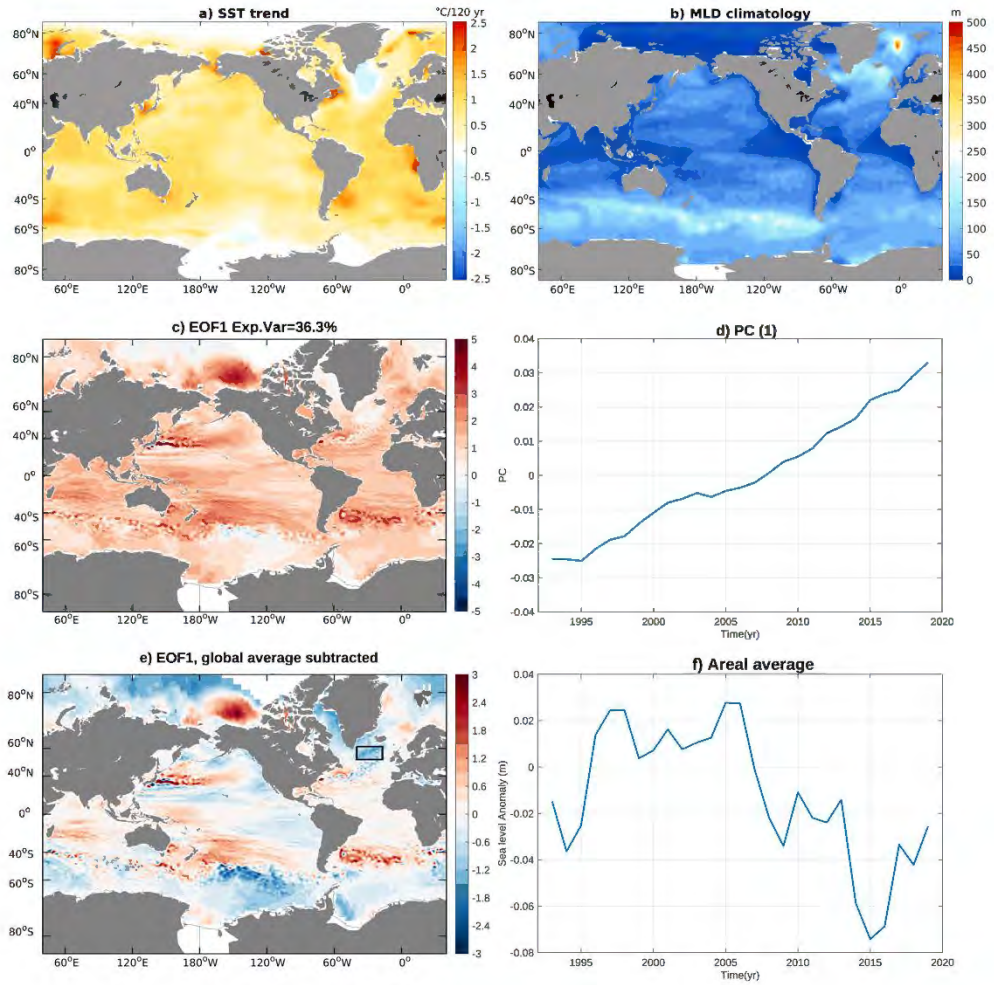

Fig. S1: a) Linear trends of sea surface temperature (SST, °C/120 years) during 1900-2019. b) Mean mixed layer Depth (MLD, m) averaged over 1961-2008. The criterion for defining MLD is based on a fixed threshold of 0.03 kg/m^3. c) Leading variance-maximizing mode of sea-level variability (EOF1, m)) during 1993-2019, d) time series (principal component) of EOF1 (PC1), e) as c) but with the global average removed. f) Time series of EOF1-related dynamic sea level (m) shown in e) averaged over the box southeast of Greenland (40°W-17°W, 53°N-61°N). The globally averaged trend in annual-mean sea level during 1993-2019 amounts to 2.86 mm/year. EOF1 accounts for 36.3% of the total sea-level variance.

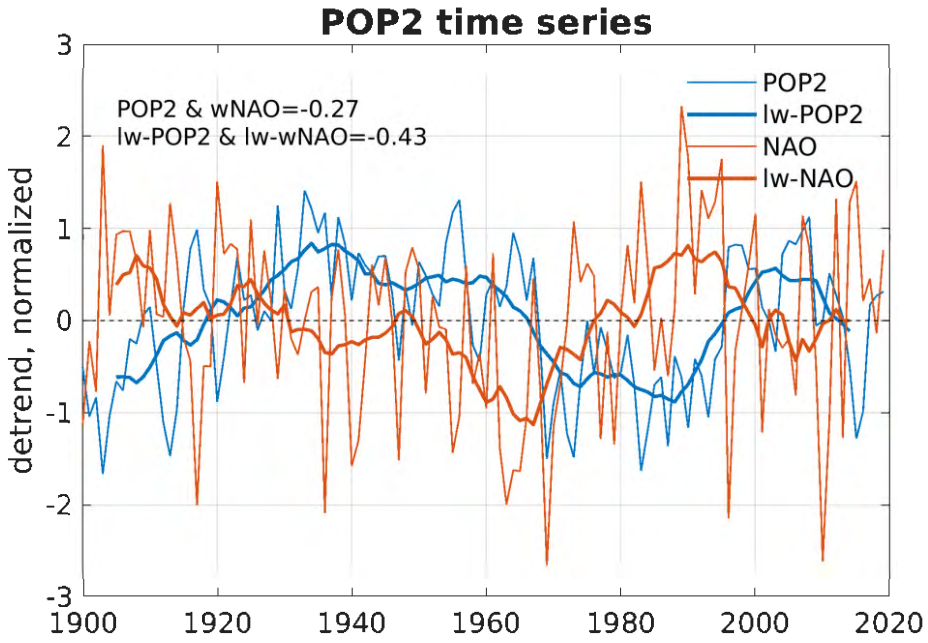

Fig. S2: Detrended POP2 time series (PC2) and detrended winter (December-March, DJFM) NAO index (thin lines), and the low-pass filtered time series (applying an 11-year running mean) denoted by lw (thick lines).

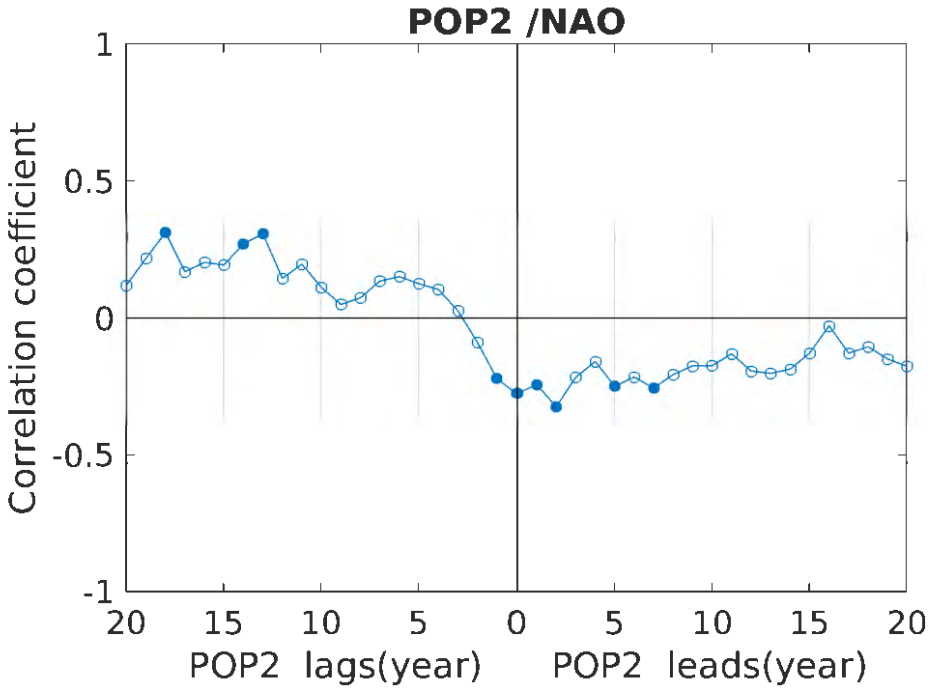

Fig. S3: Lag-correlation function between the detrended POP2 time series (PC2) and the detrended winter (December-March, DJFM) NAO index. Full circles indicate statistical significance at the 95% level.

Chapter 6 Summary and discussion

6.1 Summary

This thesis focuses on the multidecadal variability in the North Atlantic (NA) in climate models and observations, especially on sea surface temperature (SST) and Atlantic meridional overturning circulation (AMOC) variability. Different datasets are used in this work, including unforced preindustrial control runs of coupled climate models, including Kiel Climate Model (KCM), unforced preindustrial control and historical simulations from the phase 5/6 of the Coupled Model Intercomparison Project (CMIP5/6) and several observational datasets.

In this context, different driving factors operating on extratropical and tropical NA SST on different timescales are investigated in Chapter 3. This is done by cross-spectral analysis between different indices by using observational data, KCM results and CMIP5 individual model outputs and ensemble mean data. Then, the roles of ocean circulation and air-sea interactions in multidecadal variability in the NA, especially over subpolar region, are analyzed in Chapter 4. This is done by a multivariant statistical method, Principal Oscillation Pattern (POP) based on a multi-millennial control integration of a version of KCM. In addition, the recent observed possible AMOC slowdown and cooling in the NA warm hole are discussed in Chapter 5. Multivariant statistical methods, POP and EOF (Empirical Orthogonal Function) are used on observational datasets and a large ensemble of historical simulations of CMIP5/6.

The questions raised in the introduction are summarized here.

1. *What are the driving mechanisms of NA SST over different regions on different timescales in observations and climate models and how does climate model bias influence these results?*

In order to address this question, observations and preindustrial control climate model simulations from KCM and CMIP5 are analyzed. Two indices are used, an annual index, termed the NASST (North Atlantic sea surface temperature) index, and a low-pass filtered index that serves as the AMO (Atlantic multidecadal oscillation) index. In observations, the

AMO index highlights the extratropical NA SST variability and the NASST index related pattern is influenced by the NAO (North Atlantic oscillation) related SST variability.

By using cross-spectral analysis, the NA basin-averaged SST index is shown to be superimposed of SST variability influenced by different factors: NAO, AMOC (Atlantic meridional overturning circulation), SPG (subpolar gyre) and ENSO (El Niño–Southern Oscillation). SST variability associated with AMOC and SPG is restricted to the extratropical NA on multidecadal timescales while the NA tropical SST can be influenced by local trade wind changes and remote influences from tropical Pacific (ENSO) on short timescales. Moreover, the cold biases in the NA region of climate models influences the simulation of correct ocean dynamics, especially the AMOC. The corrected climate models exhibit more realistic ocean dynamics, thus enhancing the predictability of NA quantities, especially over the extratropical NA on multidecadal timescales.

2. *How do ocean circulation and atmosphere-ocean coupling influence the NA multidecadal variability and what is the role of stochastic atmospheric forcing?*

This question is addressed by using a multi-millennial freshwater flux corrected preindustrial control integration of KCM. By applying statistical method, Principal Oscillation Pattern (POP) analysis jointly on oceanic and atmospheric variables, a multidecadal coupled mode is found. This mode indicates that the interactions between ocean circulation (SPG and AMOC) and atmosphere are essential to understanding the nature of the NA multidecadal variability.

This mode includes a fast positive feedback between SPG, SST, SLP (sea level pressure) and wind stress over the Southern Greenland area and a slow negative feedback between SPG, AMOC and associated oceanic variables. SPG plays an important role in connecting the ocean and atmosphere. An anomalously strong SPG transports positive SST to the South Greenland region, driving atmospheric responses shown in SLP and related wind stress changes, thus further reinforcing SPG changes, thereby maintaining the (damped) multidecadal oscillation against dissipation and providing the positive feedback. While SPG and AMOC mutually influence each other and together provide the delayed negative feedback. SPG drives higher surface salinity and density in the NA's sinking region. In response, oceanic deep convection and AMOC intensify, which, with a time delay of about a decade, reduces SPG strength by enhancing upper-ocean heat content. The weaker gyre

leads to lower surface salinity and density in the sinking region, which reduces deep convection and eventually AMOC strength. This positive feedback is important for enhancing and maintaining the multidecadal variability. Meanwhile, the negative feedback shows the adjustment and phase reversal of AMOC. By using cross-spectral analysis, this mode also supports that the ocean variability is the response of the atmospheric stochastic forcing. The heat-flux variability associated with NAO keeps exciting the damped multidecadal mode in KCM.

3. *Does AMOC slow in response to global warming? As an indirect indicator of AMOC in observation, what is the cause of the cooling of SST in NA warming hole?*

In this study, observed SSTs since the beginning of 20th century and results of a large ensemble of historical simulations of CMIP are used to answer these questions. The results suggest the prevalence of internal AMOC variability. POP analysis is applied to the annual observed NA SSTs and the first two leading modes are analyzed. The leading POP, POP1 describes the externally forced Atlantic SST variability, which exhibits warming over most of global ocean except NA warming hole. The associated time evolution of POP1 shows a pronounced upward trend and highly correlated with the net radiative forcing (RF). POP2 exhibits an interhemispheric dipole pattern which is linked to the long-term AMOC variability and further analysis indicates that POP2 describes the SST variability related to the internal AMOC variability.

In addition, historical simulations with climate models suggest that the sustained anthropogenic AMOC slowing during the last decades is within the range of natural variability. Furthermore, an analysis of satellite sea levels indicates that the AMOC-slowing event around 2010 could be a realization of internal variability. However, some studies point out that the CMIP ensemble may underestimate the cooling in the NA warming hole. Due to the limited observations and model biases, this study does not rule out the possibility that external forcing played a major role during the recent decadal AMOC decline. Therefore, the systematic and sustained in-situ monitoring systems of AMOC are needed to detect and attribute an anthropogenic AMOC signal with high confidence.

6.2 Outlook

This thesis supports previous studies, suggesting that the ocean dynamics are crucial for the generation of the multidecadal variability in the NA region (e.g., Delworth et al. 2017; Zhang et al. 2019). However, the limited length of observations, especially direct observations of the AMOC, inhibits verifying by data the relationship between AMOC and SST and the existence of a multidecadal eigenmode including ocean-atmosphere interactions in the NA sector. For this reason, the majority of analyses in this thesis are based on climate models, which are known to suffer from large SST biases over the NA (Wang et al. 2014). The cold biases have a major influence on the origin of multidecadal NA SST variability. Enhancing model resolution and better understanding of the physical mechanisms are crucial for better model simulations of the NA multidecadal variability.

In addition, recent studies emphasis the decadal component (10-20 years) of the NA SST, which is driven by different dynamics compared with the multidecadal component. The decadal variability may be connected to the meridional shift of the Gulf stream or linked directly to the dynamics over the tropical Atlantic (Nigma et al. 2018; Lin et al. 2019; Wills et al. 2019). The second leading POP in Chapter 4 has a rotation period of 18.9 years. Further research on the mechanisms of the POP2 about the decadal variability in the NA and on potential observations to verify the model results will be done in the future.

One challenging problem in this study is to characterize the roles of internal and external forcing in multidecadal variability over the NA. Due to the uncertainties with a robust estimation of external forcing and limited instrumental records, it is difficult to clearly separate the internal multidecadal characteristics from non-linear global-scale signal in observations. For example, in Chapter 3, the SST-anomaly pattern associated with the AMO index, when calculated from the short instrumental observations, likely contains large components from atmospheric heat-flux forcing, ocean dynamical heating, and external forcing. Therefore, in addition to the improvement of the systematic observations, a better understanding about the mechanisms of external forcing is also important.

The internal variability is the natural variability of the climate system without role of external forcing, such as anthropogenic global warming (Stocker et al. 2013). ENSO would be an example of internal variability which results from the interactions between atmosphere and ocean in the tropical Pacific. Understanding the internal variability is crucial for the climate change projections, especially for the global surface warming slowdown over the last decades. Mann et al. (2021) suggested that the AMO is forced externally by volcano

activities and AMO is not a natural internal variability but a manifestation of competing time-varying effects of anthropogenic greenhouse gases and sulfate aerosols. However, this work is based on a climate model ensemble, which may not simulate the internal multidecadal variability realistically. This motivates more investigations about the nature of the multidecadal variability, in particular on the relative role of internal variability and external forcing in multidecadal variability in the past centuries.

Another interesting aspect would be the cross-basin interactions. Wang (2019) reviewed that the interactions among Pacific, Atlantic and Indian Oceans through ocean–atmosphere coupling influence climate variability. Moreover, a detailed structure between low-frequency NAO, AMO and North Pacific decadal variability is found in observations (Nigam et al. 2019). Related work has already been done by applying POP over the Pacific and Atlantic basin by using KCM, and upcoming analyses will provide more information about cross-basin interactions. This would help to compose a better understanding about the multidecadal variability in the NA.

Bibliography

Allan, R. and Ansell, T., 2006. A new globally complete monthly historical gridded mean sea level pressure dataset (HadSLP2): 1850–2004. *Journal of Climate*, **19(22)**, 5816-5842.

Álvarez-García, F., M. Latif, and A. Biastoch, 2008. On Multidecadal and Quasi-Decadal North Atlantic Variability. *Journal of Climate*, **21**, 3433–3452.

Bellomo, K., Murphy, L. N., Cane, M. A., Clement, A. C., and Polvani, L. M., 2018. Historical forcings as main drivers of the Atlantic multidecadal variability in the CESM large ensemble. *Climate Dynamics*, **50(9-10)**, 3687–3698.

Bjerknes, J., 1964. Atlantic air-sea interaction. *In Advances in geophysics*, **10**, 1-82, Elsevier.

Bloomfield, P., 2004: Fourier analysis of time series: an introduction. *John Wiley & Sons*.

Booth, B., N. J. Dunstone, P. R. Halloran, T. Andrews, and N. Bellouin, 2012. Aerosols implicated as a prime driver of twentieth-century North Atlantic climate variability, *Nature*, **484(7393)**, 228–232.

Böning, C.W., Scheinert, M., Dengg, J., Biastoch, A. and Funk, A., 2006. Decadal variability of subpolar gyre transport and its reverberation in the North Atlantic overturning. *Geophysical Research Letters*, **33(21)**.

Born, A. and Mignot, J., 2012. Dynamics of decadal variability in the Atlantic subpolar gyre: a stochastically forced oscillator. *Climate dynamics*, **39(1-2)**, 461-474.

Booth, B.B., Dunstone, N.J., Halloran, P.R., Andrews, T. and Bellouin, N., 2012. Aerosols implicated as a prime driver of twentieth-century North Atlantic climate variability. *Nature*, **484(7393)**, 228-232.

de Boyer Montégut, C., Madec, G., Fischer, A.S., Lazar, A. and Iudicone, D., 2004. Mixed layer depth over the global ocean: An examination of profile data and a profile-based climatology. *Journal of Geophysical Research: Oceans*, **109(C12)**.

Brown, P. T., M. S. Lozier, R. Zhang, and W. Li, 2016. The necessity of cloud feedback for a basin-scale Atlantic Multidecadal Oscillation. *Geophysical Research Letters*, **43**, 3955–3963.

Bryan, K., 1962. Measurements of meridional heat transport by ocean currents. *Journal of Geophysical Research*, **67(9)**, 3403-3414.

Buckley, M.W. and Marshall, J., 2016. Observations, inferences, and mechanisms of the Atlantic Meridional Overturning Circulation: A review. *Reviews of Geophysics*, **54(1)**, 5-63.

Caesar, L., Rahmstorf, S., Robinson, A., Feulner, G. and Saba, V., 2018. Observed fingerprint of a weakening Atlantic Ocean overturning circulation. *Nature*, **556(7700)**, 191-196.

Cayan, D.R., 1992. Latent and sensible heat flux anomalies over the northern oceans: Driving the sea surface temperature. *Journal of Physical Oceanography*, **22(8)**, 859-881.

Chemke, R., Zanna, L. and Polvani, L.M., 2020. Identifying a human signal in the North Atlantic warming hole. *Nature communications*, **11(1)**, 1-7.

Chen, X., and Tung, K. K., 2018. Global surface warming enhanced by weak Atlantic overturning circulation. *Nature*, **559(7714)**, 387–391.

Clement, A., Bellomo, K., Murphy, L. N., Cane, M. A., Mauritsen, T., Rädel, G., and Stevens, B., 2015. The Atlantic Multidecadal Oscillation without a role for ocean circulation. *Science*, **350(6258)**, 320–324.

Curry, R.G., McCartney, M.S. and Joyce, T.M., 1998. Oceanic transport of subpolar climate signals to mid-depth subtropical waters. *Nature*, **391(6667)**, 575-577.

Cunningham, S. A., and Coauthors, 2007. Temporal variability of the Atlantic Meridional Overturning Circulation at 26.5°N. *Science*, **317**, 935-938.

Danabasoglu, G., 2008. On multidecadal variability of the Atlantic meridional overturning circulation in the Community Climate System Model version 3. *Journal of Climate*, **21(21)**, 5524-5544.

Delworth, T., Manabe, S. and Stouffer, R.J., 1993. Interdecadal variations of the thermohaline circulation in a coupled ocean-atmosphere model. *Journal of Climate*, **6(11)**, 1993-2011.

Delworth, T. L., and Greatbatch, R. J. 2000. Multidecadal Thermohaline Circulation Variability Driven by Atmospheric Surface Flux Forcing, *Journal of Climate*, **13(9)**, 1481-1495.

Delworth, T.L. and Mann, M.E., 2000. Observed and simulated multidecadal variability in the Northern Hemisphere. *Climate Dynamics*, **16(9)**, 661-676.

Delworth, T.L., Zeng, F., Vecchi, G.A., Yang, X., Zhang, L. and Zhang, R., 2016. The North Atlantic Oscillation as a driver of rapid climate change in the Northern Hemisphere. *Nature Geoscience*, **9(7)**, 509-512.

Delworth, T.L., Zeng, F., Zhang, L., Zhang, R., Vecchi, G.A. and Yang, X., 2017. The central role of ocean dynamics in connecting the North Atlantic Oscillation to the extratropical component of the Atlantic multidecadal oscillation. *Journal of Climate*, **30(10)**, 3789-3805.

Deser, C., Alexander, M.A., Xie, S.P. and Phillips, A.S., 2010. Sea surface temperature variability: Patterns and mechanisms. *Annual review of marine science*, **2**, 115-143.

Dickson, R.R. and Brown, J., 1994. The production of North Atlantic Deep Water: sources, rates, and pathways. *Journal of Geophysical Research: Oceans*, **99(C6)**, 12319-12341.

Dickson, R., Lazier, J., Meincke, J., Rhines, P. and Swift, J., 1996. Long-term coordinated changes in the convective activity of the North Atlantic. *Progress in Oceanography*, **38(3)**, 241-295.

Dong, B. and Sutton, R., 2002. Variability in North Atlantic heat content and heat transport in a coupled ocean–atmosphere GCM. *Climate dynamics*, **19(5-6)**, 485-497.

Dong, B. and Sutton, R.T., 2005. Mechanism of interdecadal thermohaline circulation variability in a coupled ocean–atmosphere GCM. *Journal of climate*, **18(8)**, 1117-1135.

Drews, A. and Greatbatch, R.J., 2016. Atlantic multidecadal variability in a model with an improved North Atlantic Current. *Geophysical Research Letters*, **43(15)**, 8199-8206.

Drijfhout, S., Van Oldenborgh, G.J. and Cimatoribus, A., 2012. Is a decline of AMOC causing the warming hole above the North Atlantic in observed and modeled warming patterns?. Journal of Climate, **25(24)**, 8373-8379.

Ebisuzaki, W., 1997. A method to estimate the statistical significance of a correlation when the data are serially correlated. *Journal of Climate*, **10(9)**, 2147-2153.

Eden, C. and Jung, T., 2001. North Atlantic interdecadal variability: oceanic response to the North Atlantic Oscillation (1865–1997). *Journal of Climate*, **14(5)**, 676-691.

Eden, C. and Willebrand, J., 2001. Mechanism of interannual to decadal variability of the North Atlantic circulation. *Journal of Climate*, **14(10)**, 2266-2280.

Eden, C. and Greatbatch, R.J., 2003. A damped decadal oscillation in the North Atlantic climate system. *Journal of climate*, **16(24)**, 4043-4060.

Enfield, D. B., A. M. Mestas-Nuñez, and P. J. Trimble, 2001. The Atlantic Multidecadal Oscillation and its relation to rainfall and river flows in the continental U.S. *Geophysical Research Letters*, **28**, 2077–2080.

Flato G and Coauthors, 2013. Evaluation of climate models. In: Stocker TF, Qin D, Plattner G-K, Tignor M, Allen SK, Boschung J, Nauels A, Xia Y, Bex V, Midgley PM (eds) Climate change 2013: the physical science basis. Contribution of working group I to the fifth assessment report of the intergovernmental panel on climate change. *Cambridge University Press, Cambridge*.

Folland, C. K., T. N. Palmer, and D. E. Parker, 1986. Sahel rainfall and worldwide sea temperatures, 1901–85. *Nature*, **320 (6063)**, 602.

Frankignoul, C., Czaja, A. and L'Heveder, B., 1998. Air–sea feedback in the North Atlantic and surface boundary conditions for ocean models. *Journal of climate*, **11(9)**, 2310-2324.

Frankignoul, C., Gastineau, G., and Kwon, Y. O., 2017. Estimation of the SST response to anthropogenic and external forcing and its impact on the Atlantic Multidecadal Oscillation and the Pacific Decadal Oscillation. *Journal of Climate*, **30(24)**, 9871–9895.

Friedman, A. R., Reverdin, G., Khodri, M., and Gastineau, G., 2017. A new record of Atlantic sea surface salinity from 1896 to 2013 reveals the signatures of climate variability and long-term trends. *Geophysical Research Letters*, **44**, 1866–1876.

Fu, Y., Li, F., Karstensen, J. and Wang, C., 2020. A stable Atlantic Meridional Overturning Circulation in a changing North Atlantic Ocean since the 1990s. *Science advances*, **6(48)**, eabc7836.

Ganachaud, A. and Wunsch, C., 2000. Improved estimates of global ocean circulation, heat transport and mixing from hydrographic data. *Nature*, **408(6811)**, 453-457.

Gervais, M., Shaman, J. and Kushnir, Y., 2018. Mechanisms governing the development of the North Atlantic warming hole in the CESM-LE future climate simulations. *Journal of climate*, **31(15)**, 5927-5946.

Goldenberg, S. B., C. W. Landsea, A. M. Mestas-Nuñez, and W. M. Gray, 2001. The recent increase in Atlantic hurricane activity: Causes and implications. *Science*, **293 (5529)**, 474–479.

Gregory, J.M., and Coauthors, 2005. A model intercomparison of changes in the Atlantic thermohaline circulation in response to increasing atmospheric CO2 concentration. *Geophysical Research Letters*, **32(12)**.

Gulev, S.K., Latif, M., Keenlyside, N., Park, W. and Koltermann, K.P., 2013. North Atlantic Ocean control on surface heat flux on multidecadal timescales. *Nature*, **499(7459)**, 464-467.

Hansen, J., Ruedy, R., Glascoe, J. and Sato, M., 1999. GISS analysis of surface temperature change. *Journal of Geophysical Research: Atmospheres*, **104(D24)**, 30997-31022.

Hasselmann, K., 1976. Stochastic climate models part I. Theory. *tellus*, **28(6)**, 473-485.

Hasselmann, K., 1988: PIPs and POPs: The reduction of complex dynamical systems using principal interaction and oscillation patterns. *Journal of Geophysical Research: Atmospheres*, **93(D9)**, 11015-11021.

Holland, D.M., Thomas, R.H., de Young, B., Ribergaard, M.H. and Lyberth, B., 2008. Acceleration of Jakobshavn Isbræ triggered by warm subsurfaceocean waters. *Nature Geoscience*, **1**, 659–664.

Huang, B., and Coauthors, 2017. Extended reconstructed sea surface temperature, version 5 (ERSSTv5): upgrades, validations, and intercomparisons. *Journal of Climate*, **30(20)**, 8179-8205.

Hurrell J, 1995. Decadal trends in the north atlantic oscillation: regional temperatures and precipitation. *Science*, **269(5224)**, 676–678.

Hurrell, J. W., Y. Kushnir, G. Ottersen, and M. Visbeck, 2013. An overview of the North Atlantic Oscillation. The North Atlantic Oscillation. Geophys. Monogr., Vol. 134, *Amer. Geophys. Union*, **1–35**.

Jackson, L.C., Peterson, K.A., Roberts, C.D. and Wood, R.A., 2016. Recent slowing of Atlantic overturning circulation as a recovery from earlier strengthening. *Nature Geoscience*, **9(7)**, 518-522.

Kanzow, T., S. A. Cunningham, D. Rayner, J. J.-M. Hirschi, W. E. Johns, M. O. Baringer, H. L. Bryden, L. M. Beal, C. S. Meinen, andJ. Marotzke, 2007. Observed flow compensation associated with the MOC at 26.5°N in the Atlantic, *Science*, **317**, 938–941.

Keil, P., Mauritsen, T., Jungclaus, J., Hedemann, C., Olonscheck, D. and Ghosh, R., 2020. Multiple drivers of the North Atlantic warming hole. *Nature Climate Change*, **10(7)**, 667-671.

Kerr, R. A., 2000. A North Atlantic climate pacemaker for the centuries. *Science*, **288**, 1984–1985.

Klotzbach, P. J., and W. M. Gray, 2008. Multidecadal variability in North Atlantic tropical cyclone activity, *Journal of Climate*, **21**, 3929–3935.

Knight, J.R., Allan, R.J., Folland, C.K., Vellinga, M. and Mann, M.E., 2005. A signature of persistent natural thermohaline circulation cycles in observed climate. *Geophysical Research Letters*, **32(20)**.

Kaplan, A., Cane, M.A., Kushnir, Y., Clement, A.C., Blumenthal, M.B. and Rajagopalan, B., 1998. Analyses of global sea surface temperature 1856–1991. *Journal of Geophysical Research: Oceans*, **103(C9)**, 18567-18589.

Kushnir, Y., 1994. Interdecadal variations in North Atlantic sea surface temperature and associated atmospheric conditions. *Journal of Climate*, **7 (1)**, 141–157.

Latif, M., Roeckner, E., Botzet, M., Esch, M., Haak, H., Hagemann, S., Jungclaus, J., Legutke, S., Marsland, S., Mikolajewicz, U. and Mitchell, J., 2004. Reconstructing, monitoring, and predicting multidecadal-scale changes in the North Atlantic thermohaline circulation with sea surface temperature. *Journal of Climate*, **17(7)**, 1605-1614.

Latif, M., Böning, C., Willebrand, J., Biastoch, A., Dengg, J., Keenlyside, N., Schweckendiek, U. and Madec, G., 2006. Is the thermohaline circulation changing? *Journal of Climate*, **19(18)**, 4631-4637.

Latif, M., and N. S. Keenlyside, 2011. A perspective on decadal climate variability and predictability. *Deep Sea Research Part II: Topical Studies in Oceanography*, **58 (17-18)**, 1880–1894.

Latif, M., Park, T. and Park, W., 2019. Decadal Atlantic Meridional Overturning Circulation slowing events in a climate model. *Climate dynamics*, **53(1)**, 1111-1124.

Lin, P., Yu, Z., Lü, J., Ding, M., Hu, A. and Liu, H., 2019. Two regimes of Atlantic multidecadal oscillation: cross-basin dependent or Atlantic-intrinsic. *Science Bulletin*, **64(3)**, 198-204.

Liu, W., Fedorov, A.V., Xie, S.P. and Hu, S., 2020. Climate impacts of a weakened Atlantic Meridional Overturning Circulation in a warming climate. *Science advances*, **6(26)**, eaaz4876.

Lobelle, D., Beaulieu, C., Livina, V., Sevellec, F. and Frajka-Williams, E., 2020. Detectability of an AMOC decline in current and projected climate changes. *Geophysical Research Letters*, **47(20)**, e2020GL089974.

Locarnini R. A., and Coauthors, 2018. World Ocean Atlas 2018, Volume 1: Temperature. A. Mishonov Technical Ed.; NOAA Atlas NESDIS 81, 52.

Lohmann, K., Drange, H. & Bentsen, M., 2009. Response of the North Atlantic subpolar gyre to persistent North Atlantic oscillation like forcing. *Climate Dynamics*, **32**, 273–285.

Mann, M.E. and Park, J., 1994. Global-scale modes of surface temperature variability on interannual to century timescales. *Journal of Geophysical Research: Atmospheres*, **99(D12)**, 25819-25833.

Mann, M.E., Steinman, B.A., Brouillette, D.J. and Miller, S.K., 2021. Multidecadal climate oscillations during the past millennium driven by volcanic forcing. *Science*, **371(6533)**, 1014-1019.

Marshall, J., Donohoe, A., Ferreira, D. et al., 2014. The ocean's role in setting the mean position of the Inter-Tropical Convergence Zone. *Climate Dynamics*, **42**, 1967–1979.

McCarthy, G., Frajka-Williams, E., Johns, W.E., Baringer, M.O., Meinen, C.S., Bryden, H.L., Rayner, D., Duchez, A., Roberts, C. and Cunningham, S.A., 2012. Observed interannual variability of the Atlantic meridional overturning circulation at 26.5 N. *Geophysical Research Letters*, **39(19)**.

McCarthy, G.D., Haigh, I.D., Hirschi, J.J.-M., Grist, J.P. and Smeed, D.A., 2015. Ocean impact on decadal Atlantic climate variability revealed by sea-level observations. *Nature*, **521**, 508–510.

Mecking, J.V., Keenlyside, N.S. and Greatbatch, R.J., 2014. Stochastically-forced multidecadal variability in the North Atlantic: a model study. *Climate dynamics*, **43(1-2)**, 271-288.

Medhaug, I., Langehaug, H.R., Eldevik, T., Furevik, T. and Bentsen, M., 2012. Mechanisms for decadal scale variability in a simulated Atlantic meridional overturning circulation. *Climate dynamics*, **39(1-2)**, 77-93.

Madec, G., 2008. NEMO ocean engine, Note du Pole de modélisation, Institut Pierre-Simon Laplace (IPSL), France, *No 27. Tech. rep., ISSN-1288-1619*.

Msadek, R. and Frankignoul, C., 2009. Atlantic multidecadal oceanic variability and its influence on the atmosphere in a climate model. *Climate dynamics*, **33(1)**, 45-62.

Nigam, S., Ruiz-Barradas, A. and Chafik, L., 2018. Gulf Stream excursions and sectional detachments generate the decadal pulses in the Atlantic multidecadal oscillation. *Journal of Climate*, **31(7)**, 2853-2870.

Nigam, S., Sengupta, A. and Ruiz-Barradas, A., 2020. Atlantic–Pacific links in observed multidecadal SST variability: is the Atlantic multidecadal oscillation's phase reversal orchestrated by the Pacific decadal oscillation?. *Journal of Climate*, **33(13)**, 5479-5505.

Pachauri, R.K., and Coauthors, 2014. Climate change 2014: synthesis report. Contribution of Working Groups I, II and III to the fifth assessment report of the Intergovernmental Panel on Climate Change (151). IPCC.

Park, T., W. Park, and M. Latif, 2016: Correcting North Atlantic sea surface salinity biases in the Kiel Climate Model: influences on ocean circulation and Atlantic Multidecadal Variability. *Climate dynamics*, **47 (7-8)**, 2543–2560.

Park, W. and Latif, M., 2008. Multidecadal and multicentennial variability of the meridional overturning circulation. *Geophysical Research Letters*, **35(22)**.

Park, W., N. Keenlyside, M. Latif, A. Ströh, R. Redler, E. Roeckner, and G. Madec, 2009. Tropical Pacific climate and its response to global warming in the Kiel Climate Model. *Journal of Climate*, **22 (1)**, 71–92.

Pierce, D.W., Barnett, T.P., AchutaRao, K.M., Gleckler, P.J., Gregory, J.M. and Washington, W.M., 2006. Anthropogenic warming of the oceans: Observations and model results. *Journal of Climate*, **19(10)**, 1873-1900.

Te Raa, L.A. and Dijkstra, H.A., 2002. Instability of the thermohaline ocean circulation on interdecadal timescales. *Journal of physical oceanography*, **32(1)**, 138-160.

Rahmstorf, S., Box, J.E., Feulner, G., Mann, M.E., Robinson, A., Rutherford, S. and Schaffernicht, E.J., 2015. Exceptional twentieth-century slowdown in Atlantic Ocean overturning circulation. *Nature climate change*, **5(5)**, 475-480.

Rasmusson, E.M. and Carpenter, T.H., 1982. Variations in tropical sea surface temperature and surface wind fields associated with the Southern Oscillation/El Niño. *Monthly Weather Review*, **110(5)**, 354-384.

Rayner, N. A., and Coauthors, 2003. Global analyses of sea surface temperature, sea ice, and night marine air temperature since the late nineteenth century. *Journal of Geophysical Research*, **108(D14)**, 4407.

Rhein, M., Kieke, D., Hüttl-Kabus, S., Roessler, A., Mertens, C., Meissner, R., Klein, B., Böning, C.W. and Yashayaev, I., 2011. Deep water formation, the subpolar gyre, and the meridional overturning circulation in the subpolar North Atlantic. *Deep Sea Research Part II. Topical Studies in Oceanography*, **58(17-18)**, 1819-1832.

Roberts, C.D., Jackson, L. and McNeall, D., 2014. Is the 2004–2012 reduction of the Atlantic meridional overturning circulation significant?. *Geophysical Research Letters*, **41(9)**, 3204-3210.

Robson, J., Sutton, R. and Smith, D., 2014. Decadal predictions of the cooling and freshening of the North Atlantic in the 1960s and the role of ocean circulation. *Climate dynamics*, **42(9)**, 2353-2365.

Roeckner, E., and Coauthors, 2003. The atmospheric general circulation model ECHAM 5. PART I: Model description. *MPI-Report 349, Hamburg, Germany.*

Sévellec, F. and Fedorov, A.V., 2013. The leading, interdecadal eigenmode of the Atlantic meridional overturning circulation in a realistic ocean model. *Journal of Climate*, **26(7)**, 2160-2183.

Smeed, D.A., and Coauthors, 2014. Observed decline of the Atlantic meridional overturning circulation 2004–2012. *Ocean Science*, **10(1)**, 29-38.

Stocker, T. F., and Coauthors, 2013: Climate change 2013: The physical science basis. Contribution of working group I to the fifth assessment report of the intergovernmental panel on climate change. Intergov. Panel Clim. Chang. (IPCC), *Cambridge Univ. Press.* Cambridge, **1535** Doi: 10.1017/CBO9781107415324.

Stouffer, R. J., and Coauthors, 2006. Investigating the Causes of the Response of the Thermohaline Circulation to Past and Future Climate Changes, *Journal of Climate*, **19(8)**, 1365-1387.

Stommel, H., 1958. The abyssal circulation. *Deep-Sea Research*, **5**, 80-82.

Stommel, H., 1961. Thermohaline convection with two stable regimes of flow. *Tellus*, **13(2)**, 224-230.

von Storch, H., Bürger, G., Schnur, R. and von Storch, J.S., 1995: Principal oscillation patterns: A review. *Journal of Climate*, **8(3)**, 377-400.

Sutton, R. T., and D. L. Hodson, 2005. Atlantic Ocean forcing of North American and European summer climate. *Science*, **309**, 115–118.

Sutton, R.T., McCarthy, G.D., Robson, J., Sinha, B., Archibald, A.T. and Gray, L.J., 2018. Atlantic multidecadal variability and the UK ACSIS program. *Bulletin of the American Meteorological Society*, **99(2)**, 415-425.

Svendsen, L., Hetzinger, S., Keenlyside, N. and Gao, Y., 2014. Marine-based multiproxy reconstruction of Atlantic multidecadal variability. *Geophysical Research Letters*, **41(4)**, 1295-1300.

Timmermann, A., Latif, M., Voss, R. and Grötzner, A., 1998. Northern Hemispheric interdecadal variability: A coupled air–sea mode. *Journal of Climate*, **11(8)**, 1906-1931.

Ting, M., Kushnir, Y., Seager, R. and Li, C., 2009. Forced and internal twentieth-century SST trends in the North Atlantic. *Journal of Climate*, **22(6)**, 1469-1481.

Toole, J.M., Andres, M., Le Bras, I.A., Joyce, T.M. and McCartney, M.S., 2017. Moored observations of the Deep Western Boundary Current in the NW Atlantic: 2004–2014. *Journal of Geophysical Research: Oceans*, **122(9)**, 7488-7505.

Trenberth, K.E. and Solomon, A., 1994. The global heat balance: Heat transports in the atmosphere and ocean. *Climate Dynamics*, **10(3)**, 107-134.

Trenberth, K.E. and Shea, D.J., 2006. Atlantic hurricanes and natural variability in 2005. *Geophysical research letters*, **33(12)**.

Valcke, S., E. Guilyardi, and C. Larsson, 2006: PRISM and ENES: A European approach to Earth system modelling. *Concurr. Comput.: Pract. Exper.*, **18**, 247–262.

Venzke, S., M. R. Allen, R. T. Sutton, and D. P. Rowell, 1999: The atmospheric response over the North Atlantic to decadal changes in sea surface temperature. *J. Climate*, 12, 2562–2584.

Van Vuuren, D.P., and Coauthors, 2011. The representative concentration pathways: an overview. *Climatic change*, **109(1)**, 5-31.

Wang, C., Zhang, L., Lee, S.K., Wu, L. and Mechoso, C.R., 2014. A global perspective on CMIP5 climate model biases. *Nature Climate Change*, **4(3)**, 201-205.

Wang, C., 2019. Three-ocean interactions and climate variability: A review and perspective. *Climate Dynamics*, **53(7)**, 5119-5136.

Weyer, W., and Coauthors, 2020. CMIP6 Models Predict Significant 21st Century Decline of the Atlantic Meridional Overturning Circulation. *Geophys. Res. Lett.*, **47**, e2019GL086075.

Wills, R. C., Armour, K. C., Battisti, D. S. and Hartmann, D. L., 2019. Ocean–atmosphere dynamical coupling fundamental to the Atlantic Multidecadal Oscillation. *Journal of Climate*, **32(1)**, 251–272.

Xie, S.P. and Philander, S.G.H., 1994. A coupled ocean-atmosphere model of relevance to the ITCZ in the eastern Pacific. *Tellus A*, **46(4)**, 340-350.

Zhao, J. and Johns, W., 2014. Wind-forced interannual variability of the Atlantic Meridional Overturning Circulation at 26.5 N. *Journal of Geophysical Research: Oceans*, **119(4)**, 2403-2419.

Zhang, R. and Delworth, T.L., 2005. Simulated tropical response to a substantial weakening of the Atlantic thermohaline circulation. *Journal of climate*, **18(12)**, 1853-1860.

Zhang, R. and Delworth, T.L., 2006. Impact of Atlantic multidecadal oscillations on India/Sahel rainfall and Atlantic hurricanes. *Geophysical Research Letters*, **33(17)**, L17712.

Zhang, R., 2007. Anticorrelated multidecadal variations between surface and subsurface tropical North Atlantic. *Geophysical Research Letters*, **34**, L12713.

Zhang, R., 2008. Coherent surface-subsurface fingerprint of the Atlantic meridional

965 overturning circulation. *Geophysical Research Letters*, **35(20)**.

Zhang, R., and Coauthors, 2013. Have aerosols caused the observed Atlantic multidecadal variability? *Journal of the Atmospheric Sciences*, **70(4)**, 1135-1144.

Zhang, R., Sutton, R., Danabasoglu, G., Kwon, Y.-O., Marsh, R., Yeager, S. G., et al., 2019. A review of the role of the Atlantic Meridional Overturning Circulation in Atlantic Multidecadal Variability and associated climate impacts. *Reviews of Geophysics*, **57**, 316–375.

Zhu, C. and Liu, Z., 2020. Weakening Atlantic overturning circulation causes South Atlantic salinity pile-up. *Nature Climate Change*, **10(11)**, 998-1003.

Own Publications

Jing Sun, Mojib Latif, Wonsun Park, and Taewook Park (2020). On the Interpretation of the North Atlantic Averaged Sea Surface Temperature, *Journal of Climate*, 33(14): 6025-6045, https://doi.org/10.1175/JCLI-D-19-0158.1.

Jing Sun, Mojib Latif, and Wonsun Park (2021). Subpolar Gyre – AMOC – Atmosphere Interactions on Multidecadal Timescales in a version of the Kiel Climate Model, *Journal of Climate*, 34(16): 6583-6602, https://doi.org/10.1175/JCLI-D-20-0725.1.

Mojib Latif, Jing Sun, Martin Visbeck, and M. Hadi Bordbar (2021) " Natural variability prevalence in Atlantic Meridional Overturning since 1900 ", *Nature Climate Change*, under review.

Acknowledgments

First and foremost, I would like to give a huge thank you to my supervisor, Prof. Dr. Mojib Latif. It has been such an honor to be his Ph.D. student. I appreciate his generosity, kindness and encouragement during my study. He sets an excellent example as a scientist and as a supervisor, and without his patient assistance and guidance, my research could not be possible to be completed.

I would also like to thank Dr. Wonsun Park for his generous guidance and advice. He helped me a lot about doing the analysis and offering the scientific suggestions. I am also thankful to Dr. Taewook Park, who helped me a lot about the climate model data.

I also want to thank my oral defense committee members, Prof. Dr. Eric Pieter Achterberg, Prof. Dr. Arne Biastoch and Prof. Dr. Andreas Oschlies. I would also like to thank Dr. Tobias Bayr and Dr. Yao Fu, who helped me to do the proof-reading of my thesis and gave me great comments.

Thank all the ME members at GEOMAR, for the kindness and nice scientific environment. Especially the assistance from Tania and Silke, your help makes many things much easier. And Dr. Zhaoyang Song not only helped me a lot on science, but also daily life in Germany. And Dr. Wenjuan Huo, we had such a good time for having lunch together.

Futher, I would like to thank My two besties, Yongpei and Jingran. We knew each other since high school. We shared all the stories, and you will always be there when I need you. I also want to thank my friend Zelin, he is like my "German-life teacher". He helped me almost everything I encountered in Germany. And to Kechen, Yihe and all my friends in Kiel, thanks for making my life in Germany much more interesting.

I would like to thank the China Scholarship Council (CSC) and GEOMAR for the financial support during my PhD studies.

Last but not least, I would like to say thank you to my beloved boyfriend Xiaoshuai, he supported me and accompanied me during the darkest time of my life. He gave me confidence and encouraged me to seek for science. I will always thank my beloved parents, Xiaochun Sun and Guangrong Wang, who always trust me and support me for everything. Without their help, I cannot finish my PhD degree.

Thank you all.

Declaration

I hereby declare that this work is my own work apart from my supervisors' guidance and acknowledged assistance. This thesis has not been submitted for a degree to any other examining body. This thesis was prepared in accordance with the Rules of Good Scientific Practice of the German Research Foundation.

Kiel, May 2021

Jing Sun